GRAPHENE OXIDE SUPPORTED METAL OXIDE NANOHYBRIDS FOR AQUEOUS ARSENIC REMOVAL

A Dissertation
Submitted to the Graduate Faculty
of the
North Dakota State University
of Agriculture and Applied Science

By

Tonoy Kumar Das

In Partial Fulfillment of the Requirements
for the Degree of
DOCTOR OF PHILOSOPHY

Major Program:
Environmental and Conservation Sciences

June 2021

Fargo, North Dakota

North Dakota State University
Graduate School

Title

GRAPHENE OXIDE SUPPORTED METAL OXIDE NANOHYBRIDS FOR AQUEOUS ARSENIC REMOVAL

By

Tonoy Kumar Das

The Supervisory Committee certifies that this ***disquisition*** complies with North Dakota State University's regulations and meets the accepted standards for the degree of

DOCTOR OF PHILOSOPHY

SUPERVISORY COMMITTEE:

Dr. Achintya Bezbaruah
Chair

Dr. Dinesh Katti

Dr. Nita Yodo

Dr. Robert Brueggeman

Approved:

July 10 , 2021
Date

Dr. Craig Stockwell
Department Chair

ABSTRACT

Arsenic contamination of drinking water is a major public health concern affecting more than 200 million people globally. Iron(Fe)-based adsorbents though promoted for aqueous arsenic removal because of their low cost and easy availability, their field application is limited due to their low efficiency and slow adsorption kinetics. In this work, two graphene oxide (GO)-Fe nanohybrids, namely GO-supported nano magnetite (GM) and GO-supported nanoscale zero-valent iron (GFeN), were compared for arsenic removal. Controls were run with bare (i.e., no GO) nanoscale zero-valent iron (FeNP) and nano magnetite (M). GFeN worked more efficiently (>90%) over a wide pH range (3-9) for both the inorganic arsenic species, As(III) and As(V). GM worked well at pH 3 (>90% efficient) for As(V), and pH 9 (80%) for As(III). GFeN exhibited better aqueous dispersibility with a zeta potential of −21.02 mV. In GFeN and FeNP, surface complexation was dominant in the adsorption of both As(III) and As(V), and electrostatic attraction played a limited role. In GM and M, As(V) removal was controlled by electrostatic attraction while As(III) adsorption was ligand exchange and surface complexation. The arsenic removal data based on normalized iron content in the adsorbents indicated that the nanohybrids (GFeN and GM) removed arsenic more efficiently compared to the bare nanoparticles (FeNP and M) with GFeN performing the best. Arsenic adsorption capacities of GFeN were found to be 306 mg/g for As(III) and 431 mg/g for As(V). The GO-sheets in GFeN acted as reservoirs for the electrons released during surface corrosion of the FeNPs. The stored electrons were transferred back to the FeNPs to reduce the oxidized iron surface, and the rejuvenated surface helped in additional arsenic removal. The arsenic desorption pattern from two As(V)-sorbed nanohybrids (GFeN and graphene oxide-supported ceria (GO-CeO_2)) was studied. GFeN released ~5.73% and GO-CeO_2 released ~0.94% of sorbed arsenic over a period of two years. While sorbed

arsenic remained as As(V) on the GFeN surface, some As(V) in GO-CeO_2 got reduced to As(III). The surface oxide composition in GFeN (FeOOH and Fe_2O_3) and GO-CeO_2 (Ce^{3+}/Ce^{4+} ratio) underwent changes over time and that played a role in arsenic desorption.

ACKNOWLEDGMENTS

First, I bow my head in reverence to God Almighty who has been always there for me.

I would like to express my sincere gratitude and appreciation to my advisor, Dr. Achintya Bezbaruah, for his continuous support and guidance during my doctoral study. His insight and tireless efforts as mentor are truly appreciated. The completion of my dissertation would not have been possible without his valuable advice, encouragement, and continuous support. Dr. Bezbaruah enriched my thinking process as a researcher and always guided me in the right direction with his immense wisdom and knowledge. I also want to extend my gratitude to my dissertation committee members, Dr. Dinesh Katti, Dr. Robert Brueggeman, and Dr. Nita Yodo for generously offering their valuable time, suggestion, and guidance during the course of my graduate study. I would like to thank Dr. Sudipta Seal and Dr. Tamil Sakthivel from the University of Central Florida for their continuous support, invaluable inputs and guidance throughout my research.

I would also like to thank all the members of Nanoenvirology Research Group and Environmental Engineering Laboratory at NDSU. I must express my appreciation to my friends, Avik, Arighna, Debankur, Hoang, Debalin, Pallavi, Raj, Sayan, Swati, Swarup, Umma.

My tenure at NDSU was supported by fellowship grants from the Indian Council of Agricultural Research, North Dakota Water Resources Research Institute, Environmental and Conservation Sciences Program, Department of Civil and Environmental Engineering, College of Engineering, North Dakota State University (Grand Challenges Initiative), College of Graduate and Interdisciplinary Studies (Doctoral Dissertation Fellowship), and National Science Foundation (NSF Grant# CBET- 1707093, PI: Bezbaruah).

Finally, I would like to thank my parents, my wife Tandrima, my brother Sudipta, and other family members for their support-and love throughout my life.

DEDICATION

This dissertation is dedicated to my mother Saraswati Das and my father Satish Chandra Das

TABLE OF CONTENTS

LIST OF TABLES

LIST OF FIGURES

LIST OF APPENDIX TABLES

LIST OF APPENDIX FIGURES

CHAPTER 1. INTRODUCTION AND LITERATURE REVIEW

1.1. Source and geochemistry of arsenic

Arsenic is a trace toxic metalloid element present in the earth's crust. The arsenic concentration is higher in the upper continental crust (5.7 mg/kg) than the average crustal presence (2.5 mg/kg) (Hu and Gao, 2008). From ancient times, arsenic is considered a poison and sometimes used at low doses for medical purposes. Arsenic is present in both organic and inorganic forms in different valence states (-3, 0, +3, and +5). The inorganic As species, arsenite [AsO_2^- which is As(III)] and arsenate [AsO_4^{3-}, As(V)], are considered more toxic than the organic forms such as monomethylarsonic acid (MMA, CH_5AsO_3) and dimethylarsinic acid (DMA, $C_2H_7AsO_2$) (Administration, 2016). Inorganic arsenic is typically present in two oxidation states, As(III) or arsenite and As(V) or arsenate in groundwater (ATSDR, 2007).

The major source of arsenic contamination is geogenic. The major mineralogical sources of arsenic deposits are associated with metal sulfides, metal oxides, and hydroxides as part of the crystal structure or adsorbed onto the surface of the minerals. The largest fraction of crustal arsenic is associated with pyrite minerals and is present as arsenopyrite (FeAsS). Arsenic typically finds its way into the environment due to natural processes like mineral weathering, biological activities, and volcanic emissions, and some extent anthropogenic activities (Bowell et al., 2014). Geogenic arsenic typically finds its way to the human food chain via water (Zhao et al., 2010) which are released into the aqueous medium due to pH and redox (E_h) fluctuations (Amini et al., 2008a). The presence of microorganisms and/or geochemistry in the aquifer help create the right environment for the release of arsenic from arsenic-bearing iron minerals. Under anoxic conditions, arsenic is released via microbial and/or chemical reductive dissolution of arsenic-bearing iron minerals in the aquifer, and under oxidizing and high-pH conditions, arsenic

is released from iron and aluminum hydroxides via chemical reductive dissolution (Oremland and Stolz, 2003; Fendorf et al., 2010; Podgorski and Berg, 2020). Additionally, aquifers with low hydraulic gradients have higher residence time and that allows arsenic in the solid phase to become dissolved leading to high concentrations in groundwater (Podgorski and Berg, 2020). The release of arsenic from arsenic-bearing sulfide minerals and arsenic-enriched geothermal deposits via oxidation also contribute to arsenic built-up in waters (Podgorski and Berg, 2020). Most of the arsenic present in groundwater is from geogenic sources (Amini et al., 2008b; Podgorski and Berg, 2020) while the anthropogenic sources include some pesticides used in the past and industrial discharge (Murcott, 2012) (Hughes et al., 2011). Anthropogenic contributions of arsenic to the environment also come from mining activities, burning of coal, oil, gasoline, and wood preservatives (FDA, 2016). In the United States, the main source of anthropogenic arsenic contamination is the past uses of As-based pesticides. In the North Dakota aquifer system, arsenic-laden sediments were deposited via glacial deposition during the late Wisconsin period.

Predominant inorganic arsenic species present in the aqueous phase are arsenite [As(III)] and arsenate [(As(V)] in oxyanions forms and they are in two distinct oxidation states (Figure 1.1a). Solution pH and redox potential are two dominant factors that control the speciation of arsenic. Solution pH affects the speciation of As(V), and in aqueous media, it is typically present as $H_2AsO_4^-$ at pH 2.2-6.9 and $HAsO_4^{2-}$ at pH 6.9-11.5 (Figure 1.1a). At pH 0-9.2, As(III) is present as a neutral ion (H_3AsO_4). At extremely high pH, (9.2<pH<12.1) $H2AsO_4^-$, (12.1<pH<13.4), $H2AsO_4^-$, and (>13.4) AsO_4^{3-} are the dominant species (Figure 1.1b) (Yoon et al., 2016). While arsenite is dominant in mild reducing (low redox conditions) environments, arsenate species are dominant in high redox potential and oxygenated environments. The

conversion of arsenite to arsenate is a thermodynamically favorable process but it is a very slow process and depends on environmental conditions like pH and redox potential.

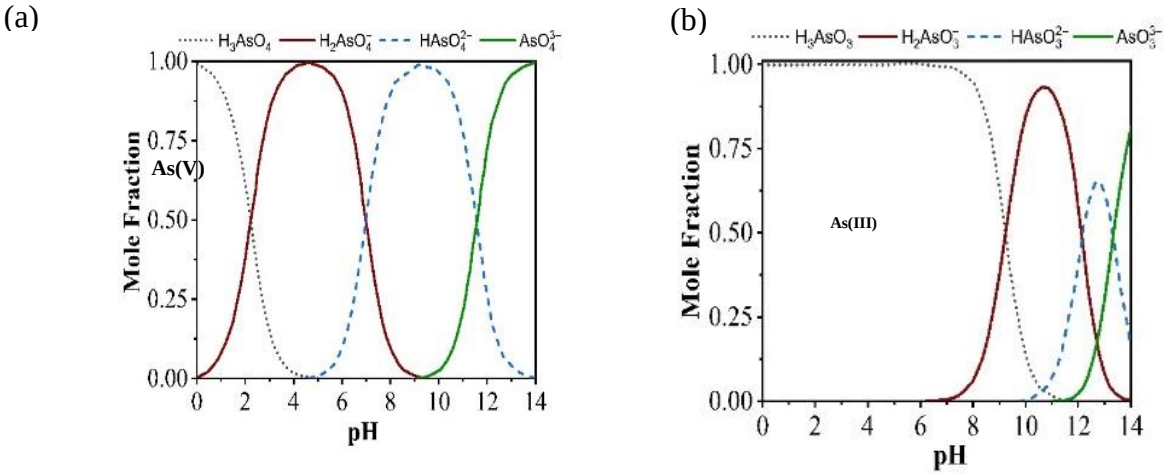

Figure 1.1. Speciation of aqueous arsenic at different pH; (a) speciation of As(V); and (b) speciation of As(III).

1.2. Occurrence of arsenic in groundwater

World Health Organization (WHO) and the United States Environmental Protection Agency (USEPA) have set the maximum contaminant level (MCL) of total inorganic arsenic in drinking water as 10 µg/L (USEPA, 2001; WHO, 2003). More than 200 million people in 50 countries are affected by groundwater arsenic contamination (Figure 1.2a) and the number is increasing rapidly (Murcott, 2012; WHO, 2017; Podgorski and Berg, 2020). Arsenic contamination of drinking water is a major public health concern across the globe with Bangladesh, India, Argentina, Canada, Chile, Japan, and Taiwan being most affected (Murcott, 2012; WHO, 2018). About 2.1 million people in the United States who rely on domestic wells for their drinking water are in danger of facing arsenic contamination (>10 µg/L) (Ayotte et al., 2017). In North Dakota, Richland and Sargent counties (name the counties) are affected by arsenic in groundwater.

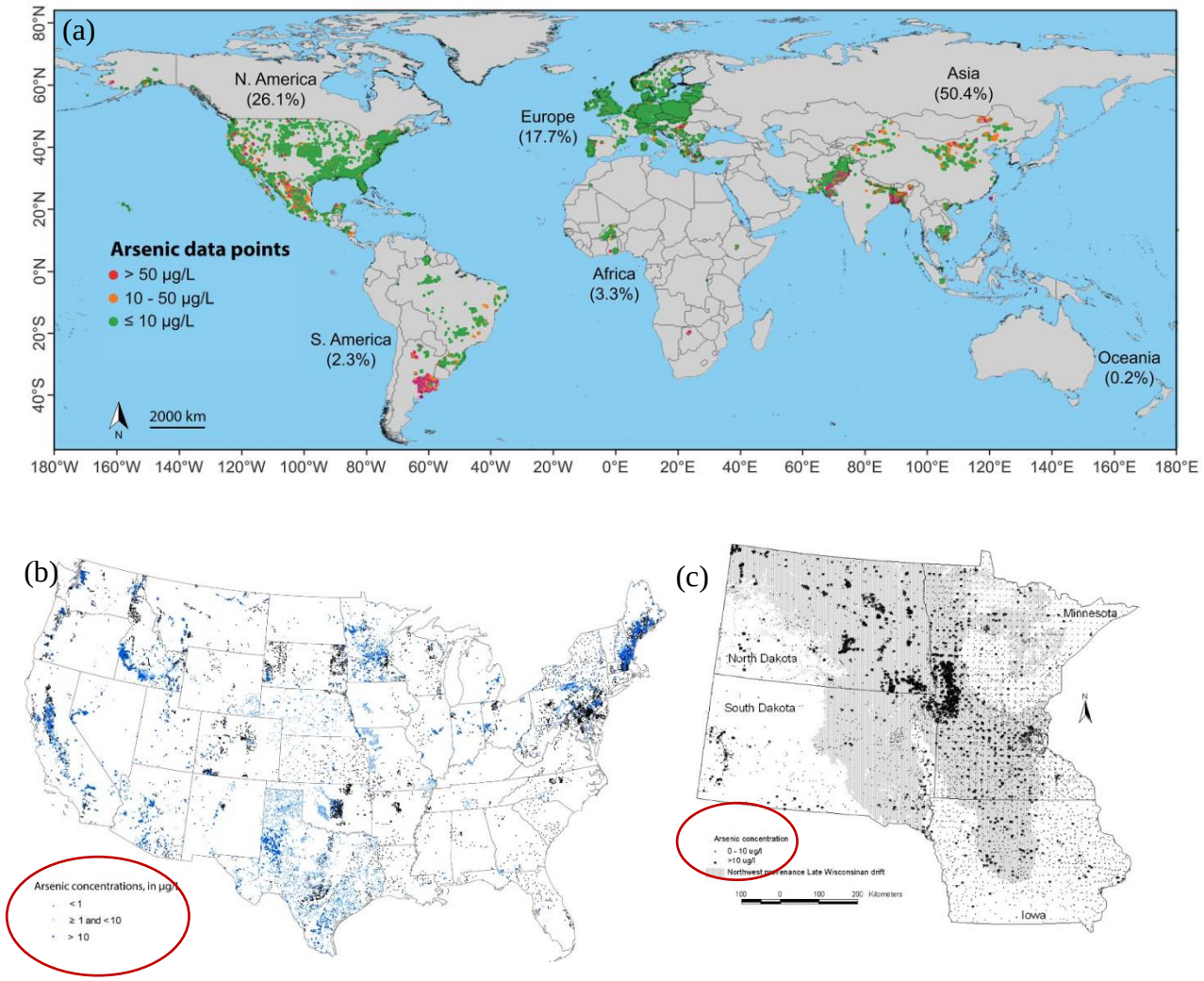

Figure 1.2. (a) Arsenic concentrations in groundwater across the globe (does not include data from aquifers of more than 100 m in depth (Podgorski and Berg, 2020). (b) Locations of domestic wells tested and arsenic concentration ranges in the US(Ayotte et al., 2017). Blue dots are As >10 µg/L, light blue 1<As<10 µg/L, black dots As<1 µg/L. (c) Arsenic concentration in upper Midwest groundwater (Erickson and Barnes, 2005). Black dots are As>10 µg/L.

Southeast Asian populations residing in India, Bangladesh, Nepal, Pakistan, China, Cambodia, and Vietnam (Figure 1.3a) are exposed to arsenic toxicity via ingestion of groundwater (Uppal et al., 2019). The world most severely affected areas with groundwater arsenic contamination are in India (Uttar Pradesh, Bihar, West Bengal, Assam) and Bangladesh in flood plains of Ganges-Padma, Brahmaputra-Jamuna, Meghna (Chakraborti et al., 2013). The sources of arsenic contamination in India and Bangladesh are geogenic in nature and they are the

arsenic-laden quaternary deposits of alluvial sediments belonging to the Holocene age (Bhattacharya et al., 2001). These As-rich sediments are transported by rivers originating from the Himalayas and are deposited into downstream basins and deltaic areas (Figure 1.3b). The extent of arsenic release from the sediments to the aquifer depends upon the geochemical environment within the sediments (Singh et al., 2020). High population density and the people's heavy dependence on groundwater as a source of water have to lead to a large number of people (> 100 million) being exposed to arsenic toxicity in these areas (Bindal and Singh, 2019; Uppal et al., 2019).

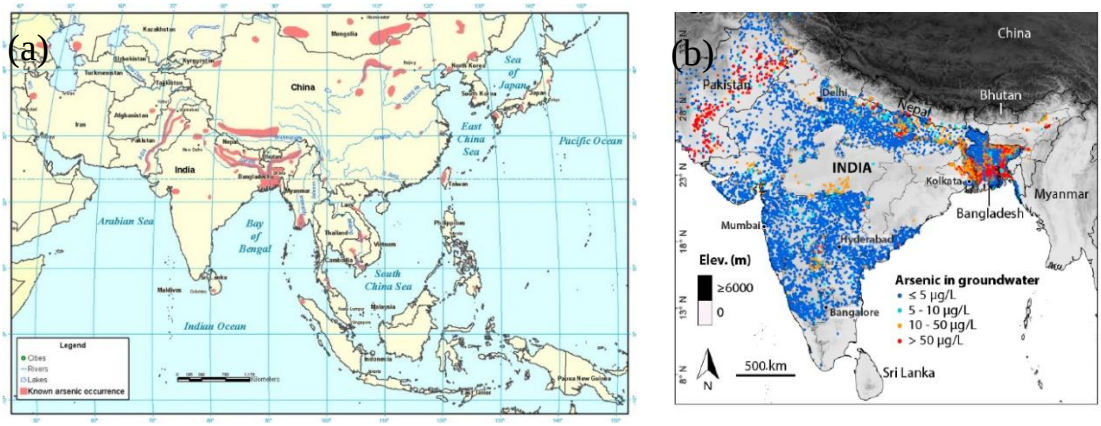

Figure 1.3. (a) Arsenic contamination of groundwater in South and South-east Asia with the pink colored patches indicating the occurrence of arsenic. Map reproduced from (Brammer and Ravenscroft, 2009). (b) Arsenic contamination in South-east Asia. The red and orange colors represent groundwater arsenic concentration more than the MCL (>10 µg/L) (Podgorski et al., 2020).

In the United States, the main source of anthropogenic arsenic contamination is the past use of arsenic-based pesticides used in cotton cultivation is still detected in the soil (Williams et al. 2007). The U.S. EPA banned inorganic arsenic applications in cotton as recently as 1987 and in other crops in 1988 (Loebenstein, 1994). Thus, millions of acres of land are now contaminated with arsenic residues. In North Dakota, there are both anthropogenic and geogenic sources of

arsenic contamination. Arsenic contamination above 50 μg/L was reported in Richland and Sargent counties during the 1980s which came from arsenic-laced bait that was extensively used for pest controls during the mid-1900s (1930-1940) (USEPA). Geologically, the Midwest region states (North Dakota, Minnesota, South Dakota, Iowa) have arsenic-bearing sediments in their aquifer. The sediments were deposited via glacial deposition during the late Wisconsin period (10,000-15,000 years ago). This geogenic arsenic contamination was reported in several parts of the upper Midwest (Figure 1.2c) in domestic and monitoring wells (Erickson and Barnes, 2005). Powers et al. (2018) reported that many American Indian communities have more than 10 μg/L of arsenic in their domestic well in North Dakota. More than 26.7% of households in North Dakota are affected by arsenic contamination in their drinking water (Powers et al., 2019).

1.3. Epidemiology of arsenic contamination and health effects

The International Agency for Research on Cancer (IARC) designated arsenic as Group 1 human carcinogen. Excess arsenic in drinking water causes several health problems including skin lesions, respiratory problems, neurological complications, reproductive and developmental effects, and circulatory disorders (Chen et al., 2009; Carlin et al., 2016; Tchounwou et al., 2019). Consumption of water high in arsenic may lead to cancers of the skin and internal organs (liver, kidney, lung, and bladder) (WHO, 2018). Prolonged ingestion of contaminated drinking water causes chronic arsenic toxicity. The major epidemiological sensitive sign and symptoms of arsenic poisoning (arsenicosis) is characteristic skin lesions (dermatological sign) like keratosis, hyperpigmentation, Bowen's disease, and hypopigmentation (Tchounwou et al., 2019). The symptoms appear major (diffuse and spotted melanosis, leucomelanosis, spotted keratosis, diffuse and spotted keratosis on palm, dorsal keratosis, gangrene, multiple squamous carcinoma, Bowen's disease) to a minor extent (Mee's line on the nail, pigmentation on the tongue,

conjunctival congestion, non-pitting oedema) depending upon amount and duration of arsenic exposure and nutritional status of exposed population (Chakraborti et al., 2013). Carcinogenesis or malignancy comes after 10-20 years of arsenic exposure. There is no medical cure available for chronic arsenic toxicity. Only some preventive measures like arsenic-free drinking water and food, healthy nutritional diet are recommended (Chakraborti et al., 2018).

Immediately upon ingestion of arsenic species (arsenate or arsenite in drinking water), they are absorbed in the gastrointestinal tract and transported to the different human organs by blood. Arsenate [(As (V)] species in the bloodstream gets reduced to arsenite [As(III)] before cellular uptake (Cohen et al., 2006). Arsenic is not a required element for human metabolism, so it does not have any specific transport pathways, but it uses the pathways of transporters of analogous essential nutrients and compounds to enter into cells. Such nutrients and compounds include phosphate (phosphate transporterPho), glucose (glucose permeases GLUT), and glycerol (aquaglyceroporins AQP)(Garbinski et al., 2019). Upon cellular absorption, inorganic arsenic undergoes a methylation process where it gets converted to organic arsenic like monomethylarsonic acid (MMA) and dimethylarsinic acid (DMA). Although methylation of arsenic is perceived as a way of reduced toxicity, both MMA and DMA cause cell toxicity, enzymatic inhibition, and genotoxicity in excess amount (Cohen et al., 2006; Tseng, 2009). The arsenic methylation process is affected by glutathione (GSH) and other thiols (-SH) groups containing biomolecule as inorganic arsenic species have a high affinity to the thiol group (Tseng, 2009). Arsenical metabolism in the human body interrupts more than two hundred essential enzymatic pathways (Khairul et al., 2017). The pathway of arsenic-induced carcinogenesis is not fully understood yet, the probable mechanism of carcinogenesis includes but not limited to the factors like oxidative stress, inhibition of DNA repair, disruptive of

transcriptional and translational activities, histone perturbations, change in gene expression, cytotoxicity, and regenerative hyperplasia and genotoxic damage (Zhou and Xi, 2018; Tchounwou et al., 2019).

1.4. Arsenic removal technologies

In the past two decades, various arsenic removal technologies were evaluated both in the field and laboratory (Mondal et al., 2013; Alka et al., 2021). The widely employed techniques for arsenic sequestration from the aqueous phase by physicochemical methods include chemical-aided precipitation, coagulation and flocculation, electrocoagulation, ion exchange, adsorption, and membrane processes. A comprehensive overview of technologies with its advantages, challenges along with the scope of improvement is summarized in Table 1.1. While each technology has its advantages, the efficient and successful implementation of any removal technologies is required to consider water quality (pH, arsenic concentration, the presence of other ions), long-term operational and maintenance options, post-treatment arsenic bearing waste management, governmental regulations, community needs, and socio-economic status of the community. In the following section, different arsenic removal technologies are discussed.

Table 1.1. Some common arsenic removal technologies.

Arsenic removal technology	**Specific approach**	**Process description**	**Advantages**	**Challenges**
Oxidation	This is a pre-required step for adsorption, ion-exchange, precipitative processes, membrane process	Direct aeration, ozonation, application of H_2O_2, MnO_4^-, Cl_2, ClO_2, (FeO_4^{2-}), and UV ray used for Oxidation to converts As(III) to As(V)	• Economical and simple process • Can treat large water volume	• Interfering substances decreases the removal process efficiency • Slow process • Chlorination generate toxic chemicals and carcinogens by-products • Oxidation implemented as added step with other removal technique, it enhances overall the operating cost of the treatment process.
Precipitative Processes	• Coagulation/ Filtration • Iron/Manganese Oxidation • Coagulation Assisted Microfiltration • Enhanced Coagulation • Lime Softening	Destabilization of arsenic ion using coagulants. Coagulants with arsenic start to aggregate and the aggregated mass precipitates and separated.	• Low operating cost • Ease of operation • Coagulants are easily available • Work over a wide pH range	• Sludge contains a concentrated amount of As. • Not so effective for As(III) • A pre-oxidation process need for As(III) • High amount of coagulant needed • Additional separation step needed
Ion Exchange		Exchangeable group of synthetic resin replaced by arsenic oxyanions	• Removal is moderately effective • Removal is independent of pH and influent concentration	• Interferences from competitive anions • Not suitable for As(III) removal and prior oxidation required • Regeneration of resins generate high amount of toxic brine • Suspended solid and other ions causes clogging
Adsorptive Processes	• Activated Alumina • Iron Oxide Coated Sand • Granular Ferric Hydroxide • Iron Filings • Nanomaterial and nanocomposites (Fe, Ce, La, Zr,) Modified clay material	As species are adsorbed either physically or chemically onto the solid surface of adsorbents.	• Economical and commercially available • Ease of application • High removal efficiencies	• Interferences from competitive anions • Regeneration for reuses of the adsorbents • Secondary arsenic release from the spent adsorbent
Membrane Processes	• Microfiltration • Ultrafiltration • Nanofiltration • Reverse Osmosis • Electrodialysis Reversal	Arsenic ions rejected based on pore size of the membrane and surface functionalization	• Technology well established and handy at households. Removes other contaminants also • Produce high-quality water and no solid waste generation	• High capital cost • Energy-intensive • Pretreatment required • Not work efficiently at low concentration • Membrane fouling and scaling Produces highly contaminated brine water.

1.4.1. Chemical-aided oxidation and precipitation

Aqueous arsenic can be present as As(V)/ As(III) but As(III) is more dominant in an anoxic neutral pH groundwater environment. The conventional treatment technologies like adsorption and coagulation-flocculation are more effective in removing anionic As(V) compared to neutral ion As(III)(USEPA, 2003). Pre-oxidation (i.e., before As removal) can significantly improve treatment performance if As is present in the source water as As(III) (i.e., arsenite) (Hering et al., 1997). Although aeration is generally economical, it is not always sufficient, and so, chemical oxidations are adopted as a pretreatment process where As(III) is converted to As(V) for efficient arsenic removal in the conventional treatment processes (Bissen and Frimmel, 2003). The most used and feasible oxidants are chlorine, potassium permanganate, persulfate, manganese dioxide, hydrogen peroxide (in Fenton's reagent and involving Fenton-like reactions), and ozone. Chlorine, permanganate, and ozone are more efficient compared to chloramine (hypochlorite) and hydrogen peroxide (Bissen and Frimmel, 2003). The major constraint of this process is the oxidation of other organic and inorganic compounds and the formation of toxic oxidation byproducts. Photochemical and photocatalytic approaches have also been investigated for As(III) oxidation (Dutta et al., 2005). UV irradiation oxidizes As(III) into As(V) in presence of oxygen, but the process is relatively slow. The addition of photocatalytic agents like iron species (ferric), citrate, and sulfite can augment the UV-aided oxidation process by generating reactive hydroxyl radicals (OH•). The standard photocatalyst material like TiO_2 was also investigated for the oxidation of As(III) (Yoon and Lee, 2005).

1.4.2. Coagulation and flocculation

The most conventional and extensively used method for arsenic removal is coagulation and flocculation (Hering et al., 1997). The coagulation and flocculation process is a standard

process in water treatment to remove total dissolved solids (TDS) using salts or polymeric compounds (USEPA, 2003; Lakshmanan et al., 2008). In this process, arsenic oxyanions react with cationic coagulants (ferric salts and aluminum alum) and become insoluble and get precipitated as heavy flocs(Wickramasinghe et al., 2004). The removal process involves three distinct pathways which include (i) co-precipitation of arsenic with newly generated metal oxyhydroxide, (ii) precipitation as $Al(AsO_4)$ or $Fe(AsO_4)$, and (iii) arsenic adsorption onto the positively charged surface of metal oxyhydroxide through electrostatic attraction. The treatment process involves oxidation flowed by coagulation and flocculation and sedimentation/filtration(Wickramasinghe et al., 2004). The main limitation of this process is the generation of large quantity arsenic-containing sludge which is difficult to manage. Improper handling of arsenic-bearing wastes causes secondary pollution (Mondal et al., 2013).

1.4.3. Electrocoagulation

Electrocoagulation (EC) is an effective technology for arsenic removal for its high removal efficiency. A simple EC reactor includes two metal electrodes, acting as cathode and anode, connected to an external power supply. Iron and aluminum are the most used anode electrode for EC due to their ease of availability, better removal performance, and low cost. (Kobya et al., 2020; Alka et al., 2021; Sandoval et al., 2021). The basic principle of EC is the in-situ generation of metallic coagulants which sequestrate the arsenic from the aqueous phase. After the introduction of the current, the anode generates metal ions and releases them into the aqueous phase. The anode also aids in reduction/oxidation releasing hydrogen ions and oxygen to the aqueous system. In the cathode regime, the water molecules dissociate into OH^- and H^+ ions. The metallic ions are released by the anode reaction with the OH^- and form metal hydroxide complexes. The freshly formed metallic hydroxide reacts with arsenic via electrostatic

attraction, co-precipitation, or complexation (Kumar et al., 2004). The arsenic sorbed metal hydroxide forms micro size flocs which ultimately grow into macro flocs and settled down as sludge. Solution pH which controls the speciation of metal ions (Fe^{2+}/Fe^{3+}, $Al^{3+}/Al^{2+}/Al^{+}$) and dissolved oxygen concentration (that helps in arsenite oxidation) have significant effects on the removal performance of arsenic in the EC system. The method has a certain advantage over the coagulation and flocculation method in terms of low chemical usage, reduction in sludge production, and higher efficiency (Nidheesh and Singh, 2017; Kobya et al., 2020). However, electrocoagulation has some operational issues like passivation of the electrode surface which significantly reduces the performance of the system, frequent replacement needs for the sacrificial electrode, and significant power consumption.

1.4.4. Ion exchange

Ion exchange is standard treatment technology for removing toxic contaminants and is very effective for arsenic removal. As arsenic is present in oxoanionic form, anionic resins are used for arsenic removal. Ion exchange resins are made of a polymeric backbone attached with charged functional groups with a covalent bond (Kim, 2001). Positively charged basic resin-saturated anions (like chloride) are used for the removal of anions like arsenic. The exchange preference of anions of strongly basic anion exchange resins follows(USEPA, 2003):

$CrO_4^{2-}>SeO_4^{2-}>SO_4^{2-}>HSO_4^{-}>NO_3^{-}>Br^{-}>HAsO_4^{2-}>SeO_3^{2-}>HSO_3^{3-}>NO_2^{-}>Cl^{-}$

Among the two dominant species of arsenic, arsenite presents as a neutral anion in a solution pH up to 9 and does not take part in the exchange process. Therefore, for optimal removal performance, the ion exchange process typically includes an oxidation step as a pretreatment to convert As(III) to As(V) (Kim, 2001). Arsenic removing resins are saturated with chloride ions by flushing the ion exchange bed with HCl acid. When arsenate, As(V), containing

water is passed through the bed, it easily replaces the Cl^- as arsenate is a stronger anion. The treated water by the ion-exchange process contains a substantial amount of chloride which requires secondary treatment to improve water quality. Naturally, present anions sulfate, nitrate, bromate, and phosphate can cause significant interferences in the arsenic exchange process. The ion exchange resins are regenerated with a concentrated NaCl solution, and the brine solution contains a very high amount of arsenic which needs safe handling and further treatment before disposal (Dominguez-Ramos et al., 2014). The need for special handling of the arsenic enriched brine is one of the major disadvantages of the ion exchange process (Sarkar and Paul, 2016).

1.4.5. Membrane processes

Arsenic removal using membrane processes presents a promising treatment option for water. The advantages of the membrane process over other technologies include reduced arsenic concentration well below the MCL (10 µg/L) in a very short time and improved finished water quality because of removal of other drinking water contaminants (bacteria, salts, and other heavy metals). Most importantly, membrane processes typically do not involve the use of any chemicals(Shih, 2005; Mondal et al., 2013; Mohanty, 2017). Different membrane technologies have been used for the removal of arsenic from water, and they are microfiltration (MF), ultrafiltration (UF), nanofiltration (NF), reverse osmosis (RO), and electrodialysis (Shih, 2005; Mondal et al., 2013). Arsenic removal through membrane technologies is a physical separation process where the separation depends on the membrane pore size. Solution chemistry (pH, and the presence of other anions) does not have any significant effects on arsenic removal performance. The MF and UF are low-pressure membranes that are not much effective for arsenic removal as the membrane pore sizes are not small enough to exclude the arsenic ions. To make it effective some particle size enhancing methods are coupled with membrane processes.

Coagulation-flocculation (Ghurye et al., 2004; Ahmad et al., 2020), and the addition of polymeric surfactant micelles (Gecol et al., 2004; Chen et al., 2020b) which sequester the arsenic in particulate form can increase the effective size of arsenic and can be subsequently removed by MF and UF. High-pressure NF and RO membranes effectively reduce arsenic concentration with their small pore size (Waypa et al., 1997; Chen et al., 2020a; Siddique et al., 2020). Although size-exclusion is the main reason for arsenic removal by NF and RO, charged RO/NF membrane showed some enhanced removal of As(V) (Brandhuber and Amy, 2001). The major disadvantages of membrane technology are the very low (10-20%) recovery rate (i.e., the amount of arsenic-free water that comes out of the membrane unit relative to the influent) which limits its application The generation of arsenic concentrated high volume of retentate is another major problem. Further, the high cost of membranes, significant energy consumption due to high operational pressure, and membrane fouling by organics also pose significant challenges.

1.4.6. Adsorption

Adsorption is an efficient and popular arsenic removal technique that is economically viable, easy to implement, and less chemical and energy-intensive (USEPA, 2003). Adsorption is a physicochemical process where the aqueous contaminant arsenic (adsorbate) is retained by the adsorbent material by either the physical or chemical adsorption process. Physical adsorption occurs due to Van der Waal forces and is reversible whereas chemosorption occurs due to chemical reaction and is irreversible. The efficiency of the arsenic adsorption process depends on adsorbent surface properties, contact time, solution pH, arsenic concentration in the feed water, temperature, presence of interfering ions, and compounds like phosphate, silicate, bicarbonate, sulphate, nitrate, and dissolved organic matters (Mohan and Pittman, 2007; Sarkar and Paul, 2016). Activated alumina (AA), iron-based sorbents, modified activated carbon, clay

minerals are the most conventional adsorbents used for arsenic removal (Mohan and Pittman, 2007; Giles et al., 2011).

Activated alumina (Al_2O_3) is promoted as one of the best available materials for arsenic adsorption. The removal process is dependent on solution pH (optimum pH 5.5-6). Arsenic removal by AA is electrostatic interaction followed by chemisorption. Due to its neutral nature at pH <9, As(III) shows very poor adsorption by AA, and so, pre-oxidation of As(III) to As(V) and adjustment of water pH are required in AA-based arsenic treatment. The adsorption rate is relatively slow in the AA-based system which leads to a significantly longer contact time (empty bed contact time ~310 min) (USEPA, 2003). Modified AA (a mixture of Al and other metal oxides) can overcome the drawbacks in AA-based adsorbent and an increased adsorption capacity can be achieved as in alum-impregnated activated alumina (Tripathy and Raichur, 2008). Such mixtures also offer greater operational flexibility over a wide range of pH (4-8) in CaO-AA, ZnO-AA, and aerogel-AA (Camacho et al., 2015) and easier oxidation of As(III) to As(V) (by Mn modified AA) (Kunzru and Chaudhuri, 2005).

Iron-based adsorption is the most popular and successfully implemented adsorption technology for arsenic removal. Iron has a greater affinity for arsenic (compared to AA), wide working pH, and rapid reaction kinetics. The commonly used iron oxide for arsenic removal is ferrihydrite ($Fe_{10}O_{14}(OH)_2$), goethite (α-FeOOH), akageneite (β-FeOOH), magnetite (Fe_3O_4), hematite (Fe_2O_3), and hydrous ferric oxide (Giles et al., 2011). Iron-oxide/hydroxide makes a strong inner-sphere complex with both the arsenic species and makes stable complexes. Iron-coated sand showed effective removal of arsenic (Joshi and Chaudhuri, 1996). Metallic iron (Fe^0) (zero-valent iron, ZVI) showed efficient arsenic removal (Nikolaidis et al., 2003; Lien and Wilkin, 2005). In the aqueous phase, ZVI generates corrosion product of fresh iron

oxyhydroxide and dissolves Fe^{2+}, and arsenic binds to the oxides and hydroxides through surface complexation and electrostatic attraction. During the surface corrosion process, the ZVI system generates a free radical that oxidize As(III) to As(V) and reduces the need for any additional oxidation. The ZVI-based system work in wide operational pH (2-9) (Sun et al., 2006). In general, the performance of iron-based filter media is significantly decreased by the presence of phosphate and silicate in the water. The filter performance also decreases if there is a large amount of dissolved iron present in the feedwater which creates iron floc that clogged the filter bed (Giles et al., 2011). More details about iron-based adsorbents are discussed in the subsequent section.

Activated carbon (AC) is also used to treat arsenic contaminated water. The effectiveness of AC depends on surface modification and the chemical composition of the material. Iron oxide-modified Zirconium loaded AC, iron salt-treated AC, iron-containing mesoporous carbon, activated carbon from agricultural by-products have been used for aqueous arsenic removal (Mohan and Pittman, 2007; Gu et al., 2005).

1.5. Arsenic removal by nano adsorbents

While conventional adsorbents showed efficient arsenic removal, there are limitations in their application (Nicomel et al., 2016). One of the major challenges faced for conventional adsorbents is low adsorption capacities that lead to a shorter life of the media or the need for a large amount of the adsorbents to achieve a longer working life (Habuda-Stanic and Nujic, 2015; Lata and Samadder, 2016). The current adsorbents also have slow adsorption kinetics and so a higher contact time is needed to achieve the desired removal leading to a large bed volume (Ray and Shipley, 2015). To overcome these challenges, nano-based adsorbents have been proposed for arsenic removal. Nanomaterials have a high specific surface area (i.e., more reactive site for

arsenic adsorption), better reactivity, and small diffusion resistance (i.e., rapid kinetics) making them superior adsorbents (Lata and Samadder, 2016; Wong et al., 2017).

Nanoscale iron oxide/hydroxide (nanoscale zerovalent iron, magnetite, goethite, ferrihydrite), manganese oxide, zirconium oxide, cerium oxide, nano alumina, copper oxide nanomaterials, titanium dioxide, nano zinc oxide, and metal-doped nanoparticles (iron-doped γ-MnO_2, Cu doped iron oxide, Fe-Ce oxide and other) are so far used or arsenic removal. (Habuda-Stanic and Nujic, 2015; Ray and Shipley, 2015; Lata and Samadder, 2016; Siddiqui et al., 2019).

1.5.1. Arsenic removal by Fe-based nano adsorbents

Iron nanoparticles are most widely studied for arsenic remediation because of iron's high affinity for arsenic (Siddiqui and Chaudhry, 2017). Iron is the fourth abundant element in the earth's crust, and it is environmentally benign (i.e., non-toxic). Iron has two dominant oxidation states: Fe^{2+} and Fe^{3+} and has various oxide forms. The major iron oxide/oxy-hydroxide nanoparticles used for arsenic removal are magnetite (Fe_3O_4), hematite (α-Fe_2O_3), maghemite (γ-Fe_2O_3), goethite (α-FeO(OH)), akaganeite (β-FeOOH), lepidocrocite (γ-FeOOH), ferrihydrite ($Fe_2O_3.0.5H_2O$) hydrated iron(III) oxide (Kanel et al., 2006; Guo et al., 2013; Ray and Shipley, 2015; Siddiqui and Chaudhry, 2017; Hao et al., 2018). A summary of Fe-based nano adsorbent is given in Table 1.2.

Nano magnetite (Fe_3O_4) recorded excellent adsorption capacity for both the arsenic species compared to its bulk counterpart due to its increased specific surface area (Shipley et al., 2009; Feng et al., 2012a). Mayo et al., (2007) reported that decreasing the particle size of magnetite from 20 nm to 12 nm enhanced the removal performance by 200 times. The adsorption capacity increased with decreasing size due to higher specific surface area and more exposed adsorption sites. Bujnakova et al. (2013) synthesized nano magnetite (20-40 nm) via ball milling

process from micron size magnetite (100 μm) to increase the specific surface area from 0.1 m^2/g to 11.9 m^2/g and surface sorption site density from 2.2 to 8.4 sites/nm. The arsenic adsorption capacity (3.65 mg/g) was enhanced by 96% in the nano magnetite compared to the bulk magnetite. Surface functionalization of magnetite with capping agent (ascorbic acid) reduces surface agglomeration of nano-magnetite and gets to better adsorption performances of 46.06 mg/g for As(III) and 16.56 mg/g for As(V). Both electrostatic attraction and surface complexation participated in the arsenic removal by the nano magnetite (Yavuz et al., 2010). As(V) adsorption onto magnetite is dependent on solution pH and point-of-zero-charge of the nanoparticles (Shipley et al., 2009; Chowdhury et al., 2011). With increasing pH (above PZC) the adsorption performance of arsenate decreased, the adsorption of arsenite was not affected. Arsenic adsorbed on the iron oxides can form various surface complexation like monodentate mononuclear corner-sharing, bidentate mononuclear edge-sharing, bidentate binuclear corner-sharing, and tridentate hexanuclear corner-sharing (Guo et al., 2013; Wang et al., 2014b). While Jönsson and Sherman (2008) reported bidentate binuclear corner-sharing complexation onto (100) surface of magnetite for both the arsenic species, Morin et al. (2009) reported tridentate hexanuclear corner-sharing complexation onto (111) surface of magnetite for As(III). Liu et al. (2015) reported the predominant formation of bidentate binuclear corner-sharing complexes for As(V) and tridentate hexanuclear corner-sharing complexes for As(III). They proposed a mechanistic model for As(III) oxidation to As(V) and As(V) reduction to As(III) on the magnetite surface (Liu et al., 2015). In addition to surface complexation, a considerable amount of arsenic precipitated as amorphous iron oxide-arsenic complexes on the magnetite surface.

Nanoscale zero-valent iron (NZVI) has been studied for decades for environmental applications due to its excellent contaminant removal capabilities. NZVI works better than bulk

ZVI for arsenic removal due to its small particle size, large specific surface area, and highly reactive nature. Due to surface corrosion, the NZVI particles surface produce various ferrous iron (Fe^{2+}), iron oxide/iron oxyhydroxide, lepidocrocite (γ-FeOOH), magnetite (Fe3O4), and maghemite (α-Fe2O3). During this surface corrosion reaction in the presence of dissolved oxygen, NZVI produces oxygen radicals ($O_2^{\bullet}$) and H_2O_2. The H_2O_2 reacts with Fe^{2+} ions and form hydroxyl radicals (OH•) which is a strong oxidizing agent. This OH• plays an important role in the oxidation of As(III) to As(V) and in enhancing arsenic removal performance. Kanel et al. (2005) demonstrated rapid and effective removal (~100%) of As(III) within 30 min) (Kanel et al., 2005) and ~100% removal of As(V) within 10 min (Kanel et al., 2006). They also investigated the arsenic removal mechanisms of NZVI and speculated that As(III) may be adsorbed either onto the corrosion products of NZVI through inner-sphere complexation or oxidized to As(V) and adsorbed on the corroded surface of NZVI via electrostatic attraction and inner-sphere complexation.

Ramos et al. (2009) confirmed that both reductive and oxidative mechanisms take place during NZVI application and elucidated the mechanism of arsenic immobilization by NZVI. They recorded the formation of As(0) on the NZVI surface after reaction with As(III) and As(V) using high-resolution X-ray photoelectronic spectroscopy (HR-XPS). NZVI was able to transform AS(III) into As(O), As(V), and As(III). These results confirmed simultaneous oxidation and reduction of arsenic by NZVI. This phenomenon was explained based on the core-shell structure of NZVI, the metallic core and thin layer of amorphous iron (oxy)hydroxide facilitated the oxidation and reduction reactions. In an anoxic environment, As(III) was adsorbed and transformed on the NZVI surface in two steps: in the first step upon adsorption, the As-O bond break at the surface of NZVI, and in the second step, arsenic further reduced and diffused

across the thin oxide layer resulting in an As-Fe intermetallic compound at the interface of core and shell of NZVI (Yan et al., 2012a) The oxidation of As(III) is facile and reversible reaction whereas reduction of As(III) is a relatively slower process (Yan et al., 2012b). Ling and Zhang (2014) have also confirmed this unique mechanism of As(V) immobilization. First, As(V) is adsorbed onto the surface via electrostatic interactions and surface reaction, and then adsorbed arsenic reduced to As(III) and start to migrate towards metallic core through amorphous oxide shell and form a layer (1.0−1.2 nm) of elemental metal-arsenic complex via chemical reduction in the interface of core and shell. These results suggest that the arsenic removal mechanism of NZVI is significantly different from conventional iron-based adsorbents. NZVI is potentially a more capacious and robust sequestration agent for arsenic abatement.

1.5.2. Other metal oxide nanomaterial

A wide variety of metal oxide (Al_2O_3, MnO_2, ZnO, TiO_2, ZrO_2, and CeO_2) and bimetallic oxide (Fe-Mn, Zr-Ce, Cu-Fe, Fe-Al) nanoparticles are reported for effective removal for arsenic. A summary of the removal performance of these nanomaterials is given in Table 1.2.

While nanomaterials have proved to be efficient adsorbents and showed high adsorption capacity, rapid kinetics, and higher reactivity towards arsenic, but they have certain limitations which are technical (agglomeration of nanoparticles, separation, and regeneration) and economical (scale-up of nanomaterial production and high synthesis cost). Nanomaterials are prone to agglomerate in aqueous media which leads to loss of their effective reactivity surface area. The majority of nanomaterials are synthesized by sol-gel or hydrothermal processes and very fine powdery materials are formed. These fine nano powders are not suitable for fixed-bed filter fabrication due to their low hydraulic conductivity. Further, the movement of nanoparticles in filter bed may lead to leaching of nanomaterials into the finished water and that is a public

health concern (Mauter et al., 2018). To address this challenge researchers have embedded the nanoparticles onto the secondary less mobile structures like activated carbon, zeolite, sand, clay, polymeric gel, and membrane (Table 1.3) (Borovik et al., 2020). Attaching nanoparticles in a bigger size substrate (supporting material) may also help to reduce the agglomeration of the particles in the aqueous phase while curtailing the leaching of nanoparticles from the filter bed.

Table 1.2. Summary of metal-metal oxide nanomaterial used in arsenic removal.

Adsorbent	**Experimental Conditions**				**Adsorption capacity (mg/g) or % removal**		**Source**
	CR (mg/L)	**pH**	**CT (min)**	**AD (g/L)**	**As(III)**	**As(V)**	
Iron/Iron oxide							
NZVI	1	7	10-60	1	96%	100%	(Kanel et al., 2006)
Akaganeite nanoparticle	5-100	7.5	1440	0.5		100-120	(Deliyanni et al., 2003)
γ-Fe_2O_3 NPs	10-200	3-6	90	1.6	74.83	105.25	(Lin et al., 2012)
Fe_3O_4	1-100		90	8		3.65	(Bujnakova et al., 2013)
Fe_3O_4	0-70	5	1440	0.1	16.56	46.06	(Feng et al., 2012a)
Ferrihydrite nanoparticles	10-125	5	1440	1	87.43	42.39	(Qi and Pichler, 2016)
Goethite nanoparticles	5-100	3	240	1	---	76	(Ghosh et al., 2012)
TiO_2							
Titanium dioxide	5-90	2	1440	4	19.88	20.53	(Nabi et al., 2009)
Hydrous titanium dioxide	0-140	7	1440	0.5	83		(Xu et al., 2010)
TiO_2 nanoparticles	0.2-50	7	1440	0.2	11.52	5.92	(Jegadeesan et al., 2010)
Al_2O_3							
γ-Al_2O_3	--	3-6	360	0.2	---	25	(Patra et al., 2012)
Nano-alumina powder	10-20	7.5	30	1	40		(Darban et al., 2013)
γ-Al_2O_3 nanoparticles	0.3	6.8	120	0.5	0.76	1	(Ghosh et al., 2019)
ZrO_2							
Ze-oxide nano	0-70	7	1440	0.1	83	32.4	(Cui et al., 2012)
zirconia nanoparticle		8-9	2840	0.5	135		(Zheng et al., 2012)
Ceria							
Hydrous cerium oxide NPs	1-100	7	1440	0.1	170	107	(Li et al., 2012)
ceria nanoparticles	0.004-0.04	3-11	60	5		17.08	(Feng et al., 2012b)
MnO_2							
α-MnO_2 nanofibers	10-270	6	360	0.5	117	60	(Luo et al., 2018)
Hydrous manganese dioxide	1-50	3	60	0.1	29	--	(Liu et al., 2020)
Cuo nanoparticles	0.1-100	8	30	2	26.9	22.6	(Martinson and Reddy, 2009)
Bi or mixed metallic nanomaterials							
Mn-Fe oxide adsorbents	5-300	7	1440	2	132	77	(Ocinski et al., 2016)
Cu doped Fe_2O_3	1-50	7	720	0.2	38	43	(Sun et al., 2017)
Fe-Cu-Mn tri-metal oxide	0-40	7	1440	0.2	85	113	(Zhang et al., 2020)
Fe-Zr oxide	5-40	7	2160	0.2	120	46.1	(Ren et al., 2011)
Fe-Al mixed oxide NPs	10-250	7	60	2	58	--	(Basu and Ghosh, 2011)
Ceria/manganese	5-50	7	60	1		18.65	(Gupta et al., 2011)
CeO_2-ZrO_2	0.5-60	6.9	1440	0.2	116.8	40.7	(Xu et al., 2013)
Fe-Ce oxide	10-250	7	60	2	86.29	55.51	(Basu et al., 2013)
Ni doped Fe_2O_4 NPs	1-1000	7	1440	0.5	169	90	(Liu et al., 2015)
Ti-Mn oxide	2-60	7	1440	0.2	107	87	(Zhang et al., 2018)

*CR: Concentration range; $^{+}$CT: Contact time; $^{\#}$AD: Adsorbent dose

Table 1.3. Metal-metal oxide nanomaterials deposited on support media and used for aqueous arsenic removal.

Adsorbent	Experimental Conditions				Adsorption capacity (mg/g) or % removal		Source
	CR* (mg/L)	pH	CT+ (min)	AD# (g/L)	As(III)	As(V)	
Carbonaceous support							
NZVI-Starbon nano composite	0.6-73.5µM	7	240	0.05	27		(Baikousi et al., 2015)
Fuller's earth immobilized NZVI	20-100	7	1440	1	50.08	45.5	(Yadav et al., 2016)
NZVI-biochar	0-400	4.1	2400	2		124.5	(Wang et al., 2017)
γ-Fe_2O_3 biochar	5-200		1440	2		3.14	(Zhang et al., 2013)
Activated carbons modified with iron-hydro (oxide)nanoparticles	0.025-1.5	6	1440	0.75		1.25	(Vitela-Rodriguez and Rangel-Mendez, 2013)
Activated carbon fiber (ACF) modified with zirconium	1-120	3	1440	0.5	21.7		(Zhao et al., 2016)
Ce-Mn activated carbon	0-100	5	1440	0.5		108.8	(Liang et al., 2020)
δ-MnO2 modified activated carbon	3-20	4	1440	1	13.30	12.56	(Wang et al., 2020)
Polymer loaded nanomaterial							
Polystyrene nano-Fe_3O_4	1-50	6	1440	0.5		139.3	(Jiang et al., 2012)
Ca-alginate loaded NZVI		7					(Bezbaruah et al., 2013)
GO-MnO_2-Goe-Ca-Alg beads	0.1-100	--	--	5	28.53	34.17	(Basu et al., 2021)
Clay supported nanomaterial							
Montmorillonite-supported NZVI	2-345	7	240	1.3	59.9	45.5	(Bhowmick et al., 2014)
nZVI-Pumice/Zeolite	25-250	--	1440	2	24.96		(Ranjan et al., 2020)
Fe-Mn oxides loaded on zeolite		7	1440	5	296.23	201.10	(Kong et al., 2014)

*CR: Concentration range; +CT: Contact time; #AD: Adsorbent dose

1.5.3. Arsenic removal by graphene oxide-based materials

1.5.3.1. Fundamentals of GO-nanohybrids

Graphene is a honeycomb-like carbon lattice with Sp^2 hybridization. It has been classified based on chemical surface, morphology, and physicochemical property. Graphene derivatives such as graphene oxide (GO), reduced graphene oxide (RGO), surface-functionalized graphene layer, and hybridized with other nanomaterials are reported (Georgakilas et al., 2012; Perreault et al., 2015). The surface functionalization of the graphene layer tunes the intrinsic properties and for various graphene-based micro/nanostructure. While the pristine graphene has

very limited applications in environmental remediation, the development of new derivatives introducing additional functional groups/materials is the main strategy for developing graphene-based material for environmental contaminant removal (Lu et al., 2009; Perreault et al., 2015). The major challenge with graphene-based materials is their production on a large scale while maintaining the unique properties of the surface layer (Neri et al., 2015). GO is a sheet-like 2 D functionalized carbon layer with a high specific surface area with aqueous stability. GO has a hydrophobic surface with a large acidic group, high charge density, surface hydrophobic π-π interaction. These unique properties of the GO make it an ideal substrate for the growing and anchoring of functional nanomaterials (Lu et al., 2009). Graphene oxide hybrids with metals/metal oxides are an emerging class of nanomaterials with applications in areas from electronics to environmental contaminant removal (Georgakilas et al., 2012; Lingamdinne et al., 2019b). The GO-based nanohybrids are developed by growing nanocrystal on the surface of GO. While both graphene and GO have a high specific surface area, GO works better than its pristine peer (graphene) because GO has more functional groups and defects present. GO provides a large number of reactive anchoring sites for nucleation and growth of nanocrystals because of the high density -COOH, -OH, C=O groups present (Liang et al., 2010; Wang et al., 2010). The GO surface interacts with the metal ions through electrostatic interaction. A robust chemical and mechanical coupling can be achieved between GO and nanocrystal through controlled nucleation, optimal chemical interaction, and bonding between the GO and the nanocrystal (Liang et al., 2010; Wang et al., 2010). Nanocrystals grown on graphene oxide surfaces have shown enhanced electron transport rate, high electrolyte contact area, and structural stability, all of which could be useful for various applications (Liang et al., 2010).

1.5.3.2. Graphene oxide metal/metal oxide nanohybrids for arsenic removal

To address the problem of agglomeration and improve its applicability in filter beds, GO-based nanohybrids have been developed where nanoparticles are deposited on the surface of micron-sized graphene oxide (GO). The nanomaterials synthesized on the GO layer are well dispersed and have been used for aqueous arsenic removal (Table 1.4). Chandra et al., (2010) chemically deposited magnetite on GO. The nanohybrid showed superparamagnetic properties and high binding capacity for both As(III) (10.2-13.1 mg/g) and As(V) (5.27-5.83 mg/g). The optimum arsenic removal was observed at 30 ℃ with an increasing trend from 10 to 30 ^{o}C and then decreased from 30to 50 ℃. While Chandra et al. (2010) was among the first to report the use of GO-supported Fe_3O_4 for arsenic removal, additional works have been reported by others which include GO supported iron oxide nanoparticles (Yoon et al., 2017; Yu et al., 2019), nanoceria (Sakthivel et al., 2017b), nano zirconia (Luo et al., 2013), nano lanthanum oxide (Lingamdinne et al., 2019a), and iron-manganese oxide (La et al., 2017). GO-supported NZVI was also used for arsenic removal (Wang et al., 2014a) which showed effective removal for both As(III) and As(V).

Iron content in GO-Fe nanohybrid plays an important role in determining arsenic adsorption performance. Yoon et al., (2016) evaluated arsenic removal performance of magnetite deposited onto GO (MGO) and RGO (M- RGO). The degree of GO layer oxidation and density of functional groups controlled the number of nanomaterials deposited onto the GO/RGO surface (Yoon et al., 2016; Yoon et al., 2017). The MGO recorded better arsenic removal for both the arsenic species (As (III)/As(V)) than M-RGO due to the presence of a higher number of magnetite particles. GO supported binary Fe-Mn oxide was explored for arsenic removal (Benjwal et al., 2015; Zhu et al., 2015). Zhu et al., (20015) observed MnO_2 on the nanohybrids

helped in the oxidation of As(III) to As(V) with Fe(III) oxide being crucial for As(V) removal. The dispersion of $FeMnO_X$ on the GO surface reduced the agglomeration of the nanomaterial. The removal was controlled by both surface complexation and electrostatic attraction, and phosphate ions show Astron interference in the removal process. Benjwal et al., (2015) reported the use of binary (rGO–TiO_2/rGO–Fe_3O_4) and ternary (rGO–Fe_3O_4–TiO_2) materials for arsenic decontamination. The rGO–Fe_3O_4–TiO_2 recorded 147 mg/g As(III) adsorption which is far better than other rGO- Fe_3O_4.

Luo et al., (2013) reported that GO-$ZrO(OH)_2$ could remove both As(III) and As(V) simultaneously with an adsorption capacity of 95.15 mg/g for As(III) and 84.89 mg/g for As(V). The performance of the nanohybrid was 3.5-4.6 times better than bare $ZrO(OH)_2$ nanoparticles. Arsenic removal by the nanohybrid was not much affected by the presence of interfering ions except phosphate. Lingamdinne et al. (2019a) developed a GO lanthanum fluoride (GO-LaF) nanohybrid which recorded 18.52 mg/g As(V) removal. Ion exchange, electrostatic interaction, and surface complexation are the major mechanisms involved in arsenic removal by GO-LaF. The solution (water) pH played an important role in arsenic removal. At low pH, electrostatic interactions were predominant where surface complexation and ion exchange were predominant at pH≥7.

Efficient arsenic removal by GO-CeO_2 was reported by Sakthivel et al., (2017). GO-CeO_2 was prepared in a one-pot hydrothermal process, and it effectively removed both As(III) (185 mg/g) and As(V) (212 mg/g). The adsorption of arsenic onto nanohybrid surfaces was highly dependent on the Ce^{3+} ion concentration. The arsenic ions first adsorbed onto the nanohybrid surface through electrostatic interaction and then made a stable complex with Ce^{3+} present on the surface. The removal performance was not much affected by the change in

solution pH (3-10) and temperature (10-40 ℃). Yu et al. (2015) used hydrous cerium oxide-modified graphene nanoplates for As(V) removal. The removal performance decreased from 60 to 20 % for an initial As(V) concentration of 10 mg/L as pH increased from 3 to 10 and the max adsorption capacity (62.33 mg/g) was recorded at pH 4. The surface-bound -OH group of hydrous cerium oxide played an important role in arsenic removal through electrostatic interaction (Yu et al., 2015).

Table 1.4. Graphene oxide-based metal oxide nanohybrids for aqueous arsenic removal.

Adsorbent	Experimental Conditions			Adsorption capacity (mg/g)		Source
	CR* (mg/L)	pH+	AD# (g/L)	As(III)	As(V)	
Magnetite-rGO[i]	3-7	7	0.2	13.10	5.83	(Chandra et al., 2010)
Magnetic-GO	0-35	6.5	0.4		59.6	(Sheng et al., 2012)
NZVI-Reduced GO	1-15	7	0.4	35.83	29.04	(Wang et al., 2014a)
Fe_3O_4-GO	0-550	7	0.1	85	38	(Yoon et al., 2016)
Fe_3O_4-non-oxidative GO	0-550	7	0.1	38	14	(Yoon et al., 2017)
GO-Fe_2O_3	0.1-1200	7	0.8	147	113	(Su et al., 2017)
Fe_2O_3 nanocubes-GO aerogel	5-70	5	0.5	172.27	217.34	(Yu et al., 2019)
CeO_2-GO	0.1-200		0.5	185	212	(Sakthivel et al., 2017a)
Mg-Al hydroxide/GO	0.1-150	5	0.5	----	180.26	(Wen et al., 2013)
rGO-Fe_3O_4-TiO_2	3-10	7	0.2	147.05	---	(Benjwal et al., 2015)
GO–$ZrO(OH)_2$	2-80	7	0.5	95.15	84.89	(Luo et al., 2013)
β-FeOOH@GO-COOH	1-200	6.5	1	77.5	45.7	(Chen et al., 2015)
GO-$MnFe_2O_4$	10-50	1-2	0.2	----	240.3	(Huong et al., 2016)
$FeMnO_x$/RGO	0.2-7		0.2	47.05	49.01	(Zhu et al., 2015)
Magnetic 3D GO hydrogel	0-150	~7	1	25.1	74.2	(Liang et al., 2019)
GNP/Fe−Mg oxide	5-90	7	0.2	---	103.9	(La et al., 2017)
GO-$CuFe_2O_4$ foam	5-500	7.2	8 l	51.64	124.69	(Wu et al., 2018)
Fe_3O_4@CuO-GO	3.75-75	7	0.3	70.36	62.60	(Wu et al., 2019)
GO-lanthanum fluoride	2-30	---	0.8	---	18.52	(Lingamdinne et al., 2019a)

*CR: Concentration range; +CT: Contact time; #AD: Adsorbent dose

1.6. Scope of this research

Arsenic contamination in drinking water is a major public health concern. It affects both rural and urban populations by restricting access to safe drinking water. Decades of research have explored processes involving membranes to adsorption to treat arsenic. Literature survey demonstrates adsorption technology outstand other treatment options due to its efficient removal of arsenic, ease of implementation, and economic viability. An ideal adsorbent should have high

adsorption capacity, an affinity for both the inorganic arsenic species, As(III) and As(V), and should be effective under relevant environmental conditions. Iron (Fe)-based adsorbents have been promoted for aqueous arsenic adsorption because of their benign nature (i.e., no known toxicity), potential cost-effectiveness, and expected ease of scale-up in production. However, their field application is, so far, limited because of their low Fe use efficiency (i.e., not all available Fe is used), slow adsorption kinetics, and low adsorption capacity. Nanomaterials, mostly nano magnetite (M) and nanoscale zero-valent iron (NZVI) are effective for arsenic removal because of their very high specific surface area and good adsorption capacity. However, these particles agglomerate easily and NZVI gets oxidized rapidly. To address these problems, graphene oxide-iron nanohybrids were synthesized and evaluated for arsenic removal (See section 1.5.3). While each reported work had high process efficiency with >99% arsenic removal, they cannot be compared one-on-one given the non-identical experimental conditions. Each researcher team used different initial arsenic concentrations, solution pH, and adsorbent dose. The reported GO-iron nanohybrids (Table 1.4) have shown limited arsenic removal capacity (6-180 mg/g) and that would limit the potential life span of the arsenic removal systems where these nanohybrids would be used. So, there is a need to optimize such nanohybrids for the most efficient arsenic removal, and to achieve that a better understanding of the mechanisms involved in arsenic removal would be needed. While attempts have been made to understand the sorption behavior of arsenic on the nanohybrid system, information regarding the desorption/release of arsenic from the nanohybrids is lacking. Secondary desorption of arsenic from the nanohybrids under relevant environmental conditions over a longer time frame is needed. The current research has attempted to address the existing gaps in research.

This work was started with two major iron-based nanomaterials reported for arsenic removal studies viz., magnetite and nanoscale zerovalent iron. Both the materials were also synthesized on the surface of GO and a comparative study under identical experimental conditions was conducted to identify the most suitable candidate for field applications. After identifying the most suitable candidate material, the arsenic removal mechanisms were investigated and the role of graphene oxide in the removal process was explored. The desorption of the adsorbed arsenic from the nanohybrids was later studied.

1.7. Research objectives

The objectives of this research are to:

a) design and synthesis of GO-iron nanohybrids and evaluate their arsenic removal potential,
b) investigate the arsenic removal mechanisms and performance of the nanohybrids under different environmental conditions.
c) evaluate the stability of adsorbed arsenic in the GO-iron nanohybrids.

1.8. Dissertation organization

There are five (5) chapters in this dissertation. Chapter 1 is the overview of the global and national arsenic problem, the health impact of arsenic, and currently available materials and methods for arsenic removal. The chapter also includes the scope of this research and the research objectives. Chapter 2 to Chapter 4 are presented in a journal paper format. Chapter 2 has been published as a peer-reviewed research article in *Science of the Total Environment* in 2021 and investigates the suitability and practical application of various graphene oxide iron nanohybrids to its bare courter part (iron nanoparticles only). Chapter 3 is a published peer-reviewed research article in *Chemosphere* (2020) that reports ultra-high arsenic adsorbing

graphene oxide iron nanohybrids. This chapter investigates in detail the mechanism of arsenic removal onto nanohybrid and its practical application. Chapter 4 is a manuscript under preparation to be submitted to *Environmental Science: Nano*. Chapter 4 explores the desorption behavior and stability of adsorbed arsenic on high adsorbing adsorbent over a long period (two years) and its environmental implication. For Chapters 2 through 4, each has an introduction, materials and methods, results and discussions, and a conclusion. Chapter 3 Finally, Chapter 5 presents the conclusions and the scope for future works. References are cited in each chapter. Some additional materials are presented as appendices.

1.9. References

Food and Drug Administration (FDA), 2016. Arsenic in rice and rice products risk assessment report.

Ahmad, A., Rutten, S., de Waal, L., Vollaard, P., van Genuchten, C., Bruning, H., Cornelissen, E., van der Wal, A., 2020. Mechanisms of arsenate removal and membrane fouling in ferric based coprecipitation-low pressure membrane filtration systems. Separation and Purification Technology 241.

Alka, S., Shahir, S., Ibrahim, N., Ndejiko, M.J., Vo, D.V.N., Abd Manan, F., 2021. Arsenic removal technologies and future trends: A mini review. Journal of Cleaner Production 278.

Amini, M., Abbaspour, K.C., Berg, M., Winkel, L., Hug, S.J., Hoehn, E., Yang, H., Johnson, C.A., 2008a. Statistical modeling of global geogenic arsenic contamination in groundwater. Environmental Science & Technology 42, 3669-3675.

Amini, M., Abbaspour, K.C., Berg, M., Winkel, L., Hug, S.J., Hoehn, E., Yang, H., Johnson, C.A., 2008b. Statistical modeling of global geogenic arsenic contamination in groundwater. Environmental Science & Technology 42, 3669-3675.

ATSDR, 2007. Toxicological profile for arsenic. Agency for Toxic Substances and Disease Registry, Division of Toxicology, Atlanta, GA.

Ayotte, J.D., Medalie, L., Qi, S.L., Backer, L.C., Nolan, B.T., 2017. Estimating the High-Arsenic Domestic-Well Population in the Conterminous United States. Environmental Science & Technology 51, 12443-12454.

Baikousi, M., Georgiou, Y., Daikopoulos, C., Bourlinos, A.B., Filip, J., Zboril, R., Deligiannakis, Y., Karakassides, M.A., 2015. Synthesis and characterization of robust

zero valent iron/mesoporous carbon composites and their applications in arsenic removal. Carbon 93, 636-647.

Basu, H., Singh, S., Venkatesh, M., Pimple, M.V., Singhal, R.K., 2021. Graphene oxide-MnO_2-goethite microsphere impregnated alginate: A novel hybrid nanosorbent for As (III) and As (V) removal from groundwater. Journal of Water Process Engineering 42, 102129.

Basu, T., Ghosh, U.C., 2011. Arsenic(III) removal performances in the absence/presence of groundwater occurring ions of agglomerated Fe(III)-Al(III) mixed oxide nanoparticles. Journal of Industrial and Engineering Chemistry 17, 834-844.

Basu, T., Nandi, D., Sen, P., Ghosh, U.C., 2013. Equilibrium modeling of As(III, V) sorption in the absence/presence of some groundwater occurring ions by iron(III)-cerium(IV) oxide nanoparticle agglomerates: A mechanistic approach of surface interaction. Chemical Engineering Journal 228, 665-678.

Benjwal, P., Kumar, M., Chamoli, P., Kar, K.K., 2015. Enhanced photocatalytic degradation of methylene blue and adsorption of arsenic(III) by reduced graphene oxide (rGO)-metal oxide (TiO2/Fe3O4) based nanocomposites. RSC Advances 5, 73249-73260.

Bezbaruah, A.N., Kalita, H., Almeelbi, T., Capecchi, C.L., Jacob, D.L., Ugrinov, A.G., Payne, S.A., 2013. Ca-alginate-entrapped nanoscale iron: arsenic treatability and mechanism studies. Journal of Nanoparticle Research 16.

Bhattacharya, P., Jacks, G., Jana, J., Sracek, A., Gustafsson, J., Chatterjee, D., 2001. Geochemistry of the Holocene alluvial sediments of Bengal Delta Plain from West Bengal, India: implications on arsenic contamination in groundwater. Groundwater arsenic contamination in the Bengal Delta Plain of Bangladesh 3084, 21-40.

Bhowmick, S., Chakraborty, S., Mondal, P., Van Renterghem, W., Van den Berghe, S., Roman-Ross, G., Chatterjee, D., Iglesias, M., 2014. Montmorillonite-supported nanoscale zero-valent iron for removal of arsenic from aqueous solution: Kinetics and mechanism. Chemical Engineering Journal 243, 14-23.

Bindal, S., Singh, C.K., 2019. Predicting groundwater arsenic contamination: Regions at risk in highest populated state of India. Water Research 159, 65-76.

Bissen, M., Frimmel, F.H., 2003. Arsenic - a review. Part II: Oxidation of arsenic and its removal in water treatment. Acta Hydrochimica Et Hydrobiologica 31, 97-107.

Borovik, A., Karanikola, V., Zucker, I., 2020. Platform selection of engineered nanomaterials for water decontamination applications. Environmental Science-Nano 7.

Bowell, R.J., Alpers, C.N., Jamieson, H.E., Nordstrom, D.K., Majzlan, J., 2014. The Environmental Geochemistry of Arsenic - An Overview. Arsenic: Environmental Geochemistry, Mineralogy, and Microbiology 79, 1-16.

Brammer, H., Ravenscroft, P., 2009. Arsenic in groundwater: A threat to sustainable agriculture in South and South-east Asia. Environment International 35, 647-654.

Brandhuber, P., Amy, G., 2001. Arsenic removal by a charged ultrafiltration membrane - influences of membrane operating conditions and water quality on arsenic rejection. Desalination 140, 1-14.

Bujnakova, Z., Balaz, P., Zorkovska, A., Sayagues, M.J., Kovac, J., Timko, M., 2013. Arsenic sorption by nanocrystalline magnetite: An example of environmentally promising interface with geosphere. Journal of Hazardous Materials 262, 1204-1212.

Camacho, L.M., Ponnusamy, S., Campos, I., Davis, T.A., Deng, S., 2015. Evaluation of novel modified activated alumina as adsorbent for arsenic removal. Handbook of Arsenic Toxicology. Elsevier, pp. 121-136.

Carlin, D.J., Naujokas, M.F., Bradham, K.D., Cowden, J., Heacock, M., Henry, H.F., Lee, J.S., Thomas, D.J., Thompson, C., Tokar, E.J., Waalkes, M.P., Birnbaum, L.S., Suk, W.A., 2016. Arsenic and Environmental Health: State of the Science and Future Research Opportunities. Environmental Health Perspectives 124, 890-899.

Chakraborti, D., Rahman, M.M., Das, B., Nayak, B., Pal, A., Sengupta, M.K., Hossain, M.A., Ahamed, S., Sahu, M., Saha, K.C., Mukherjee, S.C., Pati, S., Dutta, R.N., Quamruzzaman, Q., 2013. Groundwater arsenic contamination in Ganga-Meghna-Brahmaputra plain, its health effects and an approach for mitigation. Environmental Earth Sciences 70, 1993-2008.

Chakraborti, D., Singh, S.K., Rahman, M.M., Dutta, R.N., Mukherjee, S.C., Pati, S., Kar, P.B., 2018. Groundwater Arsenic Contamination in the Ganga River Basin: A Future Health Danger. International Journal of Environmental Research and Public Health 15.

Chandra, V., Park, J., Chun, Y., Lee, J.W., Hwang, I.-C., Kim, K.S., 2010. Water-Dispersible Magnetite-Reduced Graphene Oxide Composites for Arsenic Removal. ACS Nano 4, 3979-3986.

Chen, A.S.C., Wang, L.L., Sorg, T.J., Lytle, D.A., 2020a. Removing arsenic and co-occurring contaminants from drinking water by full-scale ion exchange and point-of-use/point-of-entry reverse osmosis systems. Water Research 172.

Chen, M., Jafvert, C.T., Wu, Y.C., Cao, X.Q., Hankins, N.P., 2020b. Inorganic anion removal using micellar enhanced ultrafiltration (MEUF), modeling anion distribution and suggested improvements of MEUF: A review. Chemical Engineering Journal 398.

Chen, M.L., Sun, Y., Huo, C.B., Liu, C., Wang, J.H., 2015. Akaganeite decorated graphene oxide composite for arsenic adsorption/removal and its preconcentration at ultra-trace level. Chemosphere 130, 52-58.

Chen, Y., Parvez, F., Gamble, M., Islam, T., Ahmed, A., Argos, M., Graziano, J.H., Ahsan, H., 2009. Arsenic exposure at low-to-moderate levels and skin lesions, arsenic metabolism,

neurological functions, and biomarkers for respiratory and cardiovascular diseases: Review of recent findings from the Health Effects of Arsenic Longitudinal Study (HEALS) in Bangladesh. Toxicology and Applied Pharmacology 239, 184-192.

Chowdhury, S.R., Yanful, E.K., Pratt, A.R., 2011. Arsenic removal from aqueous solutions by mixed magnetite-maghemite nanoparticles. Environmental Earth Sciences 64, 411-423.

Cohen, S.M., Arnold, L.L., Eldan, M., Lewis, A.S., Beck, B.D., 2006. Methylated arsenicals: The implications of metabolism and carcinogenicity studies in rodents to human risk assessment. Critical Reviews in Toxicology 36, 99-133.

Cui, H., Li, Q., Gao, S.A., Shang, J.K., 2012. Strong adsorption of arsenic species by amorphous zirconium oxide nanoparticles. Journal of Industrial and Engineering Chemistry 18, 1418-1427.

Darban, A.K., Kianinia, Y., Taheri-Nassaj, E., 2013. Synthesis of nano-alumina powder from impure kaolin and its application for arsenite removal from aqueous solutions. Journal of Environmental Health Science and Engineering 11.

Deliyanni, E.A., Bakoyannakis, D.N., Zouboulis, A.I., Matis, K.A., 2003. Sorption of As(V) ions by akaganeite-type nanocrystals. Chemosphere 50, 155-163.

Dominguez-Ramos, A., Chavan, K., Garcia, V., Jimeno, G., Albo, J., Marathe, K.V., Yadav, G.D., Irabien, A., 2014. Arsenic Removal from Natural Waters by Adsorption or Ion Exchange: An Environmental Sustainability Assessment. Industrial & Engineering Chemistry Research 53, 18920-18927.

Dutta, P.K., Pehkonen, S.O., Sharma, V.K., Ray, A.K., 2005. Photocatalytic oxidation of arsenic(III): Evidence of hydroxyl radicals. Environmental Science & Technology 39, 1827-1834.

Erickson, M.L., Barnes, R.J., 2005. Well characteristics influencing arsenic concentrations in ground water. Water Research 39, 4029-4039.

Fendorf, S., Michael, H.A., van Geen, A., 2010. Spatial and Temporal Variations of Groundwater Arsenic in South and Southeast Asia. Science 328, 1123-1127.

Feng, L.Y., Cao, M.H., Ma, X.Y., Zhu, Y.S., Hu, C.W., 2012a. Superparamagnetic high-surface-area Fe3O4 nanoparticles as adsorbents for arsenic removal. Journal of Hazardous Materials 217, 439-446.

Feng, Q.Z., Zhang, Z.Y., Ma, Y.H., He, X., Zhao, Y.L., Chai, Z.F., 2012b. Adsorption and desorption characteristics of arsenic onto ceria nanoparticles. Nanoscale Research Letters 7, 1-8.

Garbinski, L.D., Rosen, B.P., Chen, J., 2019. Pathways of arsenic uptake and efflux. Environment International 126, 585-597.

Gecol, H., Ergican, E., Fuchs, A., 2004. Molecular level separation of arsenic (V) from water using cationic surfactant micelles and ultrafiltration membrane. Journal of Membrane Science 241, 105-119.

Georgakilas, V., Otyepka, M., Bourlinos, A.B., Chandra, V., Kim, N., Kemp, K.C., Hobza, P., Zboril, R., Kim, K.S., 2012. Functionalization of graphene: covalent and non-covalent approaches, derivatives and applications. Chemical reviews 112, 6156-6214.

Ghosh, M.K., Poinern, G.E.J., Issa, T.B., Singh, P., 2012. Arsenic adsorption on goethite nanoparticles produced through hydrazine sulfate assisted synthesis method. Korean Journal of Chemical Engineering 29, 95-102.

Ghosh, S., Prabhakar, R., Samadder, S.R., 2019. Performance of -aluminium oxide nanoparticles for arsenic removal from groundwater. Clean Technologies and Environmental Policy 21, 121-138.

Ghurye, G., Clifford, D., Tripp, A., 2004. Iron coagulation and direct microfiltration to remove arsenic from groundwater. Journal American Water Works Association 96, 143-152.

Giles, D.E., Mohapatra, M., Issa, T.B., Anand, S., Singh, P., 2011. Iron and aluminium based adsorption strategies for removing arsenic from water. Journal of Environmental Management 92, 3011-3022.

Gu, Z.M., Fang, J., Deng, B.L., 2005. Preparation and evaluation of GAC-based iron-containing adsorbents for arsenic removal. Environmental Science & Technology 39, 3833-3843.

Guo, H.M., Ren, Y., Liu, Q., Zhao, K., Li, Y., 2013. Enhancement of Arsenic Adsorption during Mineral Transformation from Siderite to Goethite: Mechanism and Application. Environmental Science & Technology 47, 1009-1016.

Gupta, K., Bhattacharya, S., Chattopadhyay, D., Mukhopadhyay, A., Biswas, H., Dutta, J., Ray, N.R., Ghosh, U.C., 2011. Ceria associated manganese oxide nanoparticles: Synthesis, characterization and arsenic(V) sorption behavior. Chemical Engineering Journal 172, 219-229.

Habuda-Stanic, M., Nujic, M., 2015. Arsenic removal by nanoparticles: a review. Environmental Science and Pollution Research 22, 8094-8123.

Hao, L.L., Liu, M.Z., Wang, N.N., Li, G.J., 2018. A critical review on arsenic removal from water using iron-based adsorbents. RSC Advances 8, 39545-39560.

Hering, J.G., Chen, P.Y., Wilkie, J.A., Elimelech, M., 1997. Arsenic removal from drinking water during coagulation. Journal of Environmental Engineering-ASCE 123, 800-807.

Hu, Z.C., Gao, S., 2008. Upper crustal abundances of trace elements: A revision and update. Chemical Geology 253, 205-221.

Hughes, M.F., Beck, B.D., Chen, Y., Lewis, A.S., Thomas, D.J., 2011. Arsenic Exposure and Toxicology: A Historical Perspective. Toxicological Sciences 123, 305-332.

Huong, P.T.L., Huy, L.T., Phan, V.N., Huy, T.Q., Nam, M.H., Lam, V.D., Le, A.T., 2016. Application of Graphene Oxide-MnFe2O4 Magnetic Nanohybrids as Magnetically Separable Adsorbent for Highly Efficient Removal of Arsenic from Water. Journal of Electronic Materials 45, 2372-2380.

Jegadeesan, G., Al-Abed, S.R., Sundaram, V., Choi, H., Scheckel, K.G., Dionysiou, D.D., 2010. Arsenic sorption on TiO2 nanoparticles: Size and crystallinity effects. Water Research 44, 965-973.

Jiang, W., Chen, X.B., Niu, Y.J., Pan, B.C., 2012. Spherical polystyrene-supported nano-Fe3O4 of high capacity and low-field separation for arsenate removal from water. Journal of Hazardous Materials 243, 319-325.

Joshi, A., Chaudhuri, M., 1996. Removal of arsenic from ground water by iron oxide-coated sand. Journal of Environmental Engineering-ASCE 122, 769-771.

Kanel, S.R., Greneche, J.-M., Choi, H., 2006. Arsenic (V) removal from groundwater using nano scale zero-valent iron as a colloidal reactive barrier material. Environmental science & technology 40, 2045-2050.

Kanel, S.R., Manning, B., Charlet, L., Choi, H., 2005. Removal of arsenic(III) from groundwater by nanoscale zero-valent iron. Environmental Science & Technology 39, 1291-1298.

Khairul, I., Wang, Q.Q., Jiang, Y.H., Wang, C., Naranmandura, H., 2017. Metabolism, toxicity and anticancer activities of arsenic compounds. Oncotarget 8, 23905-23926.

Kim, M.J., 2001. Separation of inorganic arsenic species in groundwater using ion exchange method. Bulletin of Environmental Contamination and Toxicology 67, 46-51.

Kobya, M., Soltani, R.D.C., Omwene, P.I., Khataee, A., 2020. A review on decontamination of arsenic-contained water by electrocoagulation: Reactor configurations and operating cost along with removal mechanisms. Environmental Technology & Innovation 17.

Kong, S.Q., Wang, Y.X., Zhan, H.B., Yuan, S.H., Yu, M., Liu, M.L., 2014. Adsorption/Oxidation of Arsenic in Groundwater by Nanoscale Fe-Mn Binary Oxides Loaded on Zeolite. Water Environment Research 86, 147-155.

Kumar, P.R., Chaudhari, S., Khilar, K.C., Mahajan, S.P., 2004. Removal of arsenic from water by electrocoagulation. Chemosphere 55, 1245-1252.

Kunzru, S., Chaudhuri, M., 2005. Manganese amended activated alumina for adsorption/oxidation of arsenic. Journal of Environmental Engineering 131, 1350-1353.

La, D.D., Patwari, J.M., Jones, L.A., Antolasic, F., Bhosale, S.V., 2017. Fabrication of a GNP/Fe-Mg Binary Oxide Composite for Effective Removal of Arsenic from Aqueous Solution. ACS Omega 2, 218-226.

Lakshmanan, D., Clifford, D., Samanta, G., 2008. Arsenic removal by coagulation - With aluminum, iron, titanium, and zirconium. Journal American Water Works Association 100, 76-+.

Lata, S., Samadder, S.R., 2016. Removal of arsenic from water using nano adsorbents and challenges: A review. Journal of Environmental Management 166, 387-406.

Li, R.H., Li, Q., Gao, S., Shang, J.K., 2012. Exceptional arsenic adsorption performance of hydrous cerium oxide nanoparticles: Part A. Adsorption capacity and mechanism. Chemical Engineering Journal 185, 127-135.

Liang, J.J., He, B.H., Li, P., Yu, J., Zhao, X.L., Wu, H.Y., Li, J., Sun, Y.B., Fan, Q.H., 2019. Facile construction of 3D magnetic graphene oxide hydrogel via incorporating assembly and chemical bubble and its application in arsenic remediation. Chemical Engineering Journal 358, 552-563.

Liang, T., Li, L.F., Zhu, C.X., Liu, X., Li, H.N., Su, Q.Q., Ye, J., Geng, B., Tian, Y.L., Sardar, M.F., Huang, X.Y., Li, F., 2020. Adsorption of As(V) by the Novel and Efficient Adsorbent Cerium-Manganese Modified Biochar. Water 12.

Liang, Y.Y., Wang, H.L., Casalongue, H.S., Chen, Z., Dai, H.J., 2010. TiO_2 Nanocrystals Grown on Graphene as Advanced Photocatalytic Hybrid Materials. Nano Research 3, 701-705.

Lien, H.L., Wilkin, R.T., 2005. High-level arsenite removal from groundwater by zero-valent iron. Chemosphere 59, 377-386.

Lin, S., Lu, D.N., Liu, Z., 2012. Removal of arsenic contaminants with magnetic gamma-Fe_2O_3 nanoparticles. Chemical Engineering Journal 211, 46-52.

Ling, L., Zhang, W.X., 2014. Sequestration of Arsenate in Zero-Valent Iron Nanoparticles: Visualization of Intraparticle Reactions at Angstrom Resolution. Environmental Science & Technology Letters 1, 305-309.

Lingamdinne, L.P., Koduru, J.R., Chang, Y.Y., Kang, S.H., Yang, J.K., 2019a. Facile synthesis of flowered mesoporous graphene oxide-lanthanum fluoride nanocomposite for adsorptive removal of arsenic. Journal of Molecular Liquids 279, 32-42.

Lingamdinne, L.P., Koduru, J.R., Karri, R.R., 2019b. A comprehensive review of applications of magnetic graphene oxide based nanocomposites for sustainable water purification. Journal of Environmental Management 231, 622-634.

Liu, C., Ding, R.Y., Xie, F.C., 2020. Facile Synthesis of Manganese Dioxide Nanoparticles for Efficient Removal of Aqueous As(III). Journal of Chemical and Engineering Data 65, 3988-3997.

Liu, S.W., Kang, S.H., Wang, G.Z., Zhao, H.J., Cai, W.P., 2015. Micro/nanostructured porous Fe-Ni binary oxide and its enhanced arsenic adsorption performances. Journal of Colloid and Interface Science 458, 94-102.

Loebenstein, J.R., 1994. Materials flow of arsenic in the United States. US Bureau of Mines.

Lu, G.H., Mao, S., Park, S., Ruoff, R.S., Chen, J.H., 2009. Facile, Noncovalent Decoration of Graphene Oxide Sheets with Nanocrystals. Nano Research 2, 192-200.

Luo, J.M., Meng, X.Y., Crittenden, J., Qu, J.H., Hu, C.Z., Liu, H.J., Peng, P., 2018. Arsenic adsorption on alpha-MnO2 nanofibers and the significance of (100) facet as compared with (110). Chemical Engineering Journal 331, 492-500.

Luo, X.B., Wang, C.C., Wang, L.C., Deng, F., Luo, S.L., Tu, X.M., Au, C.T., 2013. Nanocomposites of graphene oxide-hydrated zirconium oxide for simultaneous removal of As(III) and As(V) from water. Chemical Engineering Journal 220, 98-106.

Martinson, C.A., Reddy, K.J., 2009. Adsorption of arsenic(III) and arsenic(V) by cupric oxide nanoparticles. Journal of Colloid and Interface Science 336, 406-411.

Mauter, M.S., Zucker, I., Perreault, F., Werber, J.R., Kim, J.H., Elimelech, M., 2018. The role of nanotechnology in tackling global water challenges. Nature Sustainability 1, 166-175.

Mayo, J., Yavuz, C., Yean, S., Cong, L., Shipley, H., Yu, W., Falkner, J., Kan, A., Tomson, M., Colvin, V., 2007. The effect of nanocrystalline magnetite size on arsenic removal. Science and Technology of Advanced Materials 8, 71.

Mohan, D., Pittman, C.U., 2007. Arsenic removal from water/wastewater using adsorbents-A critical review. Journal of Hazardous materials 142, 1-53.

Mohanty, D., 2017. Conventional as well as Emerging Arsenic Removal Technologies-a Critical Review. Water Air and Soil Pollution 228.

Mondal, P., Bhowmick, S., Chatterjee, D., Figoli, A., Van der Bruggen, B., 2013. Remediation of inorganic arsenic in groundwater for safe water supply: A critical assessment of technological solutions. Chemosphere 92, 157-170.

Morin, G., Wang, Y.H., Ona-Nguema, G., Juillot, F., Calas, G., Menguy, N., Aubry, E., Bargar, J.R., Brown, G.E., 2009. EXAFS and HRTEM Evidence for As(III)-Containing Surface Precipitates on Nanocrystalline Magnetite: Implications for As Sequestration. Langmuir 25, 9119-9128.

Murcott, S., 2012. Arsenic contamination in the world. IWA publishing.

Nabi, D., Aslam, I., Qazi, I.A., 2009. Evaluation of the adsorption potential of titanium dioxide nanoparticles for arsenic removal. Journal of Environmental Sciences 21, 402-408.

Neri, G., Scala, A., Fazio, E., Mineo, P.G., Rescifina, A., Piperno, A., Grassi, G., 2015. Repurposing of oxazolone chemistry: gaining access to functionalized graphene nanosheets in a top-down approach from graphite. Chemical Science 6, 6961-6970.

Nicomel, N.R., Leus, K., Folens, K., Van der Voort, P., Du Laing, G., 2016. Technologies for Arsenic Removal from Water: Current Status and Future Perspectives. International Journal of Environmental Research and Public Health 13.

Nidheesh, P.V., Singh, T.S.A., 2017. Arsenic removal by electrocoagulation process: Recent trends and removal mechanism. Chemosphere 181, 418-432.

Nikolaidis, N.P., Dobbs, G.M., Lackovic, J.A., 2003. Arsenic removal by zero-valent iron: field, laboratory and modeling studies. Water Research 37, 1417-1425.

Ocinski, D., Jacukowicz-Sobala, I., Mazur, P., Raczyk, J., Kociolek-Balawejder, E., 2016. Water treatment residuals containing iron and manganese oxides for arsenic removal from water - Characterization of physicochemical properties and adsorption studies. Chemical Engineering Journal 294, 210-221.

Oremland, R.S., Stolz, J.F., 2003. The ecology of arsenic. Science 300, 939-944.

Patra, A.K., Dutta, A., Bhaumik, A., 2012. Self-assembled mesoporous gamma-Al2O3 spherical nanoparticles and their efficiency for the removal of arsenic from water. Journal of Hazardous Materials 201, 170-177.

Perreault, F., De Faria, A.F., Elimelech, M., 2015. Environmental applications of graphene-based nanomaterials. Chemical Society Reviews 44, 5861-5896.

Podgorski, J., Berg, M., 2020. Global threat of arsenic in groundwater. Science 368, 845-858.

Podgorski, J., Wu, R.H., Chakravorty, B., Polya, D.A., 2020. Groundwater Arsenic Distribution in India by Machine Learning Geospatial Modeling. International Journal of Environmental Research and Public Health 17.

Powers, M., Yracheta, J., Harvey, D., O'Leary, M., Best, L.G., Bear, A.B., MacDonald, L., Susan, J., Hasan, K., Thomas, E., 2019. Arsenic in groundwater in private wells in rural North Dakota and South Dakota: Water quality assessment for an intervention trial. Environmental Research 168, 41-47.

Qi, P.F., Pichler, T., 2016. Competitive Adsorption of As(III) and As(V) by Ferrihydrite: Equilibrium, Kinetics, and Surface Complexation. Water Air and Soil Pollution 227.

Ramos, M.A.V., Yan, W., Li, X.Q., Koel, B.E., Zhang, W.X., 2009. Simultaneous Oxidation and Reduction of Arsenic by Zero-Valent Iron Nanoparticles: Understanding the Significance of the Core-Shell Structure. Journal of Physical Chemistry C 113, 14591-14594.

Ranjan, S., Yadav, B.K., Joshi, H., 2020. Development of nZVI-Pumice/Zeolite Composites for Effective Removal of Arsenic (III) from Aqueous Solution. Journal of Hazardous Toxic and Radioactive Waste 24.

Ray, P.Z., Shipley, H.J., 2015. Inorganic nano-adsorbents for the removal of heavy metals and arsenic: a review. RSC Advances 5, 29885-29907.

Ren, Z.M., Zhang, G.S., Chen, J.P., 2011. Adsorptive removal of arsenic from water by an iron-zirconium binary oxide adsorbent. Journal of Colloid and Interface Science 358, 230-237.

Sakthivel, T.S., Das, S., Pratt, C.J., Seal, S., 2017a. One-pot synthesis of a ceria-graphene oxide composite for the efficient removal of arsenic species. Nanoscale 9, 3367-3374.

Sakthivel, T.S., Das, S., Pratt, C.J., Seal, S., 2017b. One-pot synthesis of a ceria–graphene oxide composite for the efficient removal of arsenic species. Nanoscale.

Sandoval, M.A., Fuentes, R., Thiam, A., Salazar, R., 2021. Arsenic and fluoride removal by electrocoagulation process: A general review. Science of the Total Environment 753.

Sarkar, A., Paul, B., 2016. The global menace of arsenic and its conventional remediation - A critical review. Chemosphere 158, 37-49.

Sheng, G.D., Li, Y.M., Yang, X., Ren, X.M., Yang, S.T., Hu, J., Wang, X.K., 2012. Efficient removal of arsenate by versatile magnetic graphene oxide composites. RSC Advances 2, 12400-12407.

Shih, M.C., 2005. An overview of arsenic removal by pressure-driven membrane processes. Desalination 172, 85-97.

Shipley, H.J., Yean, S., Kan, A.T., Tomson, M.B., 2009. Adsorption of arsenic to magnetite nanoparticles: effect of particle concentration, pH, ionic strength, and temperature. Environmental Toxicology and Chemistry 28, 509-515.

Siddique, T.A., Dutta, N.K., Choudhury, N.R., 2020. Nanofiltration for Arsenic Removal: Challenges, Recent Developments, and Perspectives. Nanomaterials 10.

Siddiqui, S.I., Chaudhry, S.A., 2017. Iron oxide and its modified forms as an adsorbent for arsenic removal: A comprehensive recent advancement. Process Safety and Environmental Protection 111, 592-626.

Siddiqui, S.I., Naushad, M., Chaudhry, S.A., 2019. Promising prospects of nanomaterials for arsenic water remediation: A comprehensive review. Process Safety and Environmental Protection 126, 60-97.

Singh, A., Patel, A.K., Deka, J.P., Kumar, M., 2020. Natural recharge transcends anthropogenic forcing that influences arsenic vulnerability of the quaternary alluviums of the Mid-Gangetic Plain. Npj Clean Water 3.

Su, H., Ye, Z.B., Hmidi, N., Subramanian, R., 2017. Carbon nanosphere-iron oxide nanocomposites as high-capacity adsorbents for arsenic removal. RSC Advances 7, 36138-36148.

Sun, H.W., Wang, L., Zhang, R.H., Sui, J.C., Xu, G.N., 2006. Treatment of groundwater polluted by arsenic compounds by zero valent iron. Journal of Hazardous Materials 129, 297-303.

Sun, T.Y., Zhao, Z.W., Liang, Z.J., Liu, J., Shi, W.X., Cui, F.Y., 2017. Efficient As(III) removal by magnetic CuO-Fe(3)o(4) nanoparticles through photo-oxidation and adsorption under light irradiation. Journal of Colloid and Interface Science 495, 168-177.

Tchounwou, P.B., Yedjou, C.G., Udensi, U.K., Pacurari, M., Stevens, J.J., Patlolla, A.K., Noubissi, F., Kumar, S., 2019. State of the science review of the health effects of inorganic arsenic: Perspectives for future research. Environmental Toxicology 34, 188-202.

Tripathy, S.S., Raichur, A.M., 2008. Enhanced adsorption capacity of activated alumina by impregnation. with alum for removal of As(V) from water. Chemical Engineering Journal 138, 179-186.

Tseng, C.H., 2009. A review on environmental factors regulating arsenic methylation in humans. Toxicology and Applied Pharmacology 235, 338-350.

Uppal, J.S., Zheng, Q., Le, X.C., 2019. Arsenic in drinking water—recent examples and updates from Southeast Asia. Current Opinion in Environmental Science & Health 7, 126-135.

United States Environmental Protection Agency (USEPA), 2001. National primary drinking water regulations; arsenic and clarifications to compliance and new source contaminants monitoring. Fed Reg 66, 6975-7066.

United States Environmental Protection Agency (USEPA), 2003. Arsenic treatment technology evaluation handbook for small systems.

Vitela-Rodriguez, A.V., Rangel-Mendez, J.R., 2013. Arsenic removal by modified activated carbons with iron hydro(oxide) nanoparticles. Journal of Environmental Management 114, 225-231.

Wang, C., Luo, H.J., Zhang, Z.L., Wu, Y., Zhang, J., Chen, S.W., 2014a. Removal of As(III) and As(V) from aqueous solutions using nanoscale zero valent iron-reduced graphite oxide modified composites. Journal of Hazardous Materials 268, 124-131.

Wang, H., Robinson, J.T., Diankov, G., Dai, H., 2010. Nanocrystal Growth on Graphene with Various Degrees of Oxidation. Journal of the American Chemical Society 132, 3270-+.

Wang, S., Gao, B., Li, Y., Creamer, A.E., He, F., 2017. Adsorptive removal of arsenate from aqueous solutions by biochar supported zero-valent iron nanocomposite: Batch and continuous flow tests. Journal of Hazardous Materials 322, 172-181.

Wang, Y.H., Morin, G., Ona-Nguema, G., Brown, G.E., 2014b. Arsenic(III) and Arsenic(V) Speciation during Transformation of Lepidocrocite to Magnetite. Environmental Science & Technology 48, 14282-14290.

Wang, Y.L., Liu, H.P., Wang, S.F., Li, X.H., Wang, X., Jia, Y.F., 2020. Simultaneous removal and oxidation of arsenic from water by delta-MnO2 modified activated carbon. Journal of Environmental Sciences 94, 147-160.

Waypa, J.J., Elimelech, M., Hering, J.G., 1997. Arsenic removal by RO and NF membranes. Journal American Water Works Association 89, 102-114.

Wen, T., Wu, X.L., Tan, X.L., Wang, X.K., Xu, A.W., 2013. One-Pot Synthesis of Water-Swellable Mg-Al Layered Double Hydroxides and Graphene Oxide Nanocomposites for Efficient Removal of As(V) from Aqueous Solutions. ACS Applied Materials & Interfaces 5, 3304-3311.

WHO, 2003. Arsenic in drinking-water: background document for development of WHO guidelines for drinking-water quality. World Health Organization.

World Health Organization (WHO), Arsenic Fact Sheet, 2018, Available at: https://www.who.int/news-room/fact-sheets/detail/arsenic. (Access November 23, 2020)

Wickramasinghe, S.R., Han, B.B., Zimbron, J., Shen, Z., Karim, M.N., 2004. Arsenic removal by coagulation and filtration: comparison of groundwaters from the United States and Bangladesh. Desalination 169, 231-244.

Wong, W.W., Wong, H.Y., Badruzzaman, A.B.M., Goh, H.H., Zaman, M., 2017. Recent advances in exploitation of nanomaterial for arsenic removal from water: a review. Nanotechnology 28.

Wu, K., Jing, C.Y., Zhang, J., Liu, T., Yang, S.J., Wang, W.D., 2019. Magnetic Fe_3O_4@CuO nanocomposite assembled on graphene oxide sheets for the enhanced removal of arsenic(III/V) from water. Applied Surface Science 466, 746-756.

Wu, L.K., Wu, H., Zhang, H.B., Cao, H.Z., Hou, G.Y., Tang, Y.P., Zheng, G.Q., 2018. Graphene oxide/CuFe2O4 foam as an efficient absorbent for arsenic removal from water. Chemical Engineering Journal 334, 1808-1819.

Xu, W.H., Wang, J., Wang, L., Sheng, G.P., Liu, J.H., Yu, H.Q., Huang, X.J., 2013. Enhanced arsenic removal from water by hierarchically porous CeO2-ZrO2 nanospheres: Role of surface- and structure-dependent properties. Journal of Hazardous Materials 260, 498-507.

Xu, Z.C., Li, Q., Gao, S.A., Shang, J.K., 2010. As(III) removal by hydrous titanium dioxide prepared from one-step hydrolysis of aqueous TiCl4 solution. Water Research 44, 5713-5721.

Yadav, R., Sharma, A.K., Babu, J.N., 2016. Sorptive removal of arsenite As(III) and arsenate As(V) by fuller's earth immobilized nanoscale zero-valent iron nanoparticles (F-nZVI): Effect of Fe-0 loading on adsorption activity. Journal of Environmental Chemical Engineering 4, 681-694.

Yan, W., Vasic, R., Frenkel, A.I., Koel, B.E., 2012a. Intraparticle Reduction of Arsenite (As(III)) by Nanoscale Zerovalent Iron (nZVI) Investigated with In Situ X-ray Absorption Spectroscopy. Environmental Science & Technology 46, 7018-7026.

Yan, W.L., Ramos, M.A.V., Koel, B.E., Zhang, W.X., 2012b. As(III) Sequestration by Iron Nanoparticles: Study of Solid-Phase Redox Transformations with X-ray Photoelectron Spectroscopy. Journal of Physical Chemistry C 116, 5303-5311.

Yavuz, C.T., Mayo, J.T., Suchecki, C., Wang, J., Ellsworth, A.Z., D'Couto, H., Quevedo, E., Prakash, A., Gonzalez, L., Nguyen, C., Kelty, C., Colvin, V.L., 2010. Pollution magnet: nano-magnetite for arsenic removal from drinking water. Environmental Geochemistry and Health 32, 327-334.

Yoon, S.H., Lee, J.H., 2005. Oxidation mechanism of As(III) in the UV/TiO2 system: Evidence for a direct hole oxidation mechanism. Environmental Science & Technology 39, 9695-9701.

Yoon, Y., Park, W.K., Hwang, T.M., Yoon, D.H., Yang, W.S., Kang, J.W., 2016. Comparative evaluation of magnetite-graphene oxide and magnetite-reduced graphene oxide composite for As(III) and As(V) removal. Journal of Hazardous Materials 304, 196-204.

Yoon, Y., Zheng, M., Ahn, Y.-T., Park, W.K., Yang, W.S., Kang, J.-W., 2017. Synthesis of magnetite/non-oxidative graphene composites and their application for arsenic removal. Separation and Purification Technology 178, 40-48.

Yu, L., Ma, Y., Ong, C.N., Xie, J., Liu, Y., 2015. Rapid adsorption removal of arsenate by hydrous cerium oxide–graphene composite. RSC Advances 5, 64983-64990.

Yu, X.W., Wei, Y.F., Liu, C.B., Ma, J.H., Liu, H., Wei, S.D., Deng, W., Xiang, J.N., Luo, S.L., 2019. Ultrafast and deep removal of arsenic in high-concentration wastewater: A superior bulk adsorbent of porous Fe2O3 nanocubes-impregnated graphene aerogel. Chemosphere 222, 258-266.

Zhang, G.S., Liu, Y., Wang, J.Y., Li, H.S., 2020. Efficient arsenic(III) removal from aqueous solution by a novel nanostructured iron-copper-manganese trimetal oxide. Journal of Molecular Liquids 309.

Zhang, M., Gao, B., Varnoosfaderani, S., Hebard, A., Yao, Y., Inyang, M., 2013. Preparation and characterization of a novel magnetic biochar for arsenic removal. Bioresource Technology 130, 457-462.

Zhang, W., Liu, C.H., Zheng, T., Ma, J., Zhang, G.S., Ren, G.H., Wang, L., Liu, Y.L., 2018. Efficient oxidation and sorption of arsenite using a novel titanium(IV)-manganese(IV) binary oxide sorbent. Journal of Hazardous Materials 353, 410-420.

Zhao, D.D., Yu, Y., Chen, J.P., 2016. Fabrication and testing of zirconium-based nanoparticle-doped activated carbon fiber for enhanced arsenic removal in water. RSC Advances 6, 27020-27030.

Zhao, F.J., McGrath, S.P., Meharg, A.A., 2010. Arsenic as a Food Chain Contaminant: Mechanisms of Plant Uptake and Metabolism and Mitigation Strategies. Annual Review of Plant Biology, Vol 61 61, 535-559.

Zheng, Y.M., Yu, L., Wu, D., Chen, J.P., 2012. Removal of arsenite from aqueous solution by a zirconia nanoparticle. Chemical Engineering Journal 188, 15-22.

Zhou, Q., Xi, S.H., 2018. A review on arsenic carcinogenesis: Epidemiology, metabolism, genotoxicity and epigenetic changes. Regulatory Toxicology and Pharmacology 99, 78-88.

Zhu, J., Lou, Z.M., Liu, Y., Fu, R.Q., Baig, S.A., Xu, X.H., 2015. Adsorption behavior and removal mechanism of arsenic on graphene modified by iron-manganese binary oxide (FeMnOx/RGO) from aqueous solutions. RSC Advances 5, 67951-67961.

CHAPTER 2. COMPARATIVE STUDY OF ARSENIC REMOVAL BY IRON-BASED NANOMATERIALS: POTENTIAL CANDIDATES FOR FIELD APPLICATIONS[1]

2.1. Introduction

Arsenic is a naturally occurring carcinogenic metalloid that presents in inorganic forms in groundwater and typically present in two oxidation states, As(III) or arsenite and As(V) or arsenate (ATSDR, 2007). Most of the arsenic present in groundwater is from geogenic sources (Amini et al., 2008; Podgorski and Berg, 2020) while the anthropogenic sources include some pesticides used in the past and industrial discharge (Murcott, 2012). World Health Organization (WHO) and the United States Environmental Protection Agency (USEPA) have set the maximum contaminant level (MCL) of total inorganic arsenic in drinking water as 10 µg/L (USEPA, 2001; WHO, 2003). More than 200 million people in 50 countries are affected by groundwater arsenic contamination and the number is increasing rapidly (Murcott, 2012; WHO, 2017; Podgorski and Berg, 2020).

Adsorption has become a widely adapted technology for the efficient removal of aqueous arsenic with the added advantages of ease of implementation and economic viability. While the selection of the right adsorbent is always challenging (Lata and Samadder, 2016), iron (Fe)-based metal-oxide nano-adsorbents were extensively studied for arsenic remediation in the last two decades. Nano-adsorbents have a high specific surface area and good selectivity to remove both the inorganic arsenic species and exhibited rapid reaction rates (Wong et al., 2017; Siddiqui

[1] This chapter has been published as a peer-reviewed paper in *Science of The Total Environment* (2021). Das, T.K. and Bezbaruah, A.N., 2021. Comparative study of arsenic removal by iron-based nanomaterials: Potential candidates for field applications. *Science of The Total Environment*, 764, p.142914.

The material in this chapter was co-authored by Tonoy K Das and Dr. Achintya Bezbaruah. Tonoy had primary responsibility for conceptualizing the study and developing the methodology. Tonoy designed and conducted all batch experiments, analyzed all the data, and investigated the results. Tonoy also drafted and revised all versions of this chapter. Dr. Achintya served as superviser, proof reader and checked all the results and analysis conducted by Tonoy.

et al., 2019). The major problem associated with these nanomaterials is their agglomeration that reduces their contaminant (arsenic) removal efficiency and, thus, limits their application. Synthesis of these nanomaterials on a suitable support medium reduces their agglomeration and significantly improves their arsenic removal efficiency (Liu et al., 2020). Graphene oxide (GO) is one of the most promising support media extensively used by researchers (Yang et al., 2017; Sherlala et al., 2018). Graphene oxide is a 2D of carbon sheet with several functional groups (−COOH, −OH, C=O). The metal ions nucleate onto the GO surface and nanoparticles can be synthesized as well dispersed entities on the GO sheet. There are reported works on graphene oxide-supported iron nanoparticles (aka graphene oxide iron nanohybrids) for arsenic removal. Most of the studies used graphene oxide magnetite (GM) nanohybrids as the adsorbent (Chandra et al., 2010; Mishra and Ramaprabhu, 2012; Sheng et al., 2012; Hoan et al., 2016; Yoon et al., 2016; Yoon et al., 2017). There are also report on graphene oxide supported nanoscale zero-valent (GFeN) nanohybrids (Wang et al., 2014a). While each reported work had high process efficiency with >99% arsenic removal, they cannot be compared one-on-one given the non-identical experimental conditions. Each researcher team used different initial arsenic concentration (0.1-25 mg/L), solution pH (5.5-7.0), and adsorbent dose (0.1-0.4 g/L) (Table 2.1). Further, each of the reported nanohybrid had different iron content which might have significantly affected the arsenic removal efficiency. While both the materials (GM and GFeN) appear to be efficient, there is no reported comparison of the nanohybrids under similar experimental conditions. Further, a comparative analysis of the mechanisms of arsenic removal by the two nanohybrids is imperative to better understand the materials and their potential applications for drinking water arsenic removal.

In this study, we evaluated GM and GFeN, bare magnetite (M), and bare nanoscale zero-valent iron (FeNP) for aqueous arsenic removal under similar experimental conditions, and the amount of arsenic removal has been normalized with the amount of iron present in each nanomaterial. The efficiency of arsenic removal by each nanomaterial has been evaluated and the removal mechanism(s) elucidated.

Table 2.1. Experimental conditions for arsenic removal by graphene oxide supported iron nanomaterials.

Adsorbents	**pH***	**Arsenic conc. (mg/L)**	**Adsorbent dose (g/L)**	**Source**
Magnetite-rGO[ǂ]	7	3-7	0.2	(Chandra et al., 2010)
Magnetic-GO	6.5	25	0.4	(Sheng et al., 2012)
NZVI-Reduced GO	7	15	0.4	(Wang et al., 2014a)
GN-α-FeOOH Aerogel	8-9	5	0.05	(Andjelkovic et al., 2015)
β-FeOOH@GO-COOH	6.5	1	3	(Chen et al., 2015)
Fe_3O_4-GO	7	0.15-1	0.1	(Yoon et al., 2016)
Fe_3O_4-non-oxidative GO	7	1	0.1	(Yoon et al., 2017)
FeO_x GO	6.5	0.1	0.8	(Su et al., 2017)
Fe_2O_3 nanocubes-GO aerogel	5	5	0.5	(Yu et al., 2019)

*pH at which the experiment was conducted; [ǂ]rGO: Reduced graphene oxide.

2.2. Experimental methods

2.2.1. Materials and supplies

Graphene oxide (4 g/L in water, monolayer content >95%) was from Graphenea (Spain). Iron(II) chloride tetrahydrate ($FeCl_2 \cdot 4H_2O$, >98% pure), iron(III) chloride hexahydrate ($FeCl_3 \cdot 6H_2O$, 97-99%), ammonium hydroxide (NH_4OH, 30%), ferrous sulfate ($FeSO_4 \cdot 7H_2O$, >99.5%), sodium borohydride ($NaBH_4$, >97%), and other chemicals from VWR (USA). All chemicals were reagent grade and used as received unless otherwise specified. A 1000 mg/L standard stock solution (Environmental Express, USA) was used to prepare various As(III) and As(V) solutions by diluting with deoxygenated deionized (DDI) water.

2.2.2. Material synthesis

2.2.2.1. Preparation of GM and M

Graphene oxide-magnetite (GM) nanohybrids were prepared as per (Yoon et al., 2016). Briefly, 200 mg GO (i.e., 50 mL of 4 mg/L GO solution received from the manufacturer) was mixed within 150 mL DDI water in a 250 mL glass bottle and ultra-sonicated (FS30, Fisher Scientific) for 1 h to disperse the GO. Then the GO solution was transferred into a 300 mL round-bottom reaction flask. The reaction flask was placed in an oil bath connected to a temperature controller assembly (Ace Glass Inc., USA). The oil bath assembly along with the reaction flask was placed on a magnetic stirrer and continuously stirred. The content in the reaction flask was purged with nitrogen gas (N_2) for 30 min to deoxygenate the GO solution. Separately, two solutions of $FeCl_2 \cdot 4H_2O$ (0.4 g) in 0.5 M HCl (10 mL) and $FeCl_3 \bullet 6H_2O$ (1.04 g) in DDI water (20 mL) were prepared in two 50 mL centrifuge tubes and then combined to get an iron solution with a $FeCl_2$:$FeCl_3$ molarity ratio of ~2:1. The mixed iron solution was added slowly to the GO solution in the reaction flask (with continued N_2 purging and stirring). As the pH of the solution was adjusted to 10 by dropwise addition of 30% NH_4OH, the solution became blackish. To facilitate nanoparticle formation, the solution in the reaction flask was cooked for 2 h at 75-80 ^oC with continued N_2 purging and stirring (the open top of the reaction flask was wrapped with an aluminum foil to reduced evaporation losses). The black-colored solution was then transferred to two 50 mL centrifuge tubes and centrifuged at 3000 rpm for 5 min. The nanomaterials precipitated and the supernatant was decanted. The nanoparticles were then washed two times each first with DDI water and then with ethanol (analytical grade) to remove unreacted chemicals. Washing was done by filling up the tubes with DDI water or ethanol and centrifuging them at 3000 rpm for 5 min and then decanting out most of the liquid. The washed

nanomaterials were dried at 40 ^{o}C under a nitrogen environment in a vacuum oven (VWR, USA) for 40 h. The dried nanomaterials (GM nanohybrids here) were ground into powder using an agate pestle and mortar. The powdered nanohybrid was stored in 20 mL glass vials with the headspace flushed with N_2 gas. For bare magnetite (M) preparation, the same procedure was used without the addition of GO.

2.2.2.2. Preparation of GFeN and FeNP

Graphene oxide supported nanoscale zero-valent (GFeN) nanohybrids were synthesized after others (Wang et al., 2014a) with modifications to optimize the pH and borohydride dosing. GO (62.5 mL of 4 g/L GO solution received from the manufacturer = 250 mg) in DDI water (62.5 mL) was exfoliated by ultra-sonication. The GO solution was then transferred into a round-bottom reaction flask (300 mL) and placed on a temperature-controlled oil bath put on a magnetic stirrer for continuous stirring. To deoxygenate the GO solution, the content in the reaction flask was purged with N_2 gas for 30 min. On the side, a $FeSO_4 \cdot 7H_2O$ solution (2.25 g in 50 mL DDI water) was prepared in a volumetric flask (50 mL) and poured into the GO solution very slowly, and the new solution was continuously stirred and purged with N_2 gas for ~30 min. By dropwise addition of 1 M NaOH or HCl, the pH of the GO-Fe solution was adjusted to 6.1 before an aqueous solution of $NaBH_4$ (0.99 g in 30 mL of DDI) was added dropwise to the reaction flask with continuous stirring and N_2 purging on. When the solution turned blackish, the solution temperature was raised to and maintained at 60 ^{o}C for 4 h for the reaction to complete (a black-colored product was formed). The black-colored product was transferred to 50 mL centrifuge tubes for centrifugation (3000 rpm). After centrifugation, the supernatant was decanted, and the black product was washed with a copious amount of DDI water and then with ethanol (two times each). The resulting black solids were vacuum-dried (40 h, 40 ^{o}C, and under

N_2 environment). The dried nanomaterials were GFeN nanohybrids. The nanohybrids were ground using an agate pestle and mortar, and the powers were stored in a 20 mL glass bottle with the headspace flushed with N_2 gas. For bare FENP synthesis, the same procedure was used but without the addition of GO as per our previously published method (Bezbaruah et al., 2013).

2.2.3. Characterization

2.2.3.1. Scanning electron microscopy (SEM)

The GM, M, GFeN, and FeNP samples were characterized with a JEOL JSM-7600F field emission scanning electron microscope (JEOL USA Inc., Peabody, Massachusetts) operated at 2 kV. The samples of nanomaterials were placed on carbon adhesive tabs (Ted Pella, Redding, California USA) attached to aluminum mounts, and the excess material was blown off with a stream of dry N_2 gas. Images were obtained with a JEOL JSM-7600F. Energy dispersive spectroscopy (EDS) data were obtained using an UltraDry silicon drift X-ray detector and NSS-212e NORAN system 7 X-ray microanalysis system (Thermo Fisher Scientific, Madison, Wisconsin).

2.2.3.2. Transmission electron microscopy (TEM)

For TEM analysis, the specific powdered nanomaterial was placed in 100% ethanol and sonicated. A drop of the suspension was placed on a lacey-carbon support film on a 300-mesh copper TEM grid (Ted Pella, Redding, California USA) for 30 sec, then wicked off with a filter paper and allowed to air dry. High-Resolution TEM data were obtained using a JEOL JEM-2100 LaB_6 transmission electron microscope (JEOL USA, Peabody, Massachusetts) ran at 200 kV.

2.2.3.3. X-ray photoelectron spectroscopy (XPS)

The XPS analyses (K-Alpha XPS, ThermoFisher Scientific) were done for the nanomaterials. Powdered samples were packed into small wells of 3 mm diameter and 3 mm

deep. High-resolution scans were made for Fe2p, As3d, C1s, and O1s. The settings were: Pass energy = 50 eV, Dwell Time = 50 ms, spot size = 400 μm, Step size = 0.1 eV for a total of 10 scans per sample. The flood gun was also turned on to prevent charging the samples. Peak fitting was accomplished with the Avantage XPS program.

2.2.3.4. Zeta potential (ζ)

Zeta potential was measured with Zetasizer Nano ZS (Malvern, UK) at pH 7.5. The pH was adjusted to 7.5 dropwise addition of 0.1 N HCl/NaOH after putting nanomaterial in the DDI water.

2.2.3.5. Point-of-zero-charge (PZC)

PZC values were determined for the four materials used. We prepared a 0.01 M NaCl solution and adjusted the pH to the required value (pH 2-12) using 0.1 M NaOH or HCl. A measured amount (20 mg) of the nanomaterials was dispersed in 20 mL NaCl solution with different initial pH (Balistrieri and Murray, 1981; Lataye et al., 2006). The initial (0 h) and the final (48 h) pH values were recorded, and the PZC for each material was calculated by plotting initial pH vs. change in pH (dpH = Initial pH – Final pH). PZC of the adsorbent is the pH when the surface charge on the material is zero and represented by the point where the plot (initial pH vs dpH) intersects the X-axis.

2.2.4. Experimental design

The primary objective of this study was to compare the four selected nanomaterials namely Graphene oxide-magnetite nanohybrid (GM), graphene oxide-nanoscale zero-valent iron nanohybrid (GFeN), bare nano magnetite (M), and bare nanoscale zero-valent iron (FeNP) and screen out which one of these materials work most efficiently for the removal of aqueous As(III) and As(V). As(III) and As(V) were tested in separate batches. Amber glass vials (40 mL) fitted

with a plastic cap and silicon septum were used as batch reactors. Each batch reactor contained 30 mL of arsenic solution (5 mg/L) with 10 mg of adsorbents (~333 mg/L). The reactors were rotated in a custom-made end-over-end shaker (28 rpm) for 24 h at room temperature (22±2 ^{o}C). After 24 h, the reactors were withdrawn from the shaker and the content was filtered using 0.22 µm nylon housing single-use syringe filters (VWR, USA). The filtrate was acidified with concentrated HNO_3 (15.8 N) and kept in the refrigerator for later analysis. The arsenic in the filtrate was measured using a graphite furnace atomic absorption spectrophotometer (GF-AAS, Perkin Elmer AAS 900H). The percent removal efficiency of adsorbents was calculated as percent arsenic removal ($\eta = (C_0 - C_e)/ C_0 * 100\%$ where C_0 is the initial and C_e is the equilibrium arsenic concentration).

The nano-based adsorbents (333 mg/L) used in our experiments did not contain the same amount of iron. While GFeN and GM contained GO, their bare counterparts FENP and M did not, and the amount of iron in each material was different. So, 333 mg of each material used in the batch studies did not contain the same amount of iron (Fe). Therefore, we determined the total iron content in the nanomaterials for the comparison of their removal efficiencies based on the mass of iron (Fe) present. Here, 50 mg of an adsorbent was digested with 15 mL of 7M HCl by first shaking (250 rpm) for 2 h in a 50 mL test tube and then keeping it in a water bath for 1 h at 80 ^{o}C. The digested sample was filtered using a membrane filter (0.22 µm, VWR, USA) and the iron concentration in the filtrate was measured using Flame AAS (Perkin Elmer AAS 900H). The amount of arsenic adsorbed (q_e, mg/g) as per unit iron mass was determined as $q_e = (C_0 - C_e) * V/m$, where V is the volume of solution (L), and m is the mass iron in the adsorbent (g).

2.2.5. Quality control and statistical analysis

All experiments were conducted in triplicates and the average values are reported here along with the standard deviations. GF-AAS was calibrated (R^2>0.999) using a series of standard (0-100 μg/L) arsenic solutions before each instrument measurement run. All data analysis and graphical representation were done in OriginLab (OriginPro) software. ANOVA analysis was done to determine statistically significant differences in data sets and Tukey's pairwise comparison was used to identify the data that were significantly different.

2.3. Results and discussion

2.3.1. Material characterization

The four adsorbents and bare GO were examined under TEM. The GO sheets appeared as crumbled in nature and paper-like structures with irregular shapes (Figure 2.1a). The bare nanoparticles (FeNP and M) exhibited spherical morphology and were agglomerated (Figure 2. 1b-c). The particle size of FeNP ranged between 12.3 and 70.5 nm (n = 20) and for M, it was 6.7 to 20.9 nm (n = 20). On the nanohybrids, the iron nanoparticles (FeNP or M) were well dispersed on the GO surface (Figure 2.1d-f). The particles were not only deposited on the surface of GO but some of the particles were also sandwiched inside the GO layers. The particle size of FeNP deposited on GO in GFeN (Figure 2.1e-f) was 18.1-95.6 nm (n = 31), and for GM (Figure 2.1d), it was 5.5-12.5 nm (n = 22). Similar morphologies of nanohybrids were reported by others (Wang et al., 2014a; Yoon et al., 2016; Das et al., 2020). The SEM-EDS data for bare FeNP (Figure 2.2a) indicated the presence of 84.76% Fe and low oxygen (6.51% O) indicating the presence of elemental Fe (Fe0) in the FeNP particle with a thin oxide layer (core-shell structure). The presence of a very thin (2-4 nm) oxide layer on FeNP was reported by others as well (Martin et al., 2008; Krajangpan et al., 2012). In bare M (Figure 2.2c), the oxygen content was found to

be high (34.98%), and the Fe content (57.80%) was relatively low indicating the formation of iron oxides. Once nanoparticles were deposited on the GO surface (in both GFeN and GM), the total oxygen (O) content increased, and carbon (C) showed up prominently (Figure 2.2b-d) as O and C also came from the GO sheets and the functional groups present.

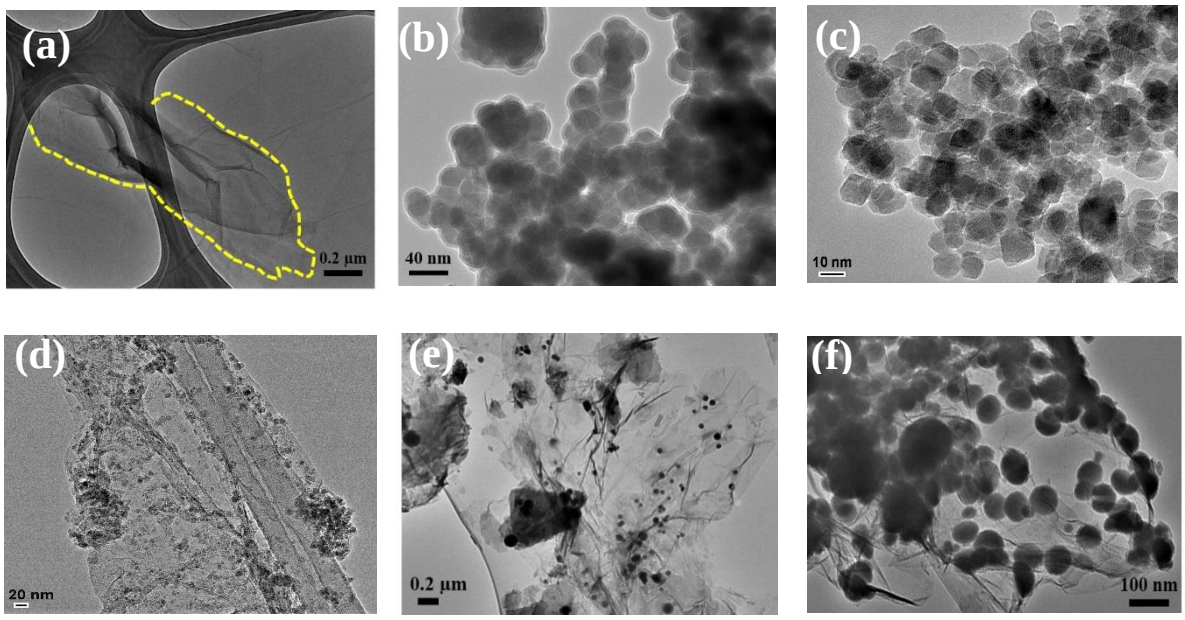

Figure 2.1. TEM micrographs of (a) GO sheet (dotted outline), (b) FeNP, (c) M, (d) GM, (e) GFeN, and (f) HRTEM of GFeN (core-shell structured FeNP particles trapped between GO layers).

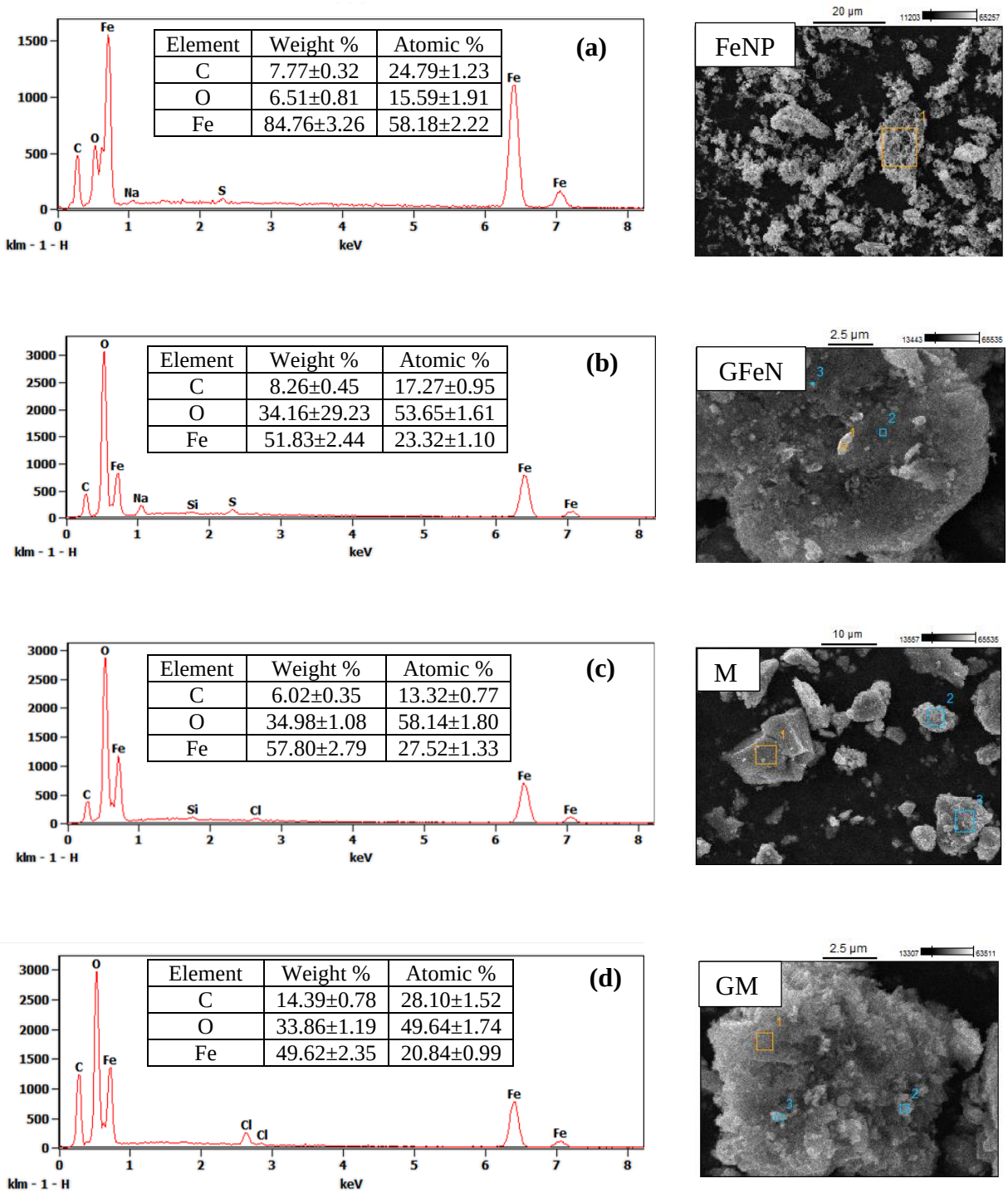

Figure 2.2. SEM-EDS of fresh (a) FeNP, (b) GFeN (c) M (d) GM.

XPS analyses of fresh FeNP (Figure 2.3a) show the presence of both Fe2p and O1s spectra suggesting that the surface layer had both Fe_2O_3 and FeOOH. The Fe2p spectrum

represents the characteristic peak for Fe ($2p_{3/2}$ and $2p_{1/2}$) and the shake-up satellite peaks indicate the existence of Fe(II) and Fe(III). A small peak for metallic iron (Fe^0) was also observed. The existence of a large fraction of iron oxides and a relatively small amount of elemental iron (Fe^0) confirms that the FeNP surface was largely made up of iron oxides. This is in conformity with the core-shell structure of FeNP which is also observed in our HRTEM micrographs (Figure 2.1b) and reported by others (Tucek et al., 2017; Martin et al., 2008). The Fe2P peaks of GFeN (Figure 2.3b) look similar to those of the FeNP sample except that there is no Fe^0 peak. The lack of Fe^0 peak may be due to the thin metal oxide layer and/or GO layer between which nanoparticles were trapped as that might have prevented the XPS beam from reaching the Fe^0 core. However, the core-shell structure is apparent in the HRTEM micrographs of GFeN (Figure 2.1f). Both Fe^{2+} and Fe^{3+} are present in the GFeN with the peak positions suggesting the presence of both Fe_2O_3 and FeOOH with the O1s peaks indicating a higher concentration of bounded OH. In M (Figure 2.3c), the $Fe2p_{3/2}$ and $Fe2p_{1/2}$ peaks confirm that both Fe^{2+} and Fe^{3+} are present, and Fe_3O_4 formation is confirmed from the characteristic peaks of $Fe2p_{3/2}$ at ~711 eV and ~724 eV and the peak of O1s at ~730 eV (Chandra et al., 2010; Yoon et al., 2016). The satellite peak situated at ~719 eV is the characteristic peak of Fe^{3+} in γ-Fe_2O_3 (Grosvenor et al., 2004) suggesting that the M (Fe_3O_4) nanoparticles were partly transformed to maghemite ($Fe_3O_4 + 2H^+ \rightarrow \gamma\text{-}Fe_2O_3 + Fe^{2+} + H_2O$). The O1s peaks confirm the dominance of Fe-O. The peaks from GM (Figure 2.3d) are similar to those from the M indicating the presence of a majority of Fe_3O_4. The XPS analyses confirmed the successful synthesis of the four nanomaterials.

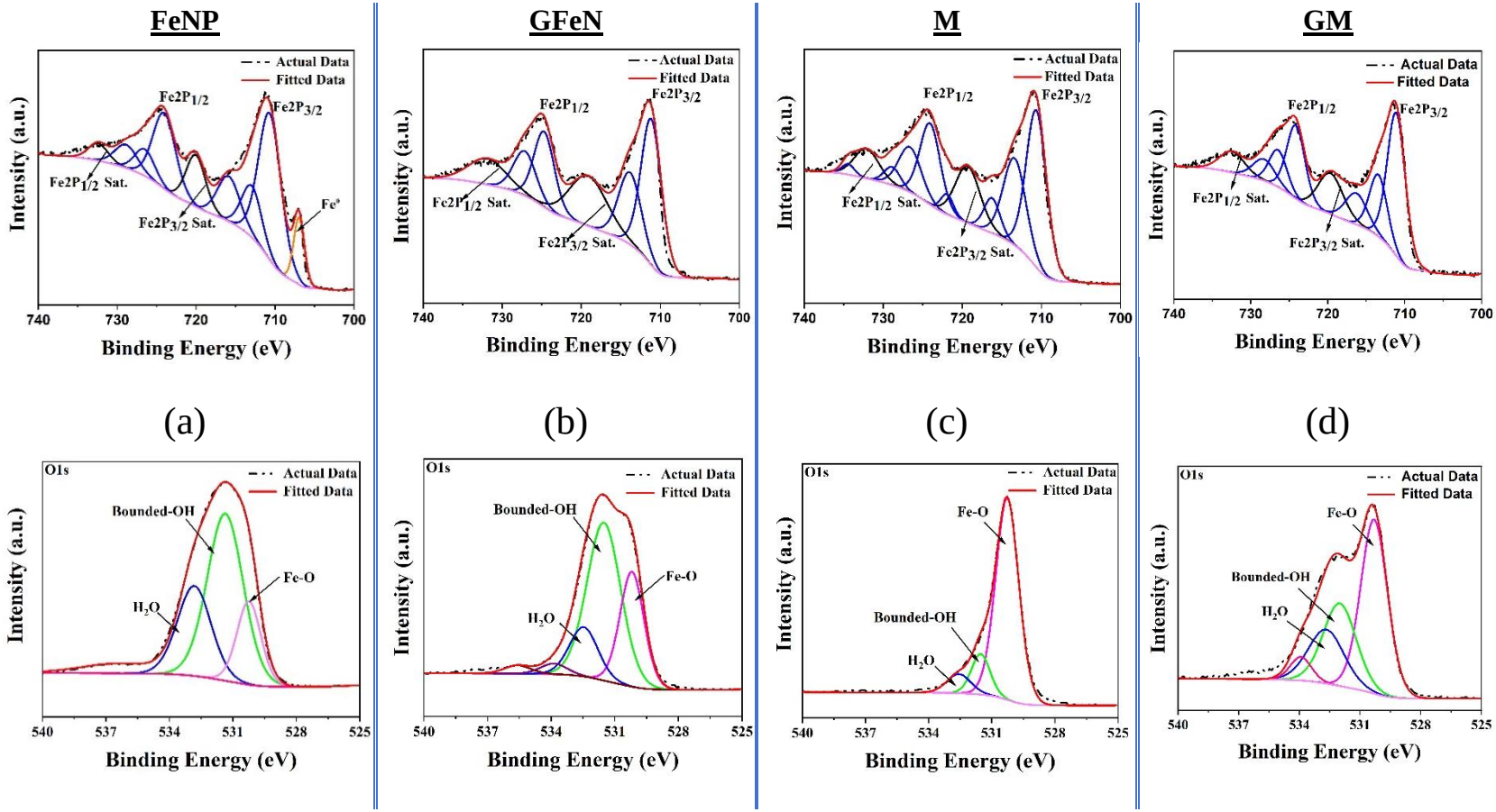

Figure 2.3. High resolution-XPS spectrum of Fe2P and O1s obtained from (a) FeNP (b) GFeN (c) M (d) GM.

2.3.2. Dispersion behavior

Table 2.2. Zeta potential (ζ) and point of zero charge (PZC) the nanomaterials used in this study.

Material	PZC	Mean ζ (mV)	Solution pH*
GO	NM	-41.76±2.27	7.5
FeNP	8.4	13.74±0.59	7.5
M	4.3	10.18±0.72	7.5
GFeN	8.05	-21.02±0.77	7.5
GM	4.8	-17.44±0.85	7.5

NM: Not measured as GO showed no significant arsenic adsorption; *pH of the test solution during ζ measurements

Zeta potential (ζ) is the interfacial potential difference between charged material surface and the counter ions in the surrounding diffuse layer and is a measure of dispersibility of nanomaterials in the aqueous phase. Particles ζ > |±25| mV make a stable suspension (ISO, 2000). The ζ values were measured for FeNP, M, GFeN, and GM as well for bare GO in DI water (Table 2.2). GO with a high negative ζ (−41.76±2.27 mV) remained well disperse (stable) in water. The high ζ values of GO can be attributed to the presence of many functional groups (−COOH,−OH, C−O−C, C=O) on the GO surface which led to the negative surface charge upon ionization in water (Gao, 2015). The bare nanoparticles (FeNP and M) showed very low positive ζ (13.74±0.59 mV for FeNP and 10.18±0.72 mV for M), and they agglomerated and settled down easily. Both the nanohybrids recorded higher ζ (GFeN: −21.02±0.77 mV and GM: −17.44±0.85 mV) than its bare counterparts leading to stable dispersions. There was, however, a reduction of ζ values in the nanohybrids compared to bare GO possibly due to the decrease in functional group and positive charge of iron nanoparticles during metal ion nucleation and because of the presence of positive changes on the surface of the nanoparticles. As the metal ions got attached to the functional groups on the GO surface, some negative charges present on the GO got neutralized leading to the decrease in net ζ values, but the values were still relatively high compared to bare particles (FeNP and M) to achieve much better stable dispersions.

2.3.3. PZC

Solution pH plays an important role in the arsenic removal process by iron-based materials (Wang et al., 2014b; Yoon et al., 2016). The PZC (pH-dependent surface charge properties) values for the four adsorbents varied from 4.3 to 8.4 (Table 2) with the nanohybrids having the PZC values as 8.05 (GFeN) and 4.8 (GM). The surface of the adsorbent is positively charged at pH below the PZC and negatively charged at pH above PZC, and that may major play a role in arsenic removal. The speciation of the arsenic oxyanions is also changed with solution pH (Figure 4). The dominant As(V) species present in aqueous solution are H_3AsO_4 (at pH<2.2), $H_2AsO_4^-$ (pH 2.2-6.9), $HAsO_4^{2-}$ (pH 6.9-11.5), and AsO_4^{3-} (pH > 11.5). On the other hand, As(III) species are present in aqueous media as neutral H_3AsO_3 (pH<9.2) and $H_2AsO_3^-$ (pH>9.3).

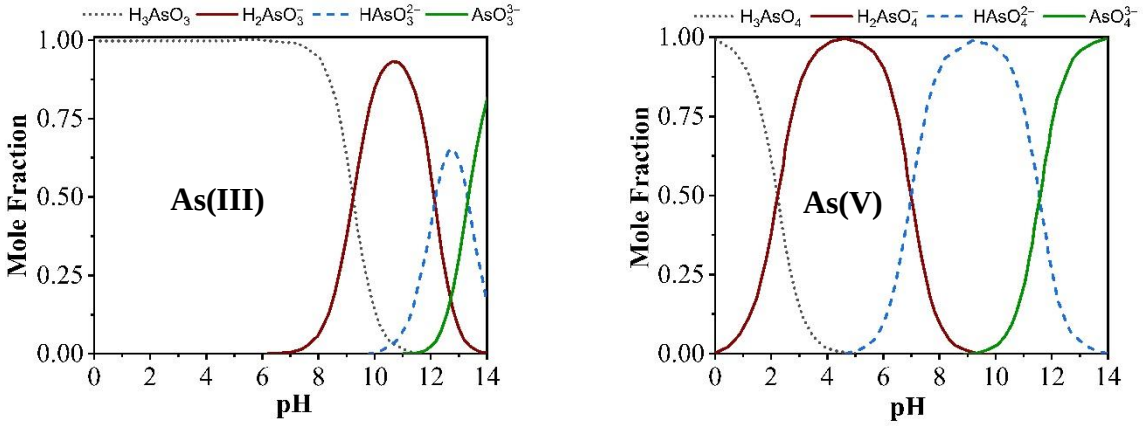

Figure 2.4. Speciation of aqueous arsenic at different pH modified from (Ben Issa et al., 2011).

2.3.4. Arsenic removal

2.3.4.1. As(III)

GFeN and FeNP removed >99% As(III) (initial concentration, C_0 = 5 mg/L) at pH 3-9 (Figure 2.5a). There was no significant difference in As(III) removal by the two nanomaterials (Two-way ANOVA, p = 0.05). The PZC values for both GFeN and FeNP were > 8, yet the

removal efficiency did not change over the wide pH range and that leads us to think that surface complexation might have played a major role in As(III) removal here.

For GM and M, there was an increase in As(III) removal efficiency with the increase in pH (Figure 2.5a). Others (Chandra et al., 2010; Yoon et al., 2016) also reported similar observations. Above the PZC, M (PZC = 4.3) and GM (4.8) becomes negatively charged while As(III) remains mostly neutral (no charge) at pH < 9.2 and without any dominant repulsive force between the adsorbent and As(III), arsenic is still adsorbed onto GM and M. Here, As (III) removal is achieved potentially via surface complexation and ligand exchange. Morin et al. (2009)(Morin et al., 2009) suggested that: (1) There are some vacant tetrahedral sites on the magnetite surface (111), and As (III) can fit into those sites by forming stable ^{3}C tridentate, hexanuclear, corner-sharing surface complexes, and (2) a portion of As(III) precipitates as amorphous Fe-As complex on the surface of magnetite. In the ligand exchange process, the surface hydroxyl groups are replaced by arsenite ions. The amount of surface hydroxyl groups increases with the increased pH (Su et al., 2017) and thus contributing towards increased As(III) removal at higher pH (Kumar and Jiang, 2017).

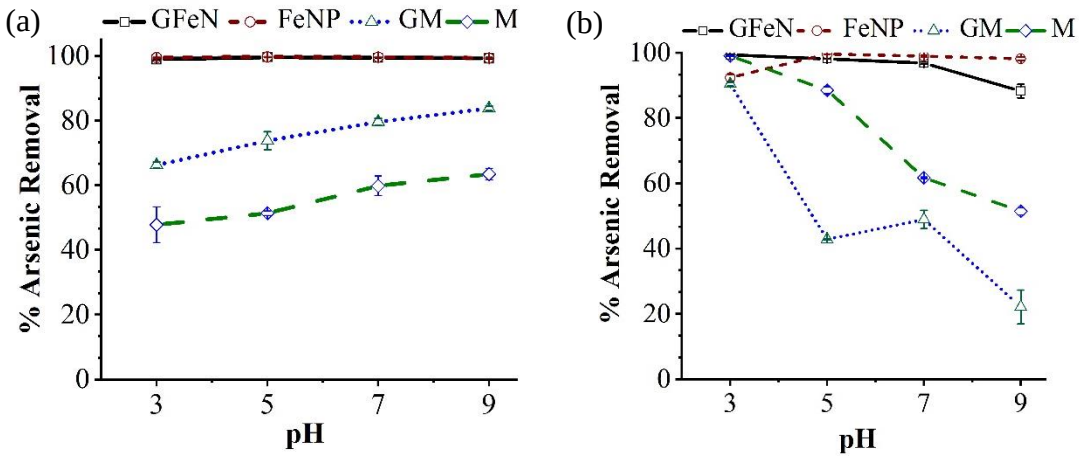

Figure 2.5. Arsenic removal at different pH by four nanomaterials: (a) As(III); note: plots for GFeN and FeNP are overlapped as both have similar removal efficiencies; (b) As(V). Initial arsenic concentration = 5 mg/L, Adsorbent dose = 333 mg/L Reaction Time = 24 h. The vertical error bars represent standard deviations. The data points are joined by straight lines for ease of reading only and do not represent trendlines.

2.3.4.2. As(V)

Both the FeNP based adsorbents, GFeN and FeNP recorded 87-98 % of As(V) removal (C_0 = 5 mg/L) over a wide pH range (3-9) (Figure 2.5b). The maximum As(V) removal efficiency (>98%) was achieved at pH 5-7 (Figure 2.5b). In our experimental pH range As(V) is present as negatively charged oxyanions ($H_2AsO_4^-$ and $HAsO_4^{2-}$). Now, the surfaces of GFeN (PZC 8.05) and FeNP (PZC 8.4) are positively charged when the solution pH is below its PZC value. The negatively charged arsenic ions can be easily adsorbed onto the positively charged material surface through the columbic attraction. The material surfaces remain positive surface due to the protonation of surface hydroxyls present on the iron oxide shell of FeNP. With the increase in solution pH, the amount of positive surface charges would decrease, and the arsenic adsorption onto the surface should decrease. However, there was no significant reduction in As(V) removal (Two-way ANOVA, p = 0.05) at pH 3 through 9 and that indicates that electrostatic attraction is not the only driving force for As(V) removal by GFeN and FeNP. Similar findings were also reported by others literature (Wang et al., 2014a; Wu et al., 2017).

The FeNP is highly reactive, the Fe^0 reacts with water to continuously form iron oxides corrosion products such as FeOOH, Fe_3O_4, and Fe_2O_3. As(V) reacts with freshly generated iron oxide via inner-sphere surface complexation forming monodentate or bidentate complexes. While electrostatic forces play a role at pH below the PZC, arsenic interactions with iron corrosion products on the surface of the FeNP particles apparently play important roles in the As(V) removal process at all pH values. While the surface positive charge decreases with the increase in pH and electrostatic As(V) adsorption goes down, the increased As(V) complexations onto surface corrosion products offset the reduction, and so a consistent high arsenic removal over a wide pH range was observed in this study.

For GM and M, As(V) removal decreased as the pH increased (Figure 2.5b). At pH 3, ~90% As(V) removal was achieved with GM and ~99% with M, and the removal decreased when pH was raised to 9 (only 22% removal by GM and 51% by M). Given that GM and M were relatively more effective at pH below their PZC (4.8 for GM and 4.3 for M), we can infer that electrostatic force was dominant in arsenic removal. At pH higher than PZC, there was a net decrease in positive surface charge on the nanomaterials and so negatively charged As(V) ions were not attracted. Further, at high pH, the competition between As(V) species ($H_2AsO_4^-$ or $HAsO_4^{2-}$) and OH^- ions for adsorption sites might have affected arsenic removal.

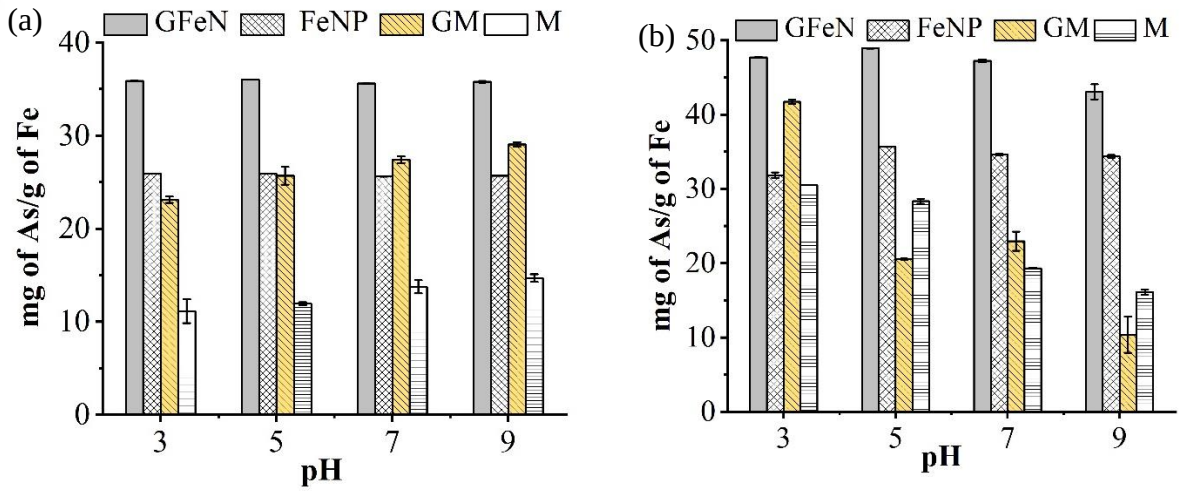

Figure 2.6. Efficacy of arsenic removal based on iron mass present in the four nanomaterials: (a) As(III) and (b) As(V).

2.3.4.3. Comparison of the nanohybrids

2.3.4.3.1. Comparison between nanohybrids and nanoparticles

In our study, we used 333 mg/L of each adsorbent (GFeN, FeNP, GM, and M) without normalizing for the amount of Fe present. We determined the Fe content in the four adsorbents (Table 3) to calculate the amount of arsenic adsorbed per unit mass of Fe (Figure 2.6a-b). The Fe mass normalized data indicate significant improvement in arsenic removal when iron nanoparticles (FeNP, M) are decorated on the GO surface (Table 2.3, Figure 2.6a-b). GFeN removed 10 mg more As(III) per g of material across all pH (3-9) compared to FeNP, and for As(V), the improvement was 11-13 mg at different pH values. As(III) removal by GM improved by 11.9-14.3 mg compared to that by M, and the improvement was ~11.2 mg for As(V). Higher arsenic removal by the nanohybrids (GFeN and GM) was achieved possibly because of their effective dispersion (reduced agglomeration) in aqueous media which ensured improved interaction with the arsenic species.

Table 2.3. Arsenic removal by the nanomaterials used in this study.

Material	Particle Size (nm)+	pH*	Fe content mg/g	As Loading mg/g**	
				As(III)	As(V)
FeNP	12.3-70.5	3-9	0.59	26	32-36
M	6.7-20.9	As(III): 9 As(V): 3	0.66	11.1-14.7	16.1-30.5
GFeN+	18.1-90.5	3-9	0.43	36	43-49
GM+	5.5-12.5	As(III): 9 As(V): 3	0.44	23-29	10.4-41.7

*pH at which >90% arsenic removal was achieved; **mg of As per g of Fe; +Size of the FeNP or M particles deposited on the graphene sheet.

2.3.4.3.2. Comparison between GFeN and GM nanohybrids

Comparison of arsenic removal by GFeN and GM indicates that GFeN is significantly ($p = 0.05$) more efficient than GM. Analysis based on normalized Fe content (Table 2.3, Figure 2.6a-b), GFeN removed ~36 mg As(III)/g of Fe and 43-49 mg As(V)/g, while GM removed 23-29 mg As(III)/g and 10-42 mg As(V)/g. It is known that iron oxides are responsible for arsenic adsorption (iron oxide + arsenic $\rightarrow$ arsenic-iron complex) onto iron nanoparticles (Kanel et al., 2006; Bezbaruah et al., 2013; Wang et al., 2014b; Tucek et al., 2017; Rashid et al., 2020). Higher removal by the FeNP-based material is achieved possibly because of the continuous corrosion leading to fresh iron oxide formation on the nanoparticle surface (shell).

2.3.4.4. Post arsenic sorption XPS analyses of the nanohybrids

The nanohybrids (GFeN and GM) so far worked better than their bare counterparts (FeNP and M), and so XPS spectra were collected after the graphene oxide-iron (GFeN and GM) sorbed arsenic (As(V)/As(III)). The As(V)-sorbed GFeN shows a strong peak at ~ 45.57 eV (Figure 2.7a, As 3d spectra) which is the characteristic peak for As(V). This indicates that As(V) was sorbed onto the surface of GFeN and the oxidation state remained unchanged. In the case of As(III)-sorbed GFeN (Figure 2.7b, As3d spectra), dual oxidation (III/V) states of adsorbed

arsenic were observed with As(V) being more noticeable than As(III). This indicates that most of the As(III) got oxidized to As(V) as they reacted with the surface iron oxide layer of the iron nanoparticles present in GFeN. The adsorption and oxidation of As(III) on the GFeN surface happened simultaneously. The deconvolution of O1s spectrum of As(III) (Figure 2.7b) and As (V) (Figure 2.7a) sorbed GFeN show reduction in surface-bound –OH concentration compared to pristine GFeN. This reveals that arsenic species reacted with surface-bound oxide and hydroxide of the iron nanoparticles present in GFeN and formed inner-sphere arsenic-iron complex. Similar observations were recorded by others for iron nanoparticle and arsenic reactions. (Kanel et al., 2006; Farrell and Chaudhary, 2013; Tucek et al., 2017; Das et al., 2020). For As(V)-sorbed GM, the characteristic peak of As(V) is present at ~ 45.67 eV (Figure 2.7c, As3d spectra) confirming the adsorption of As(V) onto the GM surface, and the oxidation state remained unchanged. In case of As(III)-sorbed GM (Figure 2.7d, As3d spectra), both As(III) and As(V) peaks can be seen with As(III) being more noticeable than As(V). This indicates most of the sorbed As(III) did not get oxidized but only a smaller fraction As(V). This indicates most of the sorbed As(III) did not get oxidized but only a smaller fraction was oxidized to As(V). Iron in GM is present in both Fe^{2+} and Fe^{3+} oxidation states, and the surface-bound Fe^{2+} induces oxidation of As(III) to As(V) either through Fenton reaction (Liu et al., 2015b) or via the formation of Fe(III) oxide-Fe(II)-As(III) surface complexation (Amstaetter et al., 2010; Yan et al., 2012b). In the O1s spectrum for As(III) and As(V) sorbed GM, the concentration of Fe-O and surface-bound hydroxyl changed compared to pristine GM. This also indicates that the arsenic species adsorbed onto the surface iron oxide layer via surface complexation.

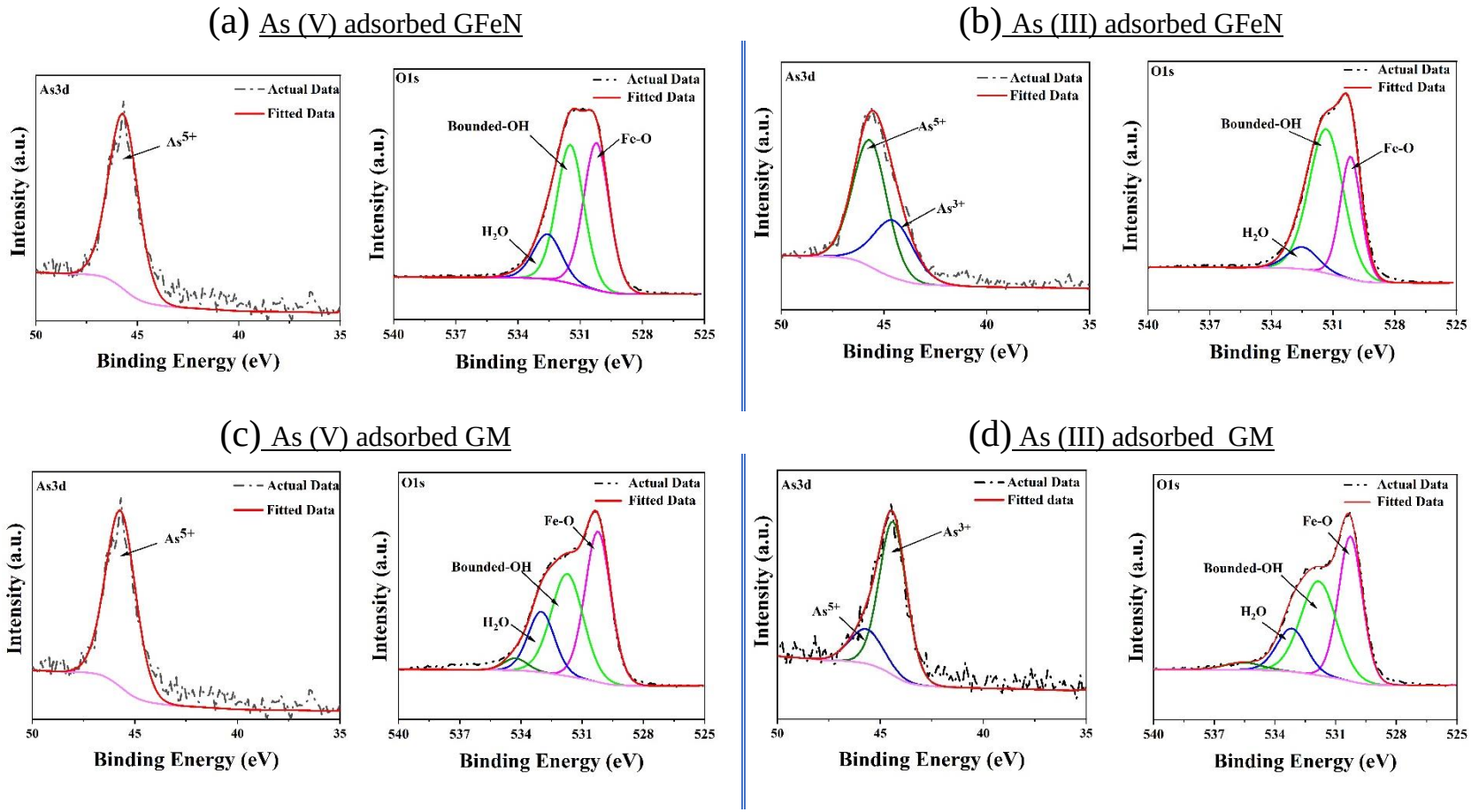

Figure 2.7. As3d and O1s XPS spectra for spent GFeN and GM (i.e., after adsorption of As(V) and As (III)). XPS spectra for GFeN after (a) As(V) adsorption, (b) As(III) adsorption; XPS spectra for GM after (c) As(V) adsorption, (d) As(III) adsorption.

2.3.5. Environmental significance

Both FeNP and magnetite are iron-based nanomaterials that are promoted as promising adsorbents for aqueous arsenic remediation. However, one of the major important aspects of its applicability is its efficiency in real water environments which is overlooked by many. Arsenic is predominately present in As(V) oxidation state and our results suggest that magnetite-based nanomaterials work most efficiently (>90%) at pH below 4 for As(V) removal. So, at typical groundwater pH (6.5-8.5), M-based materials cannot potentially perform to its full potential unless pH adjustment is made, or an increased adsorbent dosing is added at an additional cost to the treatment process. On the contrary, FeNP-based nanomaterials worked equally effectively at all environmentally relevant pH (3-9). Besides, arsenic removed per unit mass of Fe present in FeNP-based nanomaterials is much better than in M-based nanomaterials. FeNP-based materials, specifically the GFeN, hold promise for field applications for the treatment of groundwater contaminated with either or both As(III) and As(V). While M-based nanomaterials may not be effectively and easily used to treat groundwater (pH 6.5-8.5), it may find applications in industrial wastewater or mining drainage water arsenic treatment where solution pH is very low. The manufacturing of iron nanomaterials is energy and cost-intensive process compared to bulk iron-based adsorptive media. While iron nanomaterials are far more efficient and effective and required in less amount, the major roadblock for their actual application is their high production cost. In this study, the synthesized GFeN has exhibited better iron use efficiency (i.e., amount of arsenic removed per unit mass of Fe) and that is expected to lead to cost-saving in terms of materials needed and the size of treatment units. This will make the GFeN-based water treatment systems very sustainable and efficient.

2.4. Conclusions

This study has, for the first time, compared four frequently reported iron-based nanomaterials for arsenic removal under the same experimental conditions, and selected the best candidate for potential field application to remove arsenic from water. The nanoscale zero-valent iron (FeNP)-based material showed better removal performance over a wide range of pH (3-9) for both As(III) and As(V). The authors explored the potential mechanisms of arsenic removal by FeNP-based nanomaterials and opined that arsenic removal was controlled by electrostatic forces and surface complexation. The magnetite (M)-based nanomaterials worked better (>90%) at low pH (pH < 4) only for As(V) with the removal being controlled by electrostatic interactions. On the other hand, As(III) removal by M-based nanomaterials increased with an increase in pH as the process was controlled by ligand exchange and surface complexation. The deposition of nanoparticles on the GO surface (to form nanohybrids) improved arsenic removal significantly in both the nanohybrids (GFeN and GM) compared to their base counterparts (FeNP and M), and this happened because of better dispersion of iron nanoparticles on the GO surface providing better interaction between arsenic species and nanomaterial reactive surfaces. GFeN nanohybrids were found to be the most efficient in terms of arsenic removal per unit mass of iron used and the authors would promote GFeN as a potential candidate for future field application to remove arsenic from groundwater. It is, however, important to recognize that nano-based adsorbents with high arsenic adsorption capacity always pose a concern of secondary contamination through the release (desorption) of arsenic from the adsorbed phase, and so experiments should be conducted on the long-term stability of arsenic in arsenic saturated nanomaterials in actual groundwater.

2.5. References

Amini M, Abbaspour KC, Berg M, Winkel L, Hug SJ, Hoehn E, et al. Statistical modeling of global geogenic arsenic contamination in groundwater. Environmental Science & Technology 2008; 42: 3669-3675.

ATSDR. Toxicological profile for arsenic. Agency for Toxic Substances and Disease Registry, Division of Toxicology, Atlanta, GA 2007.

Balistrieri LS, Murray JW. The Surface-Chemistry Of Goethite (Alpha-Feooh) In Major Ion Seawater. American Journal of Science 1981; 281: 788-806.

Bezbaruah AN, Kalita H, Almeelbi T, Capecchi CL, Jacob DL, Ugrinov AG, et al. Ca-alginate-entrapped nanoscale iron: arsenic treatability and mechanism studies. Journal of Nanoparticle Research 2013; 16.

Chandra V, Park J, Chun Y, Lee JW, Hwang I-C, Kim KS. Water-Dispersible Magnetite-Reduced Graphene Oxide Composites for Arsenic Removal. ACS Nano 2010; 4: 3979-3986.

Das TK, Sakthivel TS, Jeyaranjan A, Seal S, Bezbaruah AN. Ultra-high arsenic adsorption by graphene oxide iron nanohybrid: Removal mechanisms and potential applications. Chemosphere 2020; 253.

Gao W. The chemistry of graphene oxide. Graphene oxide. Springer, 2015, pp. 61-95.

Hoan NTV, Thu NTA, Van Duc H, Cuong ND, Khieu DQ, Vo V. Fe3O4/Reduced Graphene Oxide Nanocomposite: Synthesis and Its Application for Toxic Metal Ion Removal. Journal of Chemistry 2016: 10.

ISO B. 14887 (2000) Sample preparation—dispersing procedures for powders in liquids. International organization for standardization, Geneva, Switzerland 2000.

Kanel SR, Greneche J-M, Choi H. Arsenic (V) removal from groundwater using nano scale zero-valent iron as a colloidal reactive barrier material. Environmental science & technology 2006; 40: 2045-2050.

Krajangpan S, Kalita H, Chisholm BJ, Bezbaruah AN. Iron Nanoparticles Coated with Amphiphilic Polysiloxane Graft Copolymers: Dispersibility and Contaminant Treatability. Environmental Science & Technology 2012; 46: 10130-10136.

Kumar ASK, Jiang SJ. Synthesis of magnetically separable and recyclable magnetic nanoparticles decorated with beta-cyclodextrin functionalized graphene oxide an excellent adsorption of As(V)/(III). Journal of Molecular Liquids 2017; 237: 387-401.

Lata S, Samadder SR. Removal of arsenic from water using nano adsorbents and challenges: A review. Journal of Environmental Management 2016; 166: 387-406.

Lataye DH, Mishra IM, Mall ID. Removal of pyridine from aqueous solution by adsorption on bagasse fly ash. Industrial & Engineering Chemistry Research 2006; 45: 3934-3943.

Liu J, Jiang J, Meng Y, Aihemaiti A, Xu Y, Xiang H, et al. Preparation, environmental application and prospect of biochar-supported metal nanoparticles: A review. Journal of Hazardous Materials 2020: 122026.

Martin JE, Herzing AA, Yan WL, Li XQ, Koel BE, Kiely CJ, et al. Determination of the oxide layer thickness in core-shell zerovalent iron nanoparticles. Langmuir 2008; 24: 4329-4334.

Mishra AK, Ramaprabhu S. Ultrahigh arsenic sorption using iron oxide-graphene nanocomposite supercapacitor assembly. Journal of Applied Physics 2012; 112.

Morin G, Wang YH, Ona-Nguema G, Juillot F, Calas G, Menguy N, et al. EXAFS and HRTEM Evidence for As(III)-Containing Surface Precipitates on Nanocrystalline Magnetite: Implications for As Sequestration. Langmuir 2009; 25: 9119-9128.

Murcott S. Arsenic contamination in the world: IWA publishing, 2012.

Podgorski J, Berg M. Global threat of arsenic in groundwater. Science 2020; 368: 845-+.

Rashid US, Saini-Eidukat B, Bezbaruah AN. Modeling arsenic removal by nanoscale zero-valent iron. Environmental Monitoring and Assessment 2020; 192.

Sheng GD, Li YM, Yang X, Ren XM, Yang ST, Hu J, et al. Efficient removal of arsenate by versatile magnetic graphene oxide composites. RSC Advances 2012; 2: 12400-12407.

Sherlala AIA, Raman AAA, Bello MM, Asghar A. A review of the applications of organo-functionalized magnetic graphene oxide nanocomposites for heavy metal adsorption. Chemosphere 2018; 193: 1004-1017.

Siddiqui SI, Naushad M, Chaudhry SA. Promising prospects of nanomaterials for arsenic water remediation: A comprehensive review. Process Safety and Environmental Protection 2019; 126: 60-97.

Su H, Ye ZB, Hmidi N. High-performance iron oxide-graphene oxide nanocomposite adsorbents for arsenic removal. Colloids and Surfaces a-Physicochemical and Engineering Aspects 2017; 522: 161-172.

Tucek J, Prucek R, Kolarik J, Zoppellaro G, Petr M, Filip J, et al. Zero-Valent Iron Nanoparticles Reduce Arsenites and Arsenates to As(0) Firmly Embedded in Core-Shell Superstructure: Challenging Strategy of Arsenic Treatment under Anoxic Conditions. ACS Sustainable Chemistry & Engineering 2017; 5: 3027-3038.

USEPA. National primary drinking water regulations; arsenic and clarifications to compliance and new source contaminants monitoring. Fed Reg 2001; 66: 6975-7066.

Wang C, Luo HJ, Zhang ZL, Wu Y, Zhang J, Chen SW. Removal of As(III) and As(V) from aqueous solutions using nanoscale zero valent iron-reduced graphite oxide modified composites. Journal of Hazardous Materials 2014a; 268: 124-131.

Wang YH, Morin G, Ona-Nguema G, Brown GE. Arsenic(III) and Arsenic(V) Speciation during Transformation of Lepidocrocite to Magnetite. Environmental Science & Technology 2014b; 48: 14282-14290.

WHO. Arsenic in drinking-water: background document for development of WHO guidelines for drinking-water quality. World Health Organization, 2003.

WHO. Arsenic. WHO. 2018. World Health Organization, 2017.

Wong WW, Wong HY, Badruzzaman ABM, Goh HH, Zaman M. Recent advances in exploitation of nanomaterial for arsenic removal from water: a review. Nanotechnology 2017; 28.

Wu C, Tu JW, Liu WZ, Zhang J, Chu SQ, Lu GN, et al. The double influence mechanism of pH on arsenic removal by nano zero-valent iron: electrostatic interactions and the corrosion of Fe-0. Environmental Science-Nano 2017; 4: 1544-1552.

Yang X, Xia L, Song S. Arsenic adsorption from water using graphene-based materials as adsorbents: A Critical Review. Surface Review and Letters 2017; 24.

Yoon Y, Park WK, Hwang TM, Yoon DH, Yang WS, Kang JW. Comparative evaluation of magnetite-graphene oxide and magnetite-reduced graphene oxide composite for As(III) and As(V) removal. Journal of Hazardous Materials 2016; 304: 196-204.

Yoon Y, Zheng M, Ahn Y-T, Park WK, Yang WS, Kang J-W. Synthesis of magnetite/non-oxidative graphene composites and their application for arsenic removal. Separation and Purification Technology 2017; 178: 40-48.

CHAPTER 3. ULTRA-HIGH ARSENIC ADSORPTION BY GRAPHENE OXIDE IRON NANOHYBRID: REMOVAL MECHANISMS AND POTENTIAL APPLICATIONS[2]

3.1. Introduction

Arsenic (As) is predominately a naturally occurring (geogenic) metalloid present in water (Meharg and Zhao, 2012). Inorganic arsenic in both As(III) and As(V) is the most prevalent species in groundwater. The maximum contaminant level (MCL) for total arsenic in drinking water is 10 µg/L (USEPA, 2001; WHO, 2003). Arsenic contamination of drinking water is a major public health concern across the globe and has affected more than 200 million people across 50 countries with Bangladesh, India, Argentina, Canada, Chile, Japan, and Taiwan being most affected (Murcott, 2012; WHO, 2018). About 2.1 million people in the United States who rely on domestic wells for their drinking water are in danger of facing arsenic contamination (>10 µg/L) (Ayotte et al., 2017). Excess arsenic in drinking water causes several health problems including skin lesions, respiratory problems, neurological complications, and circulatory disorders (Chen et al., 2009). Consumption of water high in arsenic may lead to cancers of the skin and internal organs (liver, kidney, lung, and bladder) (WHO, 2018).

While adsorption is the most adopted method for arsenic removal, coagulation, flocculation, precipitation, ion exchange, and membrane filtration are also used. An ideal

[2] This chapter has been published as a peer-reviewed paper in *Chemosphere* (2020). Das, T.K., Sakthivel, T.S., Jeyaranjan, A., Seal, S. and Bezbaruah, A.N., 2020. Ultra-high arsenic adsorption by graphene oxide iron nanohybrid: Removal mechanisms and potential applications. *Chemosphere*, 253, p.126702.

The material in this chapter was co-authored by Tonoy K Das, Dr. Tamil S.Sakthivel, Dr. Aadithya Jeyaranjan, Dr. Sudipta Seal, and Dr. Achintya Bezbaruah. Tonoy had primary responsibility for conceptualizing the study and developing the methodology. Tonoy designed and conducted all material development, batch experiments, analyzed all the data, and investigated the results. Tonoy also drafted and revised all versions of this chapter. Dr. Tamil S Sakthivel, Dr. Aadithya Jeyaranjan, Dr Sudipta Seal helped in proofreading, checked all results and analysis conducted by Tonoy. Dr. Achintya served as superviser, proofreader and checked all the results and analysis conducted by Tonoy

adsorbent should have high adsorption capacity, an affinity for both the inorganic arsenic species (As(III) and As(V)) and should be effective under relevant environmental conditions.

Among several adsorbents, iron (Fe) based adsorbents are very effective and widely used to remove arsenic (Hao et al., 2018). Nanomaterials, mostly nano magnetite (M) and nanoscale zero-valent iron (Bezbaruah et al., 2013; Ling and Zhang, 2014; Tucek et al., 2017; Xu et al., 2019), are effective for arsenic removal because of their very high specific surface area and good adsorption capacity. However, these particles agglomerate easily and get oxidized rapidly (Krajangpan et al., 2012; Stefaniuk et al., 2016). Embedding iron nanoparticles (FeNPs) on sheets of carbonaceous materials enhances aqueous dispersion of the nanoparticles (Ma et al., 2013; Mortazavian et al., 2018), and graphene-based materials are found to be one of the most promising carbonaceous materials for such applications (Wang et al., 2013; Yoon et al., 2016). Graphene oxide (GO) based nanohybrid produced with iron nanoparticles deposited on GO showed improved dispersion behavior in water (Chandra et al., 2010; Huong et al., 2016; Yoon et al., 2016). GO is a 2D carbon sheet with sp^2 hybridization with a very high specific surface area (320-940 $m^2 g^{-1}$) (Gao, 2015; Perreault et al., 2015). GO also contains a large number of hydrophilic groups (−OH, −COOH, C=O), and so has good dispersibility in aqueous media (Gao, 2015; Perreault et al., 2015). The functional groups in the GO sheet also act as the nucleation sites for nanomaterial formation and facilitate a higher number of nanoparticles to be dispersedly deposited on the GO surface (Wang et al., 2010; Tang et al., 2011). Dispersed deposition of nanoparticles ensures that the surface area of each deposited nanoparticle is available for reaction with the target contaminants. Such GO-nanohybrids are reported to be good adsorbents for various contaminants (Wang et al., 2013; Guo et al., 2014).

The use of GO-iron nanohybrids is reported for metal and metalloid removal including arsenic (Luo et al., 2012; Guo et al., 2014; Hoan et al., 2016; Ren et al., 2018). The most-reported GO-iron nanohybrid for arsenic removal is GO-Fe_3O_4 (Chandra et al., 2010; Yoon et al., 2016; Liang et al., 2019). There is also limited reporting on the use of GO-Fe^0 nanohybrid for arsenic removal (Wang et al., 2014a). The reported GO-iron nanohybrids (Table 3.1) have shown limited arsenic removal capacity (6-180 mg/g) and that limits the potential life span of the arsenic removal systems to be fabricated with these nanohybrids. To enhance the removal capacity, an iron-based nanoparticle decorated on the GO surface can potentially be used. GO-Fe nanohybrids offer such an architecture where the nanoparticles are well dispersed (less agglomerated) and, hence, will have enhanced contaminant removal efficiency. The GO layer will mediate electron transfer through the initial storage of released electrons (due to iron oxidation) and late release of electrons back to the iron nanoparticles. If a core-shell structured iron nanoparticle is used with GO, then the core-shell structure will be protected due to active electron transfer and the effective life of the GO-Fe nanohybrid will be extended. For ease of operation and maintenance, we need a treatment system that can run for a longer period of time before any maintenance intervention is needed. Further, the mechanisms of arsenic removal by these hybrid materials are not well investigated and understood.

In this study, we synthesized a GO iron nanohybrid (GFeN) using a sol-gel process where iron/iron oxide (Fe/Fe_xO_y) nanoparticles were decorated on the surface of GO. The new material was tested for its arsenic removal efficiency at environmentally relevant conditions and its field application potential was evaluated. Based on reaction kinetics, isotherm parameters, and characterization information, we have elucidated the possible arsenic removal mechanisms. We also investigated the potential role of the GO sheet in arsenic removal by GFeN.

Table 3.1. Graphene oxide iron (GO-Fe) nanohybrids used for aqueous arsenic removal.

Adsorbents	pH	Initial arsenic concentration range (mg/L)	Adsorbent dose (g/L)	Adsorption capacities (mg/g)		Source
				As (III)	As(V)	
Magnetite-rGO ǂ	7	3-7	0.2	13.10	5.83	(Chandra et al., 2010)
Fe_3O_4-GO	7	0-550	0.1	85	38	(Yoon et al., 2016)
Fe_3O_4-rGO ǂ	7	0-550	0.1	57	12	(Yoon et al., 2016)
Fe_3O_4-non-oxidative GO	7	0-550	0.1	38	14	(Yoon et al., 2017)
Magnetic-GO	6.5	0-35	0.4		59.6	(Sheng et al., 2012)
Iron oxide-rGO ǂ	5.5-6	20-100	0.2		54.48	(Hoan et al., 2016)
Fe_3O_4-HEG super capacitor *		50-300		180	172	(Mishra and Ramaprabhu, 2012)
Fe_3O_4-GO aerogel	7	0-25	0.2		40.05	(Ye et al., 2015)
NZVI-rGO ǂ	7	1-15	0.4	35.83	29.04	(Wang et al., 2014a)

ǂ rGO: Reduced graphene oxide; *HEG super-capacitor: Hydrogen exfoliated graphene super-capacitor

3.2. Experimental methods

3.2.1. Materials and supplies

Graphene oxide in water (4 g/L, monolayer content >95%) was obtained from Graphena, (Spain), ferrous sulfate ($FeSO_4 \cdot 7H_2O$, >99.5% pure), sodium borohydride ($NaBH_4$, >97% pure), and other chemicals were reagent grade and purchased from VWR (USA). All chemicals were used as received unless otherwise specified. As(III) and As(V) solutions used in this experiment were prepared using individual 1000 mg/L standard stock solutions (Environmental Express, USA). Deoxygenated deionized (DDI) water was used in this research.

3.2.2. Material synthesis

GFeN synthesis was done using a sol-gel process. The graphene oxide iron nanohybrid (GFeN) synthesis process was optimized for solution pH and borohydride dosing (Wang et al., 2014a). GO (250 mg i.e., 62.5 mL of 4 mg GO/mL solution) was exfoliated in 62.5 mL DDI water by ultra-sonication (1 h). Then the GO solution was transferred to a 300 mL round-bottom reaction flask. The reaction flask was placed on an oil bath connected to a temperature control

assembly. The oil bath assembly along with the reaction flask was placed on a magnetic stirrer and the GO solution continuously stirred. Simultaneously, the content in the reaction flask was purged with nitrogen gas (N_2) for the first 30 min to deoxygenate the GO solution. Separately, $FeSO_4 \cdot 7H_2O$ (2.25 g) was dissolved in DDI water (50 mL) in a volumetric flask and poured into the GO solution very slowly, and the mixture was kept continuously stirred and purged with nitrogen gas for 25-30 min. The pH of the GO-iron solution was adjusted to 6.1 by dropwise addition of 1 M NaOH or HCl, and then an aqueous solution of $NaBH_4$ (0.99 g in 30 mL of DDI water) was added dropwise to the reaction flask using a burette with continuous stirring and N_2 purging. At this time, the solution turned blackish, and the solution temperature was then raised to 60 ºC and maintained at that temperature for 4 h to ensure the completion of the reaction (black-colored product formed). The solution containing the black-colored product was transferred to a 50 mL centrifuge tube and centrifuged to separate the product. The supernatant was decanted, and the black product was washed with a copious amount of DDI water and then with ethanol (two times) to remove unreacted chemicals. The resulting black solids were vacuum-dried at 40 ºC under a nitrogen environment for 40 h. The dried product was ground to powders using an agate pestle and mortar to get graphene oxide iron nanohybrid (GFeN). The synthesized GFeN was stored for future use in a 20 mL glass bottle with the head space flushed with nitrogen gas. The yield of GFeN in the process was 650 ± 30 mg which was ~27% (based on total raw materials used). Iron nanoparticles (FeNPs) were also synthesized and stored using the same procedure (as in GFeN) but without the addition of GO and were used in control experiments.

3.2.3. Characterization

3.2.3.1. Transmission electron microscopy (TEM)

Transmission electron microscopy (TEM) images were obtained using a JEOL JEM-2100 LaB_6 transmission electron microscope (JEOL USA, Peabody, MA, USA) operated at 200 kV. For TEM analysis, the specific nanomaterial was placed in 100% ethanol and sonicated. A drop of the suspension was placed on a lacey-carbon support film on a 300-mesh copper TEM grid (Ted Pella, Redding, California USA) for 30 seconds, then wicked off with a filter paper and allowed to air dry. High-Resolution TEM data were obtained using a JEOL JEM-2100 LaB_6 transmission electron microscope (JEOL USA, Peabody, Massachusetts) ran at 200 kV.

3.2.3.2. XPS analysis

High-Resolution X-ray Photoelectron Spectroscopy (HR-XPS) analysis was performed on a Thermo Fisher ESCALAB 250Xi spectrometer (Thermo Fisher Scientific, Waltham, MA USA) with a monochromated Al Kα X-beams ($h\nu$ = 1486.7 eV). The specimens were set in the HR-XPS examination chamber ($5x10^{-9}$ Torr) where spectra for Fe2p, As3d, C1s, and O1s were recorded. Each of Fe2p, As3d, C1s, and O1s spectrum was aligned against the estimation of 284.6 eV binding energy (BE) for extrinsic carbon identified during the C1s scan. Peak fitting was accomplished by utilizing the Avantage XPS program. In the peak fitting method, a Smart background was chosen to represent inelastic scattering, and all peaks were depicted utilizing a Gaussian/Lorentzian proportion of 70/30. A Zetasizer Nano ZS (Malvern Panalytical Ltd, Malvern, UK) was used to measure zeta potential. The samples were vacuum degassed at 80 °C for 12 h and then the specific surface area measurements were done using a Quantachrome Nova-e surface area analyzer.

3.2.4. Batch studies

Amber glass vials (40 mL) fitted with a plastic cap and silicon septum were used as batch reactors. To understand the effects of pH on arsenic removal by GFeN, batch reactors with As(III) or As(V) (30 mL of 5 mg As/L with 10 mg of nanomaterials) were prepared and the initial solution pH was adjusted with 0.1 M HCl or 0.1M NaOH without any additional buffering and pH adjustment during the experiment. For all other studies, an adsorbent (GFeN) dose of 250 mg/L (10 mg in 40 mL) was used in a 60 mL amber glass vial containing different initial As(III) or As(V) concentrations at initial solution pH at 7. The reactors were rotated in a custom-made end-over-end shaker (28 rpm) at room temperature (22 ± 2 ºC, except in the temperature study) for 24 h. The adsorbent was filtered out from the bulk solution using 0.22 µm syringe filters (VWR, USA) and the filtrate was stored in 1 % HNO_3 for later arsenic analysis using a Graphite Furnace-Atomic Absorption Spectrophotometer (GF-AAS, Perkin Elmer AAS 900H, Waltham, MA, USA). The amount of arsenic adsorbed (q_e, mg/g) onto the adsorbent was calculated (Eq. 1). Isotherm and kinetic studies were conducted, and the effects of temperature and interferences by coexisting ions and compounds were investigated (method details in SI).

$$q_e = (C_0 - C_e) \times {}^{V}/_{m} \quad (1)$$

where, q_e, is the amount of arsenic adsorbed (mg/g) by the adsorbent, C_0 is the initial and C_e is the equilibrium arsenic concentration in the solution (mg/L), V is the volume of bulk solution (L), and m is the mass of the adsorbent (g) used.

3.2.4.1. Kinetic studies

For the kinetic studies, C_0 = 5 mg As/L was used, and multiples reactors were run for 24 h. At least three sacrificial reactors were withdrawn at definite time intervals (0.5, 1, 2, 4, 6, 8, 12, 16, 20, 24 h), and the arsenic concentration in the bulk solution was measured. The

concentration data (average of three values at each time point) were used for reaction order determination.

The linearized forms of pseudo-first-order (Eq. 2) and pseudo-second-order (Eq. 3) models (Ho and McKay, 1998) are given below.

$$\log(q_e - q_t) = log q_e - \frac{k_1 t}{2.303} \quad (2)$$

$$\frac{t}{q_t} = \frac{1}{k_2 q_e^2} + \frac{t}{q_e} \quad (3)$$

For Eqs. 2-3, q_e (mg/g) is the equilibrium adsorption capacity of the adsorbent, and q_t (mg/g) is the adsorption capacity at time t. k_1 (min^{-1}) is the rate constant for the pseudo-first-order reaction model, and K_2 (g/mg/min) is the rate constant for the pseudo-second-order reaction model. The $\log(q_e - q_t)$ vs t plot gives the value of k_1 and q_e for pseudo-first-order reaction. For pseudo-second-order reaction, t/q_t vs t data were plotted and q_e and K_2 were determined from the slope and the Y-intercept.

3.2.4.2. Isotherm studies

Isotherm studies for GFeN were carried out with 40 mL of As(III) or As(V) in 60 mL amber glass vials (reactors). The initial arsenic concentration (C_0) was varied from 0.077 to 553 mg/L. A measured amount (250 mg/L) of GFeN was used and the initial pH was adjusted to 7 with dropwise addition of 0.1 M NaOH or HCl under stirring condition. At least replicates were run for each concentration of arsenic. The reactors were put in an end-over-end shaker for 24 h. The content in each reactor was filtered using a 0.22 µm disposable syringe filter (VWR, USA), and the As content in the filtrate was measured with a GF-AAS (Perkin Elmer AAS 900H). The results were used to prepare the q_e vs C_e plot (q_e = equilibrium adsorption capacity; C_e = equilibrium concentration). The experiment was terminated once a plateau (with at least three

consecutive similar q_e data points) was achieved. The data obtained from the isotherm studies were fitted onto Langmuir and Freundlich isotherm models.

The Langmuir model is expressed as:

$$q_e = \frac{q_{max}\, C_e\, K_l}{1+K_l C_e} \quad (4)$$

The Freundlich isotherm model is expressed as:

$$q_e = k_f \sqrt[n]{Ce} \quad (5)$$

In Eqs. 4-5, q_{max} (mg/g) represents the maximum adsorption capacity, k_l (L/mg) is the Langmuir constant (which represents the affinity between the solute and adsorbent), k_f is the Freundlich constant, and 1/n is the adsorption intensity ($1 < n < 10$). The Langmuir model represents monolayer adsorption whereas if the data fit onto the Freundlich then surface heterogeneity of adsorbent will be significant.

The dimensionless parameter of the equilibrium or sorption intensity (R_L), calculated using the sorption constant K_l and the initial concentration of arsenic (C_0), indicates whether the adsorption of the contaminant (arsenic here) by the adsorbent (GFeN here) is: unfavorable if $R_L > 1$ and favorable if $0 < R_L < 1$ (Weber and Chakravorti, 1974).

$$\mathrm{RL} = \frac{1}{1+C_0\, K_l} \quad (6)$$

3.2.4.3. Interference studies

To understand how arsenic adsorption behavior of GFeN would change in the presence of coexisting ions and compounds, a separate set of studies were conducted for As(III) and As(V). To maintain equal ionic strength, arsenic solution (C_0 = 5 mg/L) was prepared using 0.01M NaCl solution. The concentrations of potential coexisting ions (phosphate (PO_4^{3-}), bicarbonate (HCO_3^-), nitrate (NO_3^-), silicate (SiO_3^{2-}), or sulfate (SO_4^-)) were varied from 0 to 10 mM and that of humic acid was varied from 0 to 10 mg/L.

3.2.4.4. Temperature studies

Temperature studies (4-45 ºC) were conducted in an environmental chamber (Walk-in Environmental Chamber, FutureDesign, USA) to know the effect of temperature on As(III) and As(V) removal by GFeN. To attain the specific solution temperature, the prepared arsenic solution (C_0 = 5 mg/L) was kept at the specified temperature in the environmental chamber at least for 12 h before the start of each batch experiment.

3.2.5. Quality control and statistical analysis

All experiments were conducted in triplicates and the average values are reported here along with the standard deviations. ANOVA analysis was done to determine statistically significant differences in data sets and Tukey's pairwise comparison was used to identify the data that were significantly different.

3.3. Results and discussion

3.3.1. Material characterization

TEM micrographs show that the fresh (unused) GO sheets (Figure 3.1a) are irregular in shape and a few micrometers in size (~0.51 µm in the shorter direction and ~4.10 µm in the longer direction) and folded in nature. Similar observations were made by others (Wang et al., 2014a; Yoon et al., 2016). The bare FeNPs are found to be spherical in shape and clustered together (diameter = 15.3-65.3 nm, n = 31, Figure 3.1b). GFeN (Figure 3.1c) has nanoparticles decorated on the GO sheets and the particles are well dispersed. The FeNPs decorated on GO (GFeN) have a size distribution of 21.1-88.5 nm (n = 50). Careful observation of the nanohybrid (GFeN) indicates that the nanoparticles are not only deposited on the GO surface but also trapped in between the GO sheets (Figure 3.1c-d). The BET specific surface area of GO was found to be 252.12 m^2/g, and it was 88.18 m^2/g for FeNP and 159.62 m^2/g for GFeN.

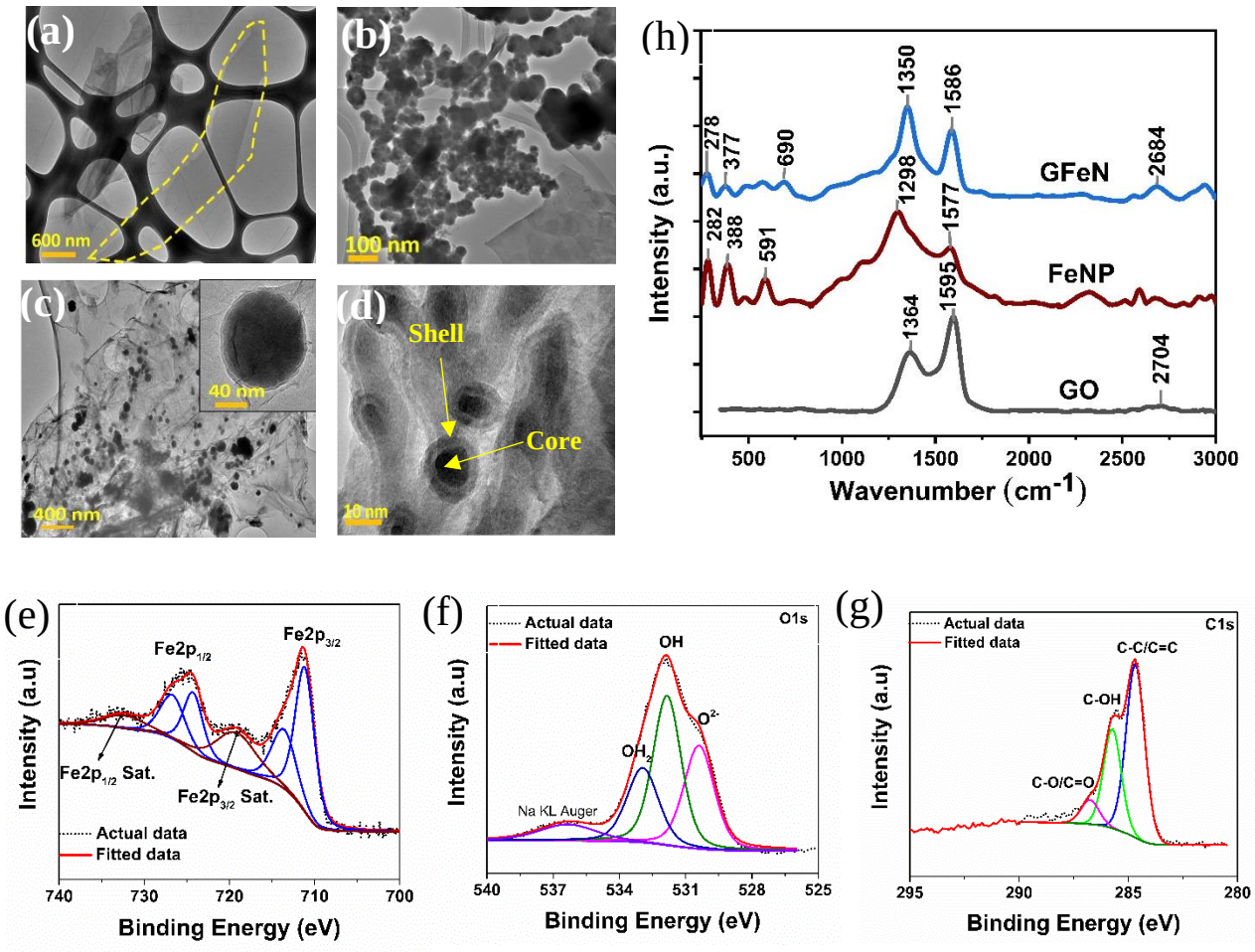

Figure 3.1. TEM micrographs (a-d) of (a) a GO sheet (dotted outline, looks irregular in shape and has layered structure), (b) FeNPs synthesized separately (not on GO), and they appear agglomerated, (c) GFeN where nanoparticles are seen dispersed on GO surface (Inset: single FeNP particle on GO), and (d) GFeN where core-shell structured FeNPs and FeNPs trapped between GO layers can be seen. High resolution-XPS spectrum (e-g) obtained from GFeN for (e) Fe 2p, (f) O1s, and (g) C1s. Fe 2p and O1s indicate that the oxidized surface of GFeN has both FeOOH and Fe_2O_3/Fe_3O_4 with FeOOH being predominant. (h) Raman spectra for GO, FeNPs, and GFeN. The characteristic D and G peaks confirm the presence GO layer. The shifts in peak locations (D and G) (in GFeN compared to GO) indicate the deposition FeNPs on GO to form GFeN.

XPS analyses of fresh bare FeNPs (Appendix A, Figure A1a) show the Fe2p core levels with the deconvoluted peaks of Fe($2p_{3/2}$), Fe($2p_{1/2}$), and the shake-up satellite peaks. The deconvoluted Fe2p envelop show a small peak of Fe^0 along with other feature peaks suggesting that the surface consists of a large fraction of iron oxides/iron hydroxide and a relatively small

amount of elemental iron (Fe^0) (Liu et al., 2014). This is in conformity with the core-shell structure of FeNPs reported by others (Li and Zhang, 2007; Martin et al., 2008; Liu et al., 2014) and also observed in our HRTEM micrographs (Figure 3.1b). This observation was expected as the nanoparticles were prepared in the water where the Fe^0 and iron oxides are eventually converted to oxyhydroxide on the surface which can be ascribed by a series of chemical reactions (Eqs. 7-9) (Roberts et al., 2004; Liu et al., 2014).

$$4Fe^0 + 3O_2 + 2H_2O \rightarrow 4FeOOH \quad (7)$$

$$4Fe_3O_4 + O_2 + 6H_2O \rightarrow 12FeOOH \quad (8)$$

$$Fe_2O_3 + H_2O \rightarrow 2FeOOH \quad (9)$$

The Fe2p core level of GFeN (Figure 3.1e) shows no elemental iron (Fe^0) suggesting that the material surface consists mostly of iron oxide/hydroxides in the form of Fe_2O_3, Fe_3O_4, or/and FeOOH. Iron oxide and hydroxide have similar XPS peak positions in this region, and therefore, the O1s spectrum (Figure 3.1f) is used to determine the existing surface oxygen states. The O1s spectrum contains three prominent peaks that are assigned to O^{2-} (~530 eV), OH (~531.8 eV), and OH_2 (~533.1 eV) (Li and Zhang, 2007). The presence of surface OH species (~68%) and Fe–O (~23%) bonds indicate that the oxidized iron is in the form of FeOOH and that is consistent with other reports (Li and Zhang, 2007; Hao et al., 2014; Liu et al., 2014). Again, the broad peak at ~530 eV suggests the presence of Fe_2O_3 and Fe_3O_4. In the spectrum of C1s core levels (Figure 3.1g), the peak at 284.6 eV represents the binding energies of C–C/C=C, the peak at 285.8 eV is for C-OH, and the one at 286.7 eV is for C–O/C=O. The intensity of C–OH is high in GFeN (compared to that in GO shown in Appendix A, Figure A2b) and that could be due to the presence of a high −OH group on the GFeN surface. Based on the XPS results, we can

suggest that FeOOH and Fe_2O_3/Fe_3O_4 are the predominant components of the oxidized surface of GFeN.

Raman spectrum of the GO (Figure 3.1h) shows two major characteristics peaks, D band peak at 1364 cm^{-1} and G band peak at 1595 cm^{-1}. The small peak at 2704 cm^{-1} belongs to the 2D band of GO. The FeNPs exhibit a broad peak at 1298 cm^{-1} and three sharp peaks at 282, 388, and 591 cm^{-1} suggesting that the surface of the nanoparticle is composed of mixed iron oxide and oxyhydroxide (Nieuwoudt et al., 2011; Liu et al., 2015a; Liu et al., 2017). The inference from the Raman data agrees very well with that from our XPS data. The Raman spectra of the nanohybrid (GFeN) show features of iron oxide and GO which demonstrates the successful deposition of FeNPs on GO. Moreover, the clear shifts of the D and G bands indicate a charge transfer between the FeNP and GO sheet (Ban et al., 2010; Cong et al., 2012). This charge transfer phenomenon can be beneficial as GO can store the electrons released during iron oxidation (and subsequent arsenic adsorption), and the stored electron can be released back to the FeNP surface to rejuvenate the iron surface. The rejuvenated iron surface can facilitate additional arsenic removal.

3.3.2. Dispersion behavior

To investigate the dispersibility of nanomaterials in an aqueous solution, zeta potential (ζ) was measured for FeNPs and GFeN as well bare GO sheets in DI water (Table 3.2). The dispersion behavior of nanomaterials was interpreted based on their Zeta potential (ζ) values (Table 3.2). An absolute ζ value greater than 25 mV ensures good electrostatic stabilization (ISO, 2000). The GO had a high ζ value (−48 ± 0.33 mV) and so the GO was electrostatically stable in the aqueous medium. The iron nanoparticles (FeNPs) had a low ζ value (11.67 ± 0.87 mV) and were not electrostatically stable in aqueous media. The lack of electrostatic stabilization and the

presence of strong interparticle attraction led to the easy agglomeration of FeNPs (preliminary observation, results not reported here; also see others (Krajangpan et al., 2012; Petcharoen and Sirivat, 2012). Even though FeNPs did not disperse well in water, the positive surface charge helped in arsenic (anionic) adsorption through electrostatic attraction. Once the Fe-nanomaterials (FeNPs) were deposited on the GO surface, some of their positive changes were neutralized by negative surface charges of the GO but the nanohybrids still had a relatively high ζ (–22.97±0.90) compared to bare nanoparticles (FeNPs) and thus made stable dispersions.

Table 3.2. Zeta potentials (ζ, mV) of the nanomaterials used in this research.

Material	Mean ζ (mV)	Solution pH
GO Sheets	–48.50±0.33	8.7
GFeN	–22.97±0.90	8.58
FeNPs	11.67±0.87	8.9

3.3.3. Point-of-zero-charge PZC

The PZC was determined (Balistrieri and Murray, 1981; Lataye et al., 2006) for the adsorbents used in this study. We prepared 0.01 M NaCl solution and adjusted the pH of the solution to the required value (pH 2-12) by dropwise addition of 0.1 M NaOH or HCl. A measured amount (20 mg) of the nanomaterials (FeNPs or GFeN) was dispersed in 20 mL of the NaCl solution with different initial solution pH. The initial (0 h) and the final (48 h) pH values were measured, and the PZC was calculated by plotting the change in pH vs initial pH (change in pH, dpH = Initial pH – Final pH). The PZC of an adsorbent is the point where the plot (dpH vs initial pH) intersects X-axis (Figure 3.2). The point-of-zero-charge (PZC), at which the pH-dependent surface charge is zero, was high for both FeNPs (PZC = 8.40) and GFeN (8.05) (Figure 3.2). This indicated that the materials would be able to effectively adsorb aqueous arsenic if the adsorption process is controlled by an electrostatic process.

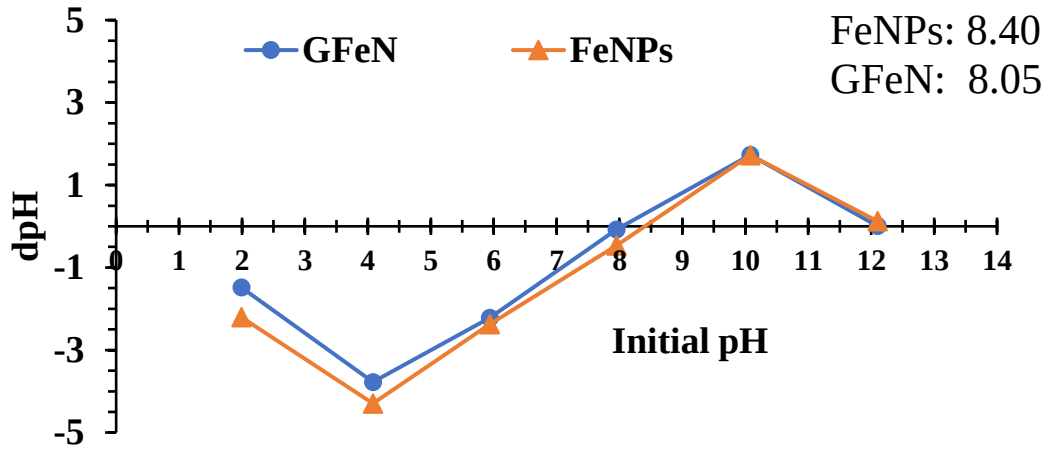

Figure 3.2. Determination of the points-of-zero-charge (PZC) of FeNPs and GFeN nanohybrid. PZC values are shown on the plot. PZC for FeNPs = 8.40 and PZC for GFeN = 8.05.

Table 3.3. Characteristics of iron nanoparticles (FeNPs) and nanohybrid (GFeN) used for arsenic removal in this study.

Material	Particle Size (nm)	Mean ζ (mV) *	Optimal pH +	PZC ǂ	Fe content g/g	As Removal mg As/ g Fe #	
						As(III)	As(V)@
FeNP	15.3-65.3	11.67±0.87	3-9	8.4	0.59	26	32-36
GFeN	21.1-88.5	-22.97±0.90	3-9	8.05	0.43	36	43-49

*: ζ = Zeta potential; +: pH at which >90% arsenic removal was achieved; ǂ: PZC: Point-of-zero-charge; #: This comparison is done based on arsenic removal by FeNPs and GFeN at C_0 = 5 mg/L and the iron content in each nanomaterial was measured for normalization purposes (Sections 3.4.2.). @: adsorption of arsenic decreased as pH increased from 3 to 9.

3.3.4. Arsenic removal

3.3.4.1. Role of pH on arsenic removal

3.3.4.1.1. As(V)

Both GFeN and FeNPs removed >90% As(V) (C_0 = 5 mg/L) over a wide pH range (pH 3-9) with maximum removal (>98%) at pH 5-7 (Figure 3.4b). Solution pH affects the speciation of As(V) (Figure 3.3), and in aqueous media, it is typically present as $H_2AsO_4^-$ at pH 2.2-6.9 and $HAsO_4^{2-}$ at pH 6.9-11.5. Further, H_3AsO_4 is the dominant species at extremely low pH (<2.2), and AsO_4^{3-} dominates at high pH (>11.5) (Yoon et al., 2016).

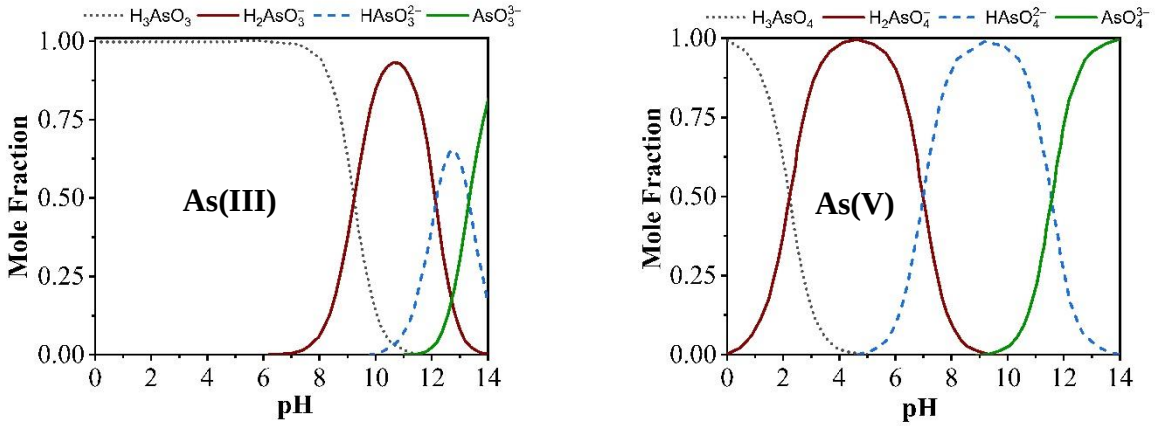

Figure 3.3. Arsenic species at different pH.

Below PZC, GFeN and FeNPs were more positively charged and attracted the negatively charged As(V) ($H_2AsO_4^-$ and $HAsO_4^{2-}$). It was expected that with increasing pH the net positive surface charge would decrease and there would be a reduction in arsenic adsorption as we hypothesized the adsorption to be controlled by the electrostatic process. However, no significant decrease in As(V) removal (Fig 3.4a, removal ~ 95%) was observed in the pH range of 3 to 9 (Two-way ANOVA, $p = 0.05$). This indicates that other driving forces besides electrostatic attraction might have helped in the removal of As(V). Besides electrostatic forces, interactions of arsenic species with iron corrosion products such as FeOOH, Fe_3O_4, and Fe_2O_3 play important roles in arsenic removal at all pH (Wu et al., 2017). As(V) was possibly removed simultaneously through electrostatic attraction and surface complexation with corrosion products, and, for that reason, high removal of As(V) by GFeN and FeNPs was observed over a wide pH range (pH 3-9).

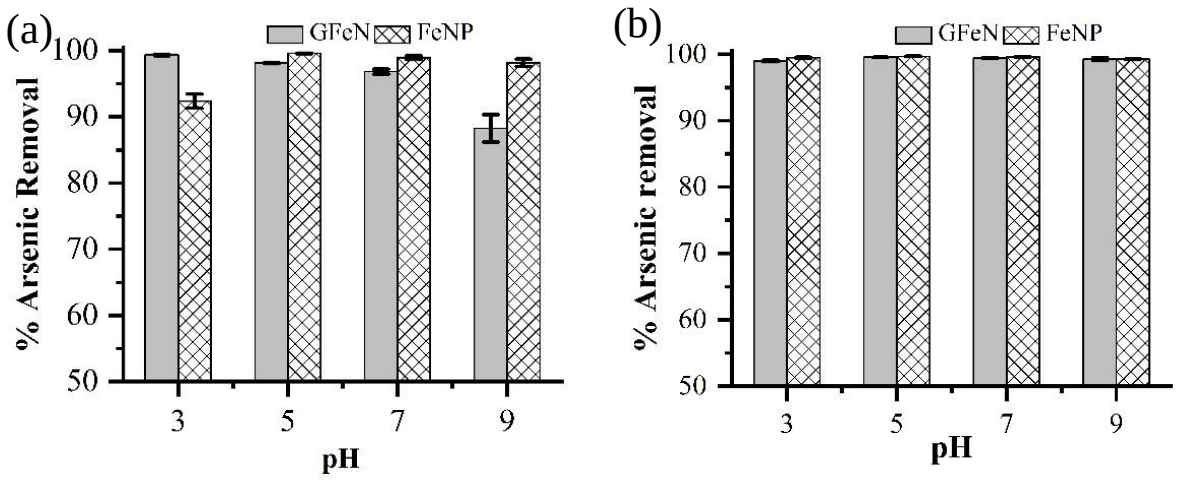

Figure 3.4. Arsenic removal at different pH: (a) As(III) and (b) As(V). Initial arsenic concentration (C_0) = 5 mg/L.

3.3.4.1.2. As(III)

We tested our new nanohybrid for the removal of As(III) as well. As(III) is present as neutral H_3AsO_3 in aqueous media at pH <9.2 (Figure 3.3). Beyond pH 9.3, H_3AsO_3 dissociates into negatively charged arsenite ions ($H_3AsO_3 \leftrightarrow H_2AsO_3^- + H^+$). The neutral As(III) was adsorbed onto the Fe-based nanohybrids through surface complexation at pH 3-9, and effective removal (>99%) was achieved (Figure 3.4b).

3.3.4.2. Roles of graphene oxide and iron

We tested the reduced GO (rGO) as the GO sheets used in GFeN synthesis might have been reduced by $NaBH_4$ used. We investigated the possible adsorption of arsenic using pristine GO and rGO sheets as controls. First, we conducted the experiment with an initial arsenic concentration (C_0) of 5 mg/L but did not record any observable removal by the adsorbents (data not shown). So, we decided to evaluate the GO and rGO sheets at C_0 = 1 mg/L (Figure 3.5a-b). The pristine GO sheets removed ~12.5 % of As(III) and 0.44% of As(V) from 1 mg/L arsenic solution (pH 7). The rGO sheets recorded only 1.8% removal for As(III) and 0.35% for As(V).

So, we can infer that our GO sheets in GFeN (present as rGO in the nanohybrid) did not significantly adsorb arsenic but only the FeNPs deposited on the GO sheets did.

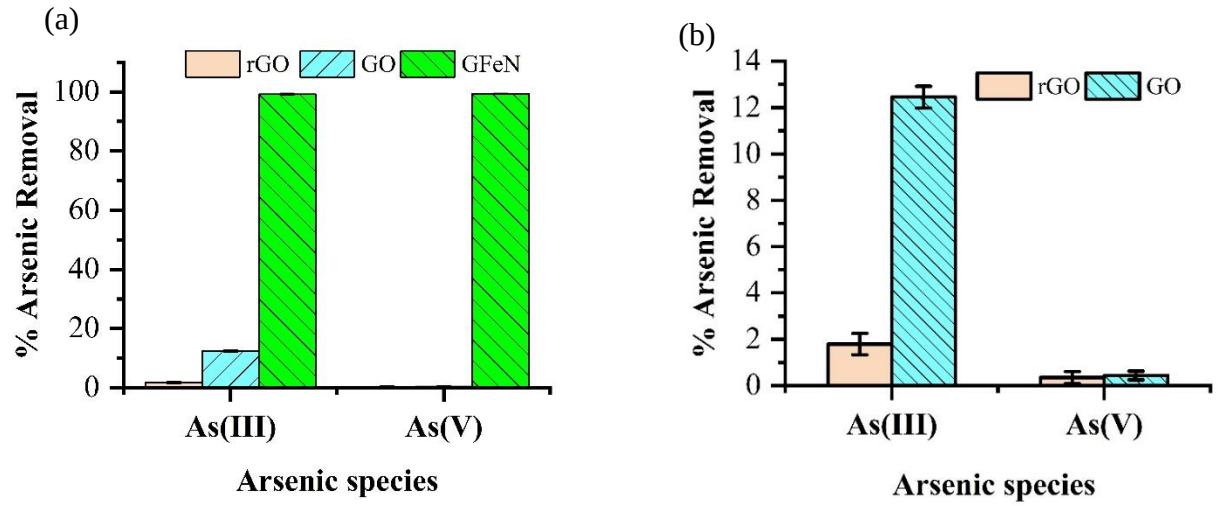

Figure 3.5. (a) Arsenic removal by GFeN, GO and rGO (Initial pH = 7 and C_0 = 1 mg/L); (b) arsenic removal by rGO and GO zoomed.

In our experiment, we used the same mass weight of each adsorbent (GFeN, FeNPs). The Fe content per unit weight of each adsorbent was determined (Table 3.3, also see Appendix A, Section A2). Even though GFeN had less iron (0.43 g/g) than FeNPs (0.59 g/g), GFeN adsorbed ~38% more As(III) than FeNP across all pH (3-9) (Table 1). In case of As(V), GFeN had ~50% more adsorption capacity than FeNP at pH 3 and ~25% more at pH 9 (Table 1). Higher arsenic removal by GFeN could be due to effective dispersion of FeNPs (reduced agglomeration) in the GO layer which ensured improved interactions with arsenic species. Given that GFeN worked as a more efficient adsorbent (than FeNPs), further investigations (subsequent sections) were carried out with GFeN only.

3.3.4.3. Arsenic removal by GFeN

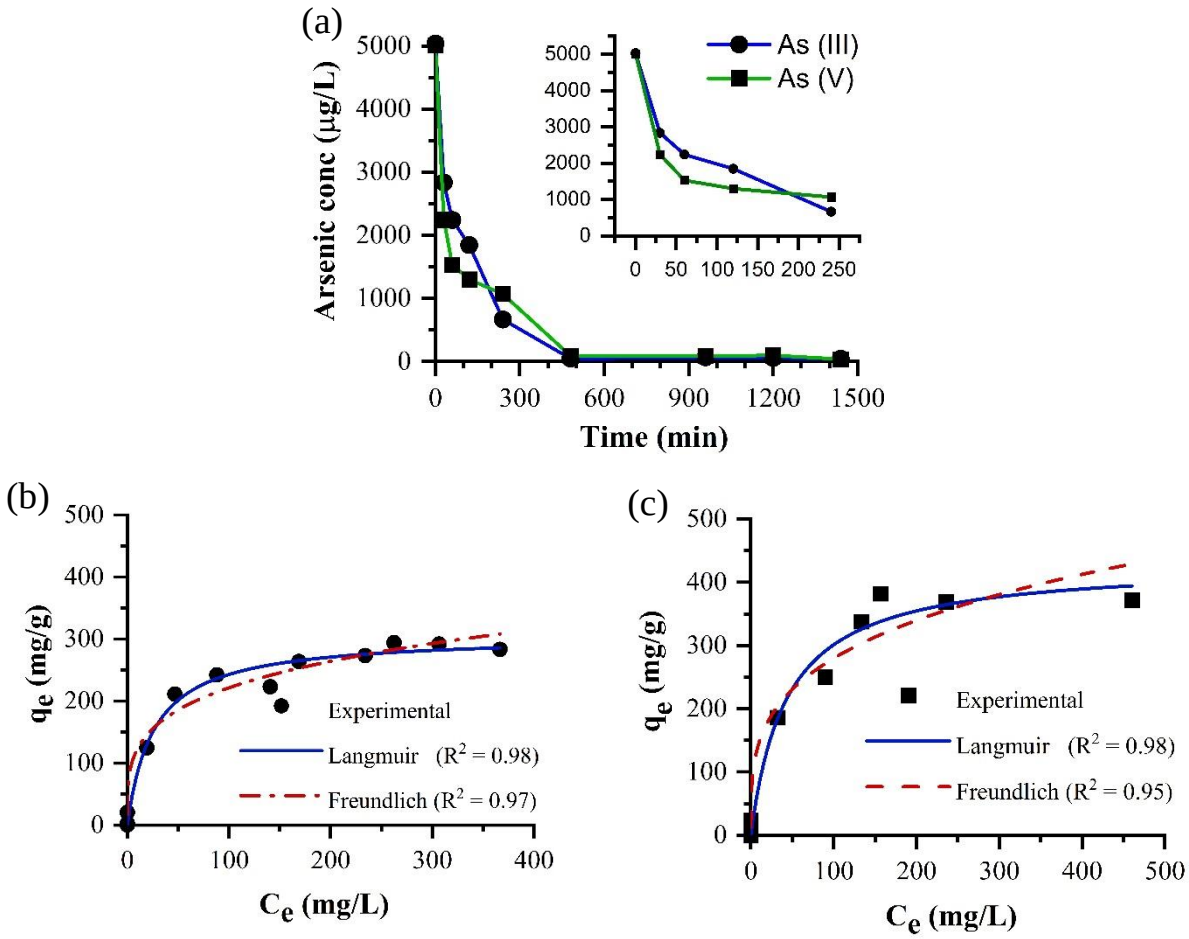

Figure 3.6. (a) Arsenic removal by GFeN overtime when initial arsenic concentration (C_0) is 5 mg/L (Inset: first 2 h data zoomed in). Langmuir and Freundlich isotherms for: (b) As(III) and (c) As(V). Langmuir fitted better for both the data sets and recorded adsorption capacities of 306.10±9.92 mg/g for As(III) and 431.41±25.95 mg/g for As(V). For all experiments: Adsorbent dose = 250 mg/L, and Initial pH = 7.

3.3.4.3.1. Kinetic studies

More than 99% removal of arsenic (C_0 = 5 mg/L) occurred within the first 6 h for As(III) and within 8 h for As(V) (Figure 3.6a). The adsorption happened in three distinct stages for both the arsenic species: (1) a rapid removal in the first 60 min (>50%) (Figure 3.6a inset), (2) relatively slower removal after 60 min till 6-8 h, and (3) minor (non-significant) removal beyond 6-8 h. The data were fitted onto zero-, first-, and second-order as well as pseudo-first- and pseudo-second-order reaction models. The pseudo-second-order model gave the best fit (R^2 ~

0.999) for both As(III) and As(V) (Figure 3.7, Table 3.4) which suggests that chemisorption is possibly responsible for the removal of arsenic by GFeN (Wang et al., 2014a).

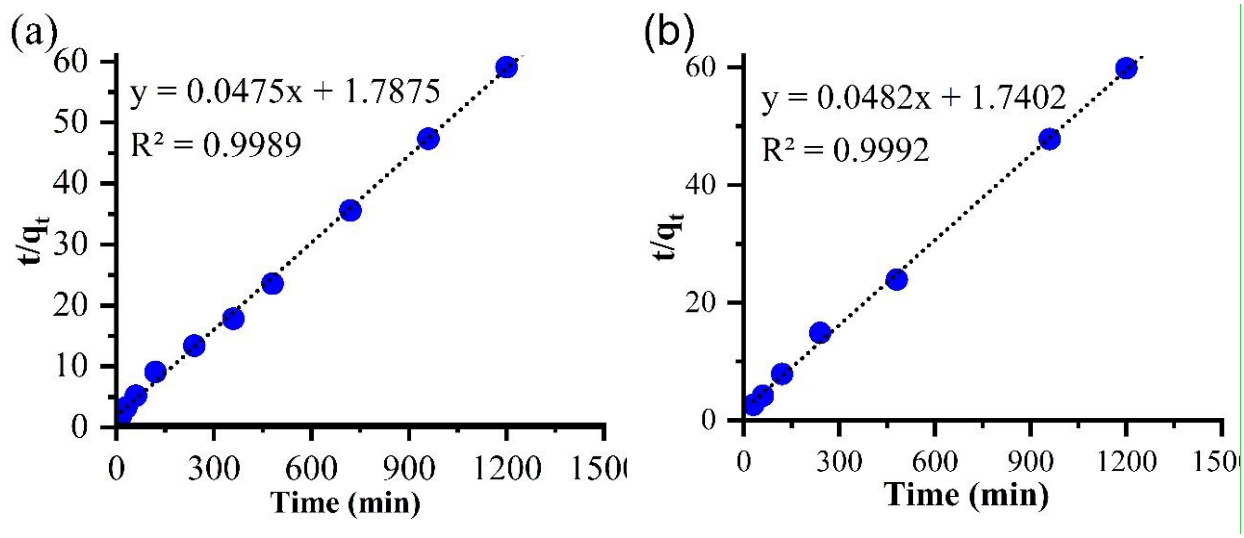

Figure 3.7. Pseudo-second order kinetic model for (a) As(III) and (b) As(V) treated with GFeN.

Table 3.4. Kinetics model parameters associated with arsenic adsorption by GFeN. Adsorbent dose = 250 mg/L and initial pH = 7.

Arsenic Species	Experimental q_e	Zero-order	1st Order	Pseudo 1st Order	2nd Order	Pseudo 2nd Order		
		R^2	R^2	R^2	R^2	R^2	Model Predicted q_e	K_2
C0 = 5 mg/L								
As(V)	20.27	0.463	0.831	0.772	0.833	0.999	20.75	1.3×10^{-3}
As(III)	20.35	0.517	0.711	0.662	0.760	0.999	21.05	3.3×10^{-4}
C_0 =100 µg/L								
As(V)	0.434	0.270	0.514	0.831	0.675	0.999	0.434	3.759
As(III)	0.434	0.269	0.539	0.648	0.854	0.999	0.438	4.280

We also measured the Fe in the bulk solution in the 24-h samples. During As(V) removal by GFeN, the total Fe release after 24 h reaction was 0.76 mg/L (0.71% of total Fe in GFeN), and for As(III), the release was 1.03 mg/L (0.95% of total Fe). The results indicate that our nanohybrid was not leaching out any significant amount of iron.

3.3.4.3.2. Adsorption isotherm

Langmuir and Freundlich isotherm models were used to understand arsenic sorption behavior by GFeN. Both As(III) and As(V) adsorption data fitted slightly better for Langmuir model (R^2 = 0.9863 for As(III) and 0.9818 for As(V)) than the Freundlich (R^2 = 0.9758 for As(III) and 0.9586 As(V)) (Figure 3.6b-c, Table 3.5).

Table 3.5. Langmuir and Freundlich isotherm model parameters for As(V) and As(III) adsorption by GFeN.

Arsenic Species	Langmuir		Freundlich	
	Parameter	**Value**	**Parameter**	**Value**
As(V)	q_m (mg/g)	431.41±25.95	N	3.57
	K_l (L/mg)	0.02314±0.005	k_f	77.12±19.01
	R^2	0.9818	R^2	0.9586
As(III)	q_m (mg/g)	306.10±9.92	N	3.93
	K_l (L/mg)	0.03846±0.006	k_f	68.75±10.73
	R^2	0.9863	R^2	0.9758

Based on the isotherm data, the adsorption capacities of GFeN were found to be 306.10±9.92 mg/g for As(III) and 431.41±25.95 mg/g for As(V) (Table 3.5). The As(III) and As(V) adsorption capacities of GFeN are very high compared to other GO-based nanocomposites so far reported (Table 3.6). For GFeN, the affinity for sorption (K_l) of As(III) is 0.03846 L/mg and that for As(V) is 0.02314 L/mg, and we used these values to calculate R_L ($R_L = 1/(1+C_0*K_l$, where C_0 is the initial arsenic concentration) to further elucidate the adsorption process. If $R_L > 1$ then the adsorption process is unfavorable and if $0 < R_L < 1$ then the adsorption is favorable (Hall et al., 1966; Weber and Chakravorti, 1974). For GFeN, arsenic adsorption was found to be favorable for both the arsenic species with R_L = 0.056-0.997 for As(III) and 0.072-0.998 for As(V).

3.3.4.4. Stability of GFeN

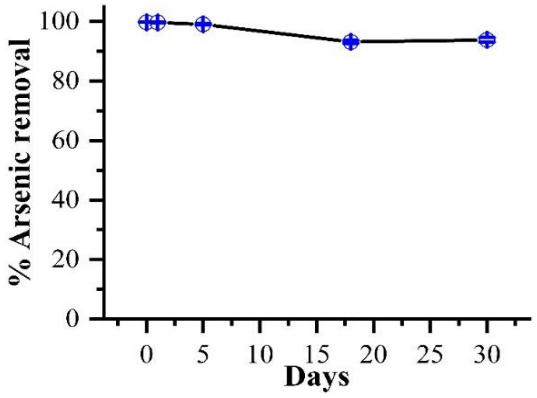

Figure 3.8. Arsenic removal by GFeN in actual arsenic contaminated groundwater. Initial arsenic concentration 450 µg/L and Adsorbent dose 250 mg/L.

A number of batch reactors (amber glass vials) were prepared with 10 mg of GFeN and 40 mL of actual arsenic contaminated groundwater (As(V) ≅ 30 µg/L) were prepared and kept in. a dark cabinet. Three randomly selected reactors were taken at a predetermined time (0, 1, 5, 18, and 30 d) and spiked with arsenic (with As(V) standard solution) to achieve an arsenic concentration of 450 µg/L. The set of three reactors put in the end-over-end shaker (28 rpm) for 12 h and the arsenic concentration was measured in the bulk solution after 12h to calculate the removal efficiency. The arsenic removal till 5 days remained ~99% and then it slightly decreased to ~93% (18 d) and remained unchanged till 30 d (Figure 3.8).

Table 3.6. Arsenic adsorption capacity for various carbon-based metallic nanohybrids.

Adsorbents	pH*	Arsenic concentration range (mg/L)	Adsorbent dose used (g/L)	Adsorption capacity (mg/g)		Source
				As(III)	As(V)	
Fe_3O_4-GO	7	0-550	0.1	85	38	(Yoon et al., 2016)
CeO_2-GO	--	0.1-200	0.5	185	212	(Sakthivel et al., 2017)
Mg-Al hydroxide/GO	5	0.1-150	0.5	----	180.26	(Wen et al., 2013)
rGO-Fe_3O_4-TiO_2	7	3-10	0.2	147.05	---	(Benjwal et al., 2015)
GO–$ZrO(OH)_2$	7	2-80	0.5	95.15	84.89	(Luo et al., 2013)
β-FeOOH@GO-COOH	6.5	1-200	1	77.5	45.7	(Chen et al., 2015)
GO-$MnFe_2O_4$	1-2	10-50	0.2	----	240.3	(Huong et al., 2016)
$FeMnO_x$/RGO		0.2-7	0.2	22.17	22.05	(Zhu et al., 2015)
Macro-porous magnetic 3D GO hydrogel	~7	0-150	1	25.1	74.2	(Liang et al., 2019)
GNP/Fe−Mg oxide	7	5-90	0.2	---	103.9	(La et al., 2017)
GO-$CuFe_2O_4$ foam	7.2	5-500	8 l	51.64	124.69	(Wu et al., 2018)
GO-Fe_2O_3	7	0.1-1200	0.8	147	113	(Su et al., 2017)
Fe_3O_4@CuO-GO	7	3.75-75	0.3	70.36	62.60	(Wu et al., 2019)
GO-lanthanum fluoride	---	2-30	0.8	---	18.52	(Lingamdinne et al., 2019)
Fe_2O_3 nanocubes-porous GO aerogel	---	5-70	0.5	172.27	217.34	(Yu et al., 2019)
GFeN	7	0.1-550	0.25	306.10	431.41	This study

*pH at which the experiment was conducted.

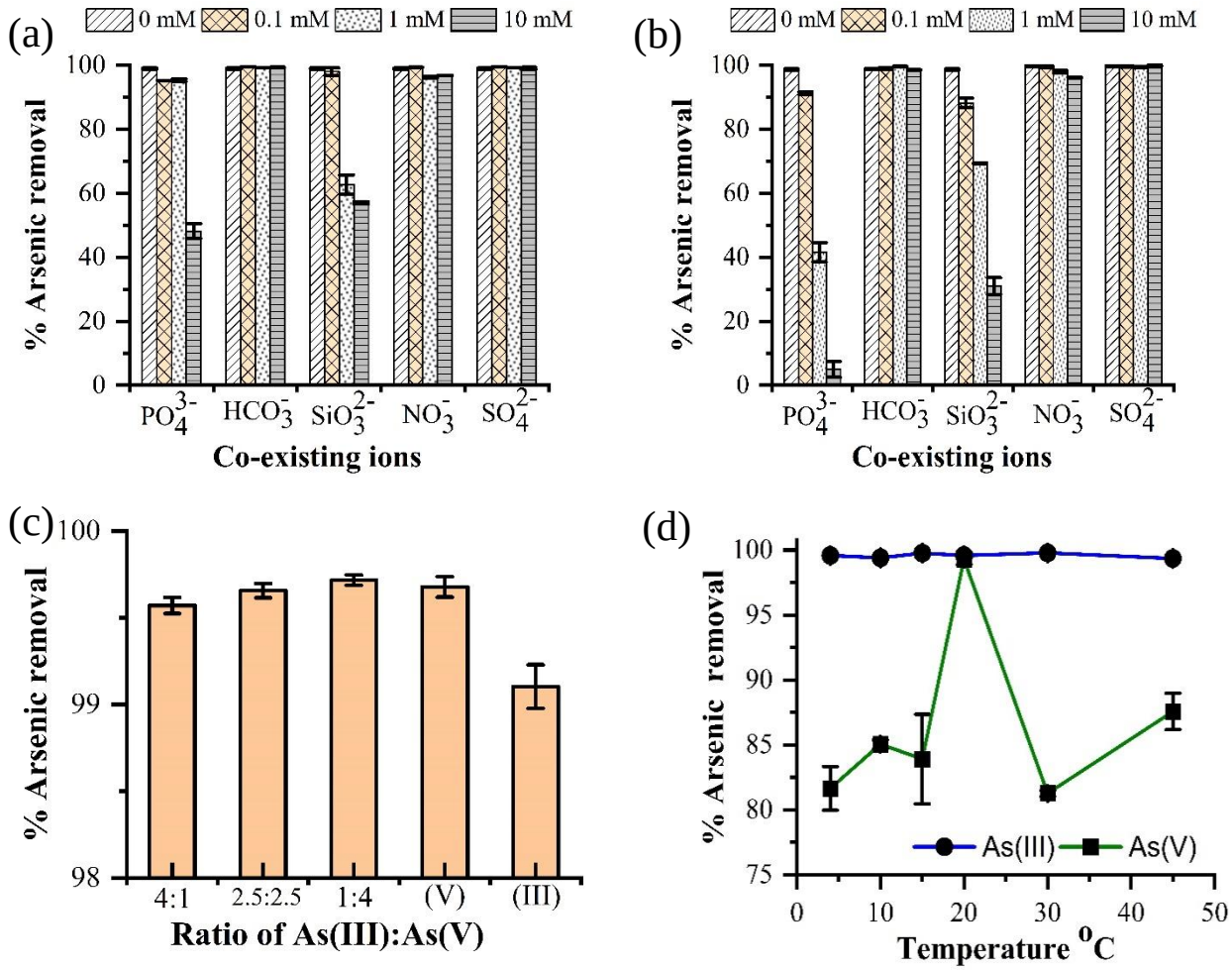

Figure 3.9. Arsenic removal by GFeN in the presence of co-existing anions while treating (a) As(III) and (b) As(V), phosphate and silicates ions interfered in arsenic removal but only at above environmental significant concentrations (c) both As(III) and As(V) co-exist (in different mass ratios, (V) and (III) on the x-axis represent 5 mg/L of only As(V) or As(III)) and (d) Arsenic removal by GFeN under different temperatures Initial arsenic concentration (C_0) = 5 mg/L, Adsorbent dose = 250 mg/L, and Initial pH = 7; for (c) C_0 = 5 mg/L total of As(III) and As(V) combined.

3.3.4.5. Interferences by co-existing ions and compounds

The ions in groundwater that may potentially interfere with arsenic removal by GFeN include phosphate (PO_4^{3-}, typical groundwater concentration ~0.32 µM), bicarbonate (HCO_3^-, ~3 mM), silicate (SiO_3^{2-}, ~0.3 mM), nitrate (NO_3^-, <0.16 mM), sulfate (SO_4^{2-}, ~1 mM) and compounds like natural organic matters (NOM, <1 mg/L) (Van der Leeden, 1990; Karanfil et al., 2002). The role of ionic strength (typical value 0.001-0.02 mM) on arsenic removal by GFeN

was also evaluated. Further, the adsorption efficiency of GFeN was determined when As(III) and As(V) are present together.

SO_4^{2-}, NO_3^- and HCO_3^- (0 to 10 mM) had a negligible effect on the removal of both the arsenic species by GFeN (Figure 3.9a-b).

In the presence of low PO_4^{3-} concentration (0.1 mM), the As(III) removal efficiency decreased from ~99% (0 mM PO_4^{3-}) to ~95% (Figure 3.9a), and As(V) removal decreased to ~91% (Figure 3.9b). The removal efficiency further decreased with the increase of PO_4^{3-} concentration (Figure 3.9a-b) and the effect was more prominent in As(V) compared to As(III). At 10 mM PO_4^{3-}, As(III) removal was ~48% and As (V) removal was ~5%. It is important to note that PO_4^{3-} concentration in groundwater is typically much below 0.1 mM (WHO, 2004) and, as such, will not affect arsenic removal by GFeN.

In the presence of low SiO_3^{2-} concentration (0.1 mM), the As(III) removal (~97%) was not significantly ($p = 0.05$) affected relative to the control (~99%) whereas As(V) removal significantly decreased to ~88% (Figure 3.9a-b). At 1 mM SiO_3^{2-} concentration, As(III) removal reduced to ~62% and As(V) removal decreased to ~69.2%. When SiO_3^{2-} concentration was increased to 10 mM, the removal efficiencies decreased to ~56% for As(III) and ~31% for As(V). The typical reported concentration of SiO_3^{2-} in groundwater is 0.3 mM, and so we expect some reduction in arsenic removal efficiency when GFeN is used.

There was a marginal (6-7%) decrease in arsenic removal when the humic acid concentration was increased from 0 to 10 mg/L (Appendix A, Figure A3a). In groundwater, organic acid concentration does not typically exceed 1 mg/L (Karanfil et al., 2002) and we did not see any significant decrease in arsenic removal efficiency when the organic acid present was 1 mg/L.

Ionic strength 0-1 M did not affect arsenic adsorption by GFeN (removal >98%) (Appendix A, Figure A3b). Typical groundwater ionic strength is 0.001-0.02 M (Wallace et al., 2012), and, as such, GFeN is expected to effectively work in any groundwater contaminated with arsenic.

3.3.4.5.1. Co-existing arsenic species

To simulate the field situation when As(III) and As(V) are present at the same time, a series of experiments were conducted with an initial combined (As(III) and As(V)) concentration of 5 mg/L with different ratios of the two species. For all combinations, ~99% removal was achieved (Figure 3.9c) indicating that GFeN can simultaneously remove both the arsenic species. This is a major advantage with GFeN as most of the reported adsorptive media can only effectively remove As(V) and pretreatment is called for to oxidize As(III) to As(V). The ability of GFeN for the simultaneous removal of both species will reduce treatment system complexity and result in cost savings.

3.3.4.6. Effect of temperature

The temperature (4-45 ℃) had significant effects on As(V) removal by GFeN. Optimal As(V) removal (>99%) was achieved at 20 ℃, but the removal decreased from 99 to 80-85% when the temperature was either increased or decreased (Figure 3.9d). However, As(III) removal was not affected by the temperature variation (4-45 ℃) and always remained >99% (Figure 3.9d). While mobility of the arsenic species increases with the increase in temperature, electrostatic attraction gets reduced (Wang et al., 2014a). Accordingly, we observed reduced As(V) removal at low temperature (low species mobility) as well as high temperature (low electrostatic attraction). However, As(III) removal was not controlled by electrostatic attraction (Section 3.3.4.1) and, thus, was not affected by temperature change.

3.3.4.7. Environmental relevance

Arsenic concentration in arsenic contaminated groundwater across the globe is typically around 100 µg/L. We evaluated the removal of both As(III) and As(V) by the GFeN in the concentration range of 0 to 140 µg/L in simulated groundwater (Appendix A, Table A1) and achieved >99% within 30 min in all cases (Figure 3.10a). At an initial arsenic concentration of 100 µg/L, GFeN remediated both As(III) and As(V) to below the MCL (10 µg/L) within 10 min (Figure 3.10b). The arsenic removal data best fitted in a pseudo-second-order model ($R^2 \sim 0.999$) for both As(III) and As(V). Effective removal of the arsenic species at these environmentally relevant concentrations in a short time (10-30 min) is promising for field applications.

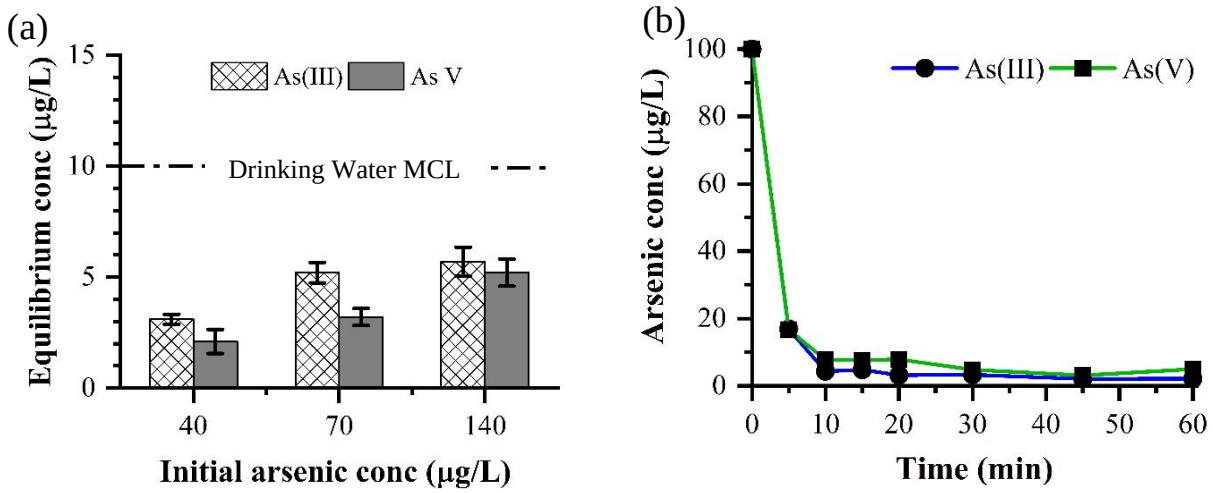

Figure 3.10. (a) Arsenic removal at environmental relevant concentrations of 40-140 µg/L (in simulated groundwater). (b) Arsenic removal by GFeN over time when initial arsenic concentration (C_0) 100 µg/L. GFeN removed As(III) and As(V) below MCL (10 µg/L) within 10 min. For all experiments: Adsorbent dose = 250 mg/L, and Initial pH = 7.

3.3.5. Removal mechanisms

Based on our experimental and characterization data, we are proposing a possible mechanism (Figure 3.12) for arsenic removal by the nanohybrid (GFeN). First, the aqueous arsenic ions come in contact with the nanohybrid surface, and the arsenic flux gradient builds up between the solution and the adsorbent (GFeN) surface. Then the arsenic adsorbs onto the

surface of GFeN through electrostatic attraction and surface complexation. Further, the adsorbed arsenic on the GFeN surface gets transformed and stabilized within the nanohybrid.

Two types of surfaces are available on the GFeN for arsenic adsorption, the GO sheet, and the FeNP surface. However, GO (rGO in GFeN) is not considered as an adsorbent for arsenic in the model as our results indicate that GO sheets do not actively participate in the adsorption process (Figure 3.5, rGO in our GFeN removed <2% arsenic, Section 3.3.4.2).

The XPS spectrum of GFeN after As(V) adsorption shows a strong peak at 45.7 eV (Figure 3.11a) which is the characteristic peak for As(V) indicating that there was no change in the oxidation state during the adsorption process. To further understand the possible mechanism, the O1s scan of GFeN after As(V) adsorption was analyzed (Figure 3.11b) and a significant reduction of the OH group (from 68% to 52%) was observed. This result indicates that surface OH species were involved in the formation of inner-sphere monodentate ($FeOAsO_2OH$) or bidentate ($(FeO)_2AsO_2$) complex leading to the lowering of OH concentration. Similar results were reported earlier (Eqs. 4-5) (Stachowicz et al., 2008; Hao et al., 2014) and our observations are consistent with that. These equations (Eqs. 10-11) are based on a surface complexation model (*aka* charge distribution model (CD model)) explained by Stachowicz et al. (2008) (Stachowicz et al., 2008) where ΔZ_0 and ΔZ_1 are the CD model coefficients, and $\Delta Z_0 + \Delta Z_1$ is equal to the charge introduced by the As(V) adsorption process.

$$\equiv FeOH^{-1/2} + 2H^+ + AsO_4^{3-} \rightarrow FeO^{-1/2+\Delta Z_0}AsO_2OH^{\Delta Z_1} + H_2O \quad (10)$$

$$2 \equiv FeOH^{-1/2} + 2H^+ + AsO_4^{3-} \rightarrow (FeO)_2{}^{-1/2+\Delta Z_0}AsO_2^{\Delta Z_1} + 2H_2O \quad (11)$$

In the case of As(III), the XPS spectrum of arsenic sorbed GFeN indicates that the adsorbed arsenic is in dual oxidation states with As(V) being mostly noticeable on the material's surface and As(III) being relatively less (Figure 3.11c). This reveals that As(III) is oxidized to

As(V) as it reacts with the iron oxide present on GFeN (Ramos et al., 2009; Tucek et al., 2017). However, during this oxidation process, elemental iron (Fe^0) also corrodes simultaneously via the Fenton reaction (Pang et al., 2011) to produce fresh/more iron oxyhydroxide/iron oxide products; in our experiment, this was confirmed by the increase in OH concentration (from 68% to 72%) in the O1s spectrum (Figure 3.11d). This suggests that the Fe-O has involved in As(III) adsorption via the formation of an inner-sphere surface complex product ($(FeO)_2AsOH$). In brief, both adsorption and oxidation of As(III) happen simultaneously on the GFeN surface. Others reported similar observations during the adsorption of arsenic onto iron nanomaterials (Kanel et al., 2006; Farrell and Chaudhary, 2013; Tucek et al., 2017). Fe^0 in FeNPs [Fe/Fe_xO_y] deposited on the GO sheet oxidize quickly due to the lower redox potential of the Fe^{2+} and Fe^{3+} couple. During this oxidation, electrons are released by Fe^0 [$Fe^0 \rightarrow Fe^{2+} + 2e^-$; $Fe^{2+} \rightarrow Fe^{3+} + e^-$], and the GO sheet acts as a reservoir for the released electrons (Lightcap et al., 2010; Wang et al., 2017; Ren et al., 2018). The GO sheet then releases the electrons back to the FeNPs, and iron oxides (on FeNP surface) are converted back to the earlier reduced form ($Fe^{3+} + e^- \rightarrow Fe^{2+}$) (Wang et al., 2017). Ren et al. (2018) (Ren et al., 2018) working with hexavalent chromium indicated that there is an active electron transfer process occurring between the decorated iron nanoparticles and the GO sheet, and Wang et al. (2017) (Wang et al., 2017) reported that ion nanoparticles deposited on GO are regenerated by electrons transferred from the graphene oxide sheets during phenol removal. The electron transfer process (from GO to FeNP) helps in maintaining an optimal amount of iron species on the FeNP surface which enhances arsenic adsorption. The major significance of this mechanism is that the overall iron oxidation process is slowed down because of the electron transfer process, and the core Fe^0 is prevented from getting quickly oxidized (Ren et al., 2018) potentially adding to the active life of the GFeN system.

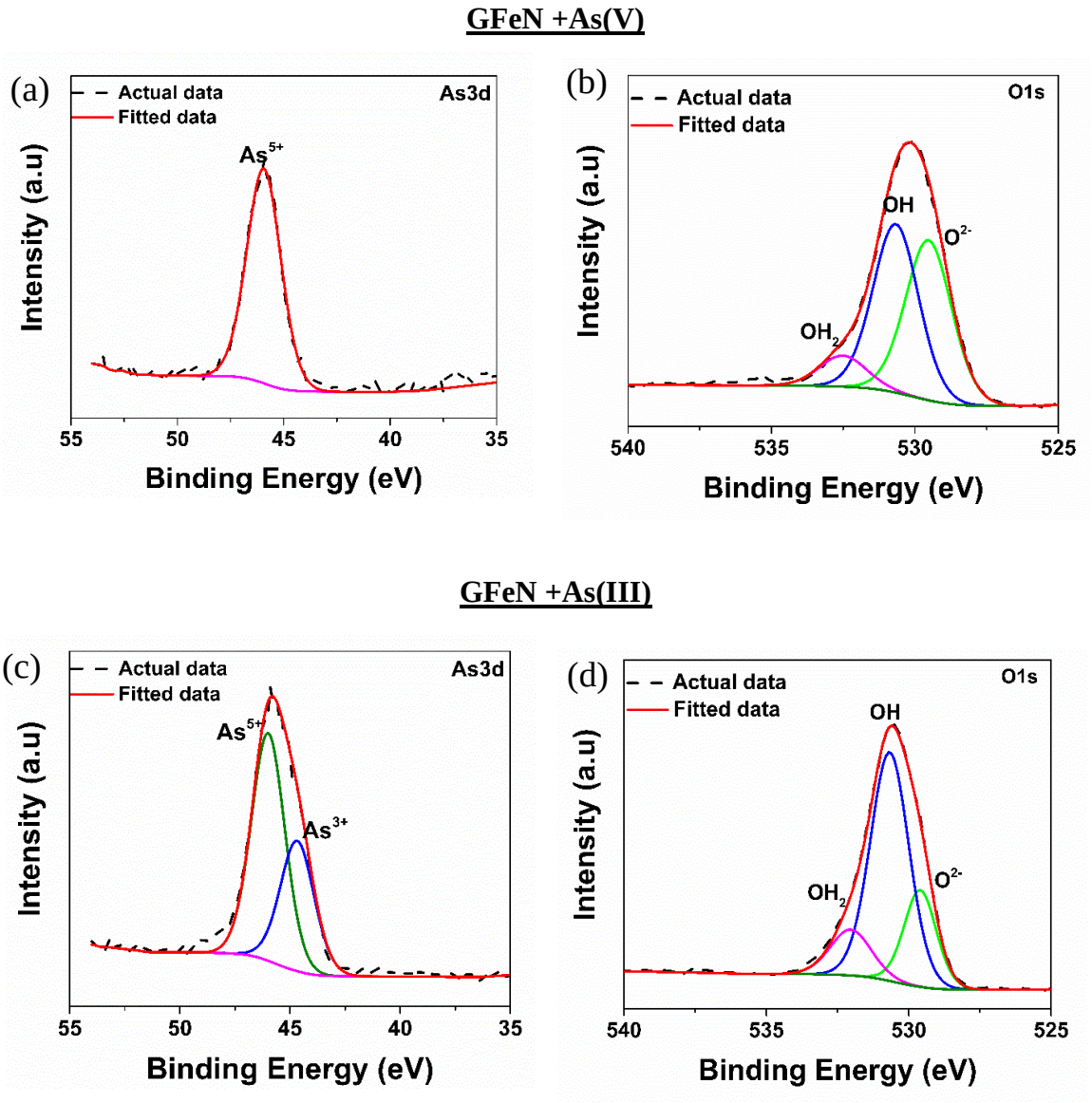

Figure 3.11. XPS spectra for GFeN after As(V) adsorption: (a) As3d and (b) O1s; and XPS spectra for GFeN after As(III) adsorption: (c) As3d and (d) O1s.

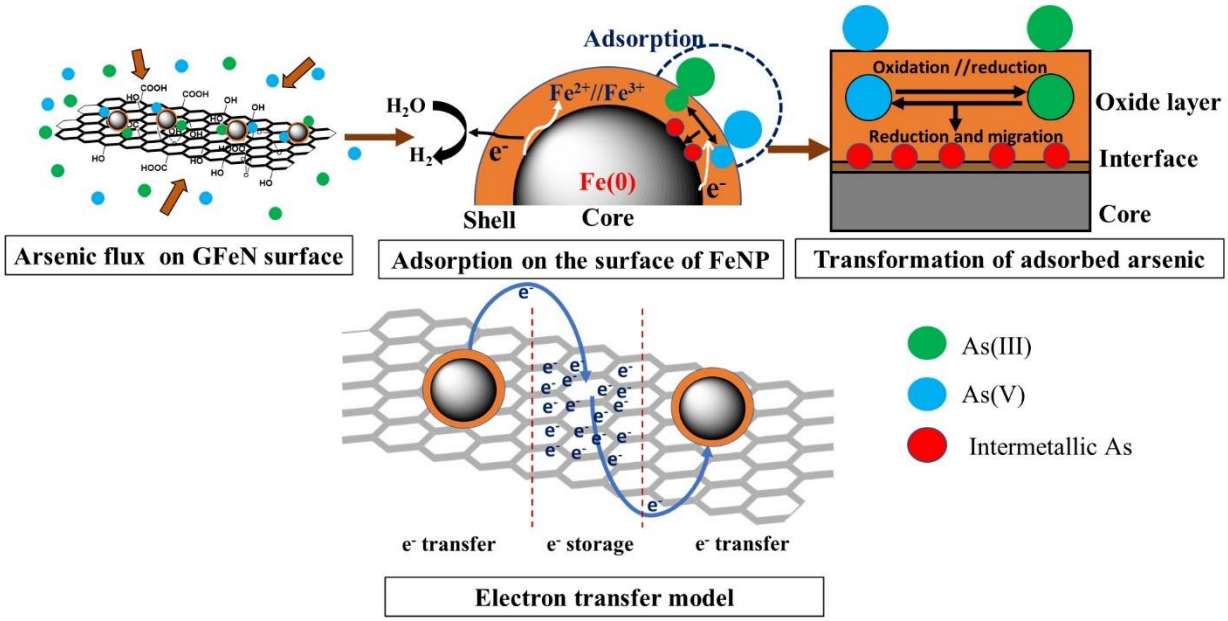

Figure 3.12. Top: The possible mechanism for arsenic removal by GFeN. The proposed mechanism involves arsenic flux built-up at the solution-adsorbent interface, followed by adsorption onto the iron nanoparticles (FeNPs) present on GFeN. Simultaneous oxidation and reduction of adsorbed arsenic occur, and the reduced arsenic moves to the core of the FeNPs. Bottom: The graphene oxide (GO) sheet acts as the reservoir for electrons (e^-) released during iron oxidation and the stored electrons are used by the oxide layer (on FeNPs) to rejuvenate itself for further adsorption of arsenic.

Additionally, the As(V) → As(0) reaction has a potential of 0.499 V while reduction potential of the Fe(0) → Fe(II) reaction is –0.477 V, and, thus, As(V) → As(0) transformation (Eqs. 12-20) is thermodynamically favorable (Melitas et al., 2002; Sasaki et al., 2009). The oxide layer on FeNP contains a mixture of amorphous and crystalline iron oxides with the amorphous phase being much larger (2-10 times) than the crystalline phase (Dixit and Hering, 2003; Yan et al., 2012b; Ling and Zhang, 2014; Wu et al., 2017). The porous nature of the amorphous phase, and the lattice disorder and oxygen vacancies in the crystalline phase facilitate faster ionic mobility of arsenic (Kerisit and Rosso, 2005). Both the arsenic species migrate toward the Fe^0 core (Figure 3.12) and get reduced to an intermetallic phase of As(0) (Yan et al., 2012b; Ling

and Zhang, 2014). Intermetallic arsenic species are known to be more stable than other species (Yan et al., 2012a; Tucek et al., 2017) and that adds to the robustness of the adsorbent (GFeN). There are two possible pathways for the reduction of arsenic by FeNPs (Tucek et al., 2017).

Pathway 1:

$$Fe^{o} + H_2AsO_4^{-} \rightarrow Fe_xO_y + H_2AsO_3^{-} \quad (12)$$

$$Fe^{o} + H^{+} + H_2AsO_3^{-} \rightarrow Fe_xO_y + As(0) + H_2O \quad (13)$$

$$Fe^{o} + HAsO_4^{2-} \rightarrow Fe_xO_y + HAsO_3^{2-} \quad (14)$$

$$Fe^{o} + H^{+} + HAsO_3^{2-} \rightarrow Fe_xO_y + As(0) + H_2O \quad (15)$$

Pathway 2:

$$Fe^{o} + H_2O \rightarrow Fe_xO_y + H_2 \quad (16)$$

$$H_2 + H_2AsO_4^{-} \rightarrow H_2AsO_3^{-} + H_2O \quad (17)$$

$$3H_2 + 2H_2AsO_3^{-} + 2H^{+} \rightarrow 2As(0) + 6H_2O \quad (18)$$

$$H_2 + HAsO_4^{2-} \rightarrow HAsO_3^{2-} + H_2O \quad (19)$$

$$3H_2 + 4H^{+} + 2HAsO_3^{2-} \rightarrow 2As(0) + 6H_2O \quad (20)$$

3.4. Practical significance

The relatively high arsenic removal capacity of GFeN (>300 mg As/g for both the species) and rapid reaction kinetics are very significant for possible field applications of the nanohybrid. Assuming that a typical four-member family needs a minimum of 20 liters of drinking water per day, the amount of GFeN needed to treat arsenic contaminated water to meet daily water demand will be 10 g per year (detailed calculations in, Table 3.7). We assumed an influent arsenic concentration in groundwater as 100 µg/L, the target MCL for arsenic as 0 µg/L (this is the MCL Goal or MCLG for arsenic (U.S.EPA, 2020). We further took the adsorption capacity of the material as 300 mg As per g GFeN for both the species although our reported arsenic adsorption capacities of GFeN are 430 mg As(V)/g and 306 mg As(III)/g. A factor of

safety of 4 was applied which means that only 25% of the experimental arsenic adsorption capacity of GFeN will be used. The water requirement for drinking and cooking is assumed as 20 L/d per 4-member family.

The amount of GFeN needed for a treatment system was calculated from Eq. 21 and presented in Table 3.7.

$$GFeN\left(\frac{g}{year}\right) = \frac{(Intial\ As - Target\ As) \times \frac{water\ requirment}{day} \times 365}{adsorption\ capacity} \times factor\ of\ safety \qquad (21)$$

Table 3.7. Point-of-Use (POU) treatment system to supply arsenic-free drinking water (20 L/d for a 4-member family).

Calculation parameters	**Value**	**Unit**
Arsenic in water	100	µg/L
Target arsenic concentration after treatment	0	µg/L
Adsorption capacity of the adsorptive material	300	mg As/g
Factor of safety	4	-
Drinking water demand /family	20	L/d
GFeN needed/family/year	10	g

It is important to note that this number is calculated assuming only 25% efficiency in arsenic adsorption by GFeN (25% of 300 mg/g = 75 mg As per g of GFeN), a raw water arsenic concentration of 100 µg/L (typical value), and a finished water arsenic concentration of 0 µg/L (MCL Goal, (U.S.EPA, 2020)). If a point-of-use (POU) treatment system is fabricated with 100 g of GFeN, then it is expected to work for ~10 years. Additionally, such systems can be scaled up for community water treatment. This is significant because such a treatment unit will reduce the need for frequent monitoring of the system and water quality. Monitoring water quality is always a challenge in rural and remote communities. Moreover, it will reduce the volume of hazardous waste generated and the frequency of such generation.

3.5. Conclusions

In this paper, we have reported an easy to adopt synthesis process for graphene oxide-iron nanohybrid (GFeN). GFeN exhibits very high adsorption capacities for As(V) (431 mg/g) and As(III) (306 mg/g) compared to other available nanohybrid sorbents (reported adsorption capacities of 12 to 240 mg/g, Table 3.6). At environmentally relevant arsenic concentrations (up to 140 µg/L), GFeN could bring down the effluent arsenic concentrations to below the MCL (10 µg/L) within 10 min. The adsorbent works for both the species of arsenic even when they were present simultaneously. GFeN nanohybrid removes >90% arsenic even in the presence of potential competing anions (SO_4^{2-}, NO_3^-, HCO_3^-, PO_4^{3-}, SiO_3^{2-}) and organic matters (organic acid) at environmentally relevant concentrations. Arsenic removal by GFeN is not controlled by electrostatic forces alone but surface complexation played a major role to make it effective across a wide pH range (pH 3–9). Iron nanoparticles (FeNPs) were well dispersed on the graphene oxide (GO) sheets and thus most of the reactive surfaces on the nanoparticles were available for arsenic removal. The GO sheet also played an important role by acting as the reservoir for the released electrons during the oxidation of Fe^0 present in GFeN and then transferring the electrons back to the nanoparticle (FeNP) surface to rejuvenate the adsorptive oxide layer. We also report a comprehensive mechanism to explain the unique arsenic adsorption behavior of the nanohybrid (GFeN). Interfacial (water and GFeN) exchange of arsenic leads to adsorption through electrostatic attraction and surface complexation, and the adsorbed arsenic then gets transformed and stabilizes in the nanohybrid. The ultra-high adsorption capacity (>300 mg/g for either arsenic species) along with quick reaction kinetics and effectiveness under different environmental conditions make GFeN an ideal candidate for potential use in aqueous arsenic remediation. Our calculations indicate that a point-of-use treatment unit with 100 g of

GFeN can potentially supply arsenic-free drinking water for ~10 years without much operation and maintenance needs.

3.6. References

Ayotte, J.D., Medalie, L., Qi, S.L., Backer, L.C., Nolan, B.T., 2017. Estimating the High-Arsenic Domestic-Well Population in the Conterminous United States. Environmental Science & Technology 51, 12443-12454.

Balistrieri, L.S., Murray, J.W., 1981. The Surface-Chemistry Of Goethite (Alpha-FeOOH) in Major Ion Seawater. American Journal of Science 281, 788-806.

Ban, C.M., Wu, Z.C., Gillaspie, D.T., Chen, L., Yan, Y.F., Blackburn, J.L., Dillon, A.C., 2010. Nanostructured Fe3O4/SWNT Electrode: Binder-Free and High-Rate Li-Ion Anode. Advanced Materials 22, E145-E149.

Benjwal, P., Kumar, M., Chamoli, P., Kar, K.K., 2015. Enhanced photocatalytic degradation of methylene blue and adsorption of arsenic(III) by reduced graphene oxide (rGO)-metal oxide (TiO2/Fe3O4) based nanocomposites. RSC Advances 5, 73249-73260.

Bezbaruah, A.N., Kalita, H., Almeelbi, T., Capecchi, C.L., Jacob, D.L., Ugrinov, A.G., Payne, S.A., 2013. Ca-alginate-entrapped nanoscale iron: arsenic treatability and mechanism studies. Journal of Nanoparticle Research 16.1: 2175.

Chandra, V., Park, J., Chun, Y., Lee, J.W., Hwang, I.-C., Kim, K.S., 2010. Water-Dispersible Magnetite-Reduced Graphene Oxide Composites for Arsenic Removal. ACS Nano 4, 3979-3986.

Chen, M.L., Sun, Y., Huo, C.B., Liu, C., Wang, J.H., 2015. Akaganeite decorated graphene oxide composite for arsenic adsorption/removal and its proconcentration at ultra-trace level. Chemosphere 130, 52-58.

Chen, Y., Parvez, F., Gamble, M., Islam, T., Ahmed, A., Argos, M., Graziano, J.H., Ahsan, H., 2009. Arsenic exposure at low-to-moderate levels and skin lesions, arsenic metabolism, neurological functions, and biomarkers for respiratory and cardiovascular diseases: Review of recent findings from the Health Effects of Arsenic Longitudinal Study (HEALS) in Bangladesh. Toxicology and Applied Pharmacology 239, 184-192.

Cong, H. P., Ren, X. C., Wang, P., Yu, S. H., 2012. Macroscopic multifunctional graphene-based hydrogels and aerogels by a metal ion induced self-assembly process. ACS nano 6, 2693-2703.

Dixit, S., Hering, J.G., 2003. Comparison of arsenic (V) and arsenic (III) sorption onto iron oxide minerals: implications for arsenic mobility. Environmental science & technology 37, 4182-4189.

Farrell, J., Chaudhary, B.K., 2013. Understanding Arsenate Reaction Kinetics with Ferric Hydroxides. Environmental Science & Technology 47, 8342-8347.

Gao, W., 2015. The chemistry of graphene oxide. Graphene oxide. Springer, pp. 61-95.

Guo, X.Y., Du, B., Wei, Q., Yang, J., Hu, L.H., Yan, L.G., Xu, W.Y., 2014. Synthesis of amino functionalized magnetic graphenes composite material and its application to remove Cr(VI), Pb(II), Hg(II), Cd(II) and Ni(II) from contaminated water. Journal of Hazardous Materials 278, 211-220.

Hall, K.R., Eagleton, L.C., Acrivos, A., Vermeulen, T., 1966. Pore and Solid-Diffusion Kinetics in Field-bed Adsorption under Constant-pattern Conditions. Industrial & Engineering Chemistry Fundamentals 5, 212-223.

Hao, L., Ouyang, T., Lai, L., Liu, Y. X., Chen, S., Hu, H., Chang, C. T., Wang, J.-J., 2014. Temperature effects on arsenate adsorption onto goethite and its preliminary application to arsenate removal from simulative geothermal water. RSC Advances 4, 51984-51990.

Hao, L.L., Liu, M.Z., Wang, N.N., Li, G.J., 2018. A critical review on arsenic removal from water using iron-based adsorbents. RSC Advances 8, 39545-39560.

Ho, Y.S., McKay, G., 1998. Kinetic models for the sorption of dye from aqueous solution by wood. Process Safety and Environmental Protection 76, 183-191.

Hoan, N.T.V., Thu, N.T.A., Van Duc, H., Cuong, N.D., Khieu, D.Q., Vo, V., 2016. Fe3O4/Reduced Graphene Oxide Nanocomposite: Synthesis and Its Application for Toxic Metal Ion Removal. Journal of Chemistry, 10.

Huong, P.T.L., Huy, L.T., Phan, V.N., Huy, T.Q., Nam, M.H., Lam, V.D., Le, A.T., 2016. Application of Graphene Oxide-MnFe2O4 Magnetic Nanohybrids as Magnetically Separable Adsorbent for Highly Efficient Removal of Arsenic from Water. Journal of Electronic Materials 45, 2372-2380.

International Organization for Standardization (ISO), ISO BS 14887 (2000) Sample preparation—dispersing procedures for powders in liquids, International Organization for Standardization, Geneva, Switzerland (2000).

Kanel, S.R., Greneche, J. M., Choi, H., 2006. Arsenic (V) removal from groundwater using nano scale zero-valent iron as a colloidal reactive barrier material. Environmental Science & Technology 40, 2045-2050.

Karanfil, T., Schlautman, M.A., Erdogan, I., 2002. Survey of DOC and UV measurement practices with implications for SUVA determination. Journal American Water Works Association 94, 68-80.

Kerisit, S., Rosso, K.M., 2005. Charge transfer in FeO: A combined molecular-dynamics and ab initio study. Journal of Chemical Physics 123, (22), 224712.

Krajangpan, S., Kalita, H., Chisholm, B.J., Bezbaruah, A.N., 2012. Iron Nanoparticles Coated with Amphiphilic Polysiloxane Graft Copolymers: Dispersibility and Contaminant Treatability. Environmental Science & Technology 46, 10130-10136.

La, D.D., Patwari, J.M., Jones, L.A., Antolasic, F., Bhosale, S.V., 2017. Fabrication of a GNP/Fe-Mg Binary Oxide Composite for Effective Removal of Arsenic from Aqueous Solution. ACS Omega 2, 218-226.

Lataye, D.H., Mishra, I.M., Mall, I.D., 2006. Removal of pyridine from aqueous solution by adsorption on bagasse fly ash. Industrial & Engineering Chemistry Research 45, 3934-3943.

Li, X. Q., Zhang, W. X., 2007. Sequestration of metal cations with zerovalent iron nanoparticles a study with high resolution X-ray photoelectron spectroscopy (HR-XPS). The Journal of Physical Chemistry C 111, 6939-6946.

Liang, J.J., He, B.H., Li, P., Yu, J., Zhao, X.L., Wu, H.Y., Li, J., Sun, Y.B., Fan, Q.H., 2019. Facile construction of 3D magnetic graphene oxide hydrogel via incorporating assembly and chemical bubble and its application in arsenic remediation. Chemical Engineering Journal 358, 552-563.

Lightcap, I.V., Kosel, T.H., Kamat, P.V., 2010. Anchoring Semiconductor and Metal Nanoparticles on a Two-Dimensional Catalyst Mat. Storing and Shuttling Electrons with Reduced Graphene Oxide. Nano Letters 10, 577-583.

Ling, L., Zhang, W.X., 2014. Sequestration of Arsenate in Zero-Valent Iron Nanoparticles: Visualization of Intraparticle Reactions at Angstrom Resolution. Environmental Science & Technology Letters 1, 305-309.

Lingamdinne, L.P., Koduru, J.R., Chang, Y.Y., Kang, S.H., Yang, J.K., 2019. Facile synthesis of flowered mesoporous graphene oxide-lanthanum fluoride nanocomposite for adsorptive removal of arsenic. Journal of Molecular Liquids 279, 32-42.

Liu, A., Liu, J., Han, J., Zhang, W.X., 2017. Evolution of nanoscale zero-valent iron (nZVI) in water: Microscopic and spectroscopic evidence on the formation of nano- and micro-structured iron oxides. Journal of Hazardous Materials 322, 129-135.

Liu, A., Liu, J., Pan, B., Zhang, W. X., 2014. Formation of lepidocrocite (γ-FeOOH) from oxidation of nanoscale zero-valent iron (nZVI) in oxygenated water. RSC Advances 4, 57377-57382.

Liu, A.R., Liu, J., Zhang, W.X., 2015. Transformation and composition evolution of nanoscale zero valent iron (nZVI) synthesized by borohydride reduction in static water. Chemosphere 119, 1068-1074.

Luo, X., Wang, C., Luo, S., Dong, R., Tu, X., Zeng, G., 2012. Adsorption of As (III) and As (V) from water using magnetite Fe3O4-reduced graphite oxide-MnO2 nanocomposites. Chemical Engineering Journal 187, 45-52.

Luo, X.B., Wang, C.C., Wang, L.C., Deng, F., Luo, S.L., Tu, X.M., Au, C.T., 2013. Nanocomposites of graphene oxide-hydrated zirconium oxide for simultaneous removal of As(III) and As(V) from water. Chemical Engineering Journal 220, 98-106.

Ma, J., Zhu, Z., Chen, B., Yang, M., Zhou, H., Li, C., Yu, F., Chen, J., 2013. One-pot, large-scale synthesis of magnetic activated carbon nanotubes and their applications for arsenic removal. Journal of Materials Chemistry A 1, 4662-4666.

Martin, J.E., Herzing, A.A., Yan, W.L., Li, X.Q., Koel, B.E., Kiely, C.J., Zhang, W.X., 2008. Determination of the oxide layer thickness in core-shell zerovalent iron nanoparticles. Langmuir 24, 4329-4334.

Meharg, A.A., Zhao, F. J., 2012. Arsenic & Rice. Springer Science & Business Media.

Melitas, N., Wang, J.P., Conklin, M., O'Day, P., Farrell, J., 2002. Understanding soluble arsenate removal kinetics by zerovalent iron media. Environmental Science & Technology 36, 2074-2081.

Mishra, A.K., Ramaprabhu, S., 2012. Ultrahigh arsenic sorption using iron oxide-graphene nanocomposite supercapacitor assembly. Journal of Applied Physics *112*(10), p.104315.

Mortazavian, S., An, H., Chun, D., Moon, J., 2018. Activated carbon impregnated by zero-valent iron nanoparticles (AC/nZVI) optimized for simultaneous adsorption and reduction of aqueous hexavalent chromium: Material characterizations and kinetic studies. Chemical Engineering Journal 353, 781-795.

Murcott, S., 2012. Arsenic Contamination in the World. IWA publishing.

Nieuwoudt, M.K., Comins, J.D., Cukrowski, I., 2011. The growth of the passive film on iron in 0.05 M NaOH studied in situ by Raman micro-spectroscopy and electrochemical polarisation. Part I: near-resonance enhancement of the Raman spectra of iron oxide and oxyhydroxide compounds. Journal of Raman Spectroscopy 42, 1335-1339.

Pang, S.Y., Jiang, J., Ma, J., 2011. Response to Comment on "Oxidation of Sulfoxides and Arsenic(III) in Corrosion of Nanoscale Zero Valent Iron by Oxygen: Evidence against Ferryl Ions (Fe(IV)) as Active Intermediates in Fenton Reaction". Environmental Science & Technology 45, 3179-3180.

Perreault, F., De Faria, A.F., Elimelech, M., 2015. Environmental applications of graphene-based nanomaterials. Chemical Society Reviews 44, 5861-5896.

Petcharoen, K., Sirivat, A., 2012. Synthesis and characterization of magnetite nanoparticles via the chemical co-precipitation method. Materials Science and Engineering B-Advanced Functional Solid-State Materials 177, 421-427.

Ramos, M.A.V., Yan, W., Li, X.Q., Koel, B.E., Zhang, W.X., 2009. Simultaneous Oxidation and Reduction of Arsenic by Zero-Valent Iron Nanoparticles: Understanding the Significance of the Core-Shell Structure. Journal of Physical Chemistry C 113, 14591-14594.

Ren, L.M., Dong, J., Chi, Z.F., Huang, H.Z., 2018. Reduced graphene oxide-nano zero value iron (rGO-nZVI) micro-electrolysis accelerating Cr(VI) removal in aquifer. Journal of Environmental Sciences 73, 96-106.

Roberts, L.C., Hug, S.J., Ruettimann, T., Billah, M., Khan, A.W., Rahman, M.T., 2004. Arsenic removal with iron(II) and iron(III) waters with high silicate and phosphate concentrations. Environmental Science & Technology 38, 307-315.

Sakthivel, T.S., Das, S., Pratt, C.J., Seal, S., 2017. One-pot synthesis of a ceria–graphene oxide composite for the efficient removal of arsenic species. Nanoscale 9(10), 3367-3374.

Salameh, Y., Al-Lagtah, N., Ahmad, M.N.M., Allen, S.J., Walker, G.M., 2010. Kinetic and thermodynamic investigations on arsenic adsorption onto dolomitic sorbents. Chemical Engineering Journal 160, 440-446.

Sasaki, K., Nakano, H., Wilopo, W., Miura, Y., Hirajima, T., 2009. Sorption and speciation of arsenic by zero-valent iron. Colloids and Surfaces a-Physicochemical and Engineering Aspects 347, 8-17.

Sheng, G.D., Li, Y.M., Yang, X., Ren, X.M., Yang, S.T., Hu, J., Wang, X.K., 2012. Efficient removal of arsenate by versatile magnetic graphene oxide composites. RSC Advances 2, 12400-12407.

Stachowicz, M., Hiemstra, T., van Riemsdijk, W.H., 2008. Multi-competitive interaction of As (III) and As (V) oxyanions with Ca2+, Mg2+, PO3−4, and CO2−3 ions on goethite. Journal of Colloid and Interface Science 320, 400-414.

Stefaniuk, M., Oleszczuk, P., Ok, Y.S., 2016. Review on nano zerovalent iron (nZVI): From synthesis to environmental applications. Chemical Engineering Journal 287, 618-632.

Su, H., Ye, Z.B., Hmidi, N., 2017. High-performance iron oxide-graphene oxide nanocomposite adsorbents for arsenic removal. Colloids and Surfaces a-Physicochemical and Engineering Aspects 522, 161-172.

Tang, X. Z., Cao, Z., Zhang, H. B., Liu, J., Yu, Z. Z., 2011. Growth of silver nanocrystals on graphene by simultaneous reduction of graphene oxide and silver ions with a rapid and efficient one-step approach. Chemical Communications 47, 3084-3086.

Tucek, J., Prucek, R., Kolarik, J., Zoppellaro, G., Petr, M., Filip, J., Sharma, V.K., Zboril, R., 2017. Zero-Valent Iron Nanoparticles Reduce Arsenites and Arsenates to As(0) Firmly Embedded in Core-Shell Superstructure: Challenging Strategy of Arsenic Treatment under Anoxic Conditions. ACS Sustainable Chemistry & Engineering 5, 3027-3038.

United States Environmental Protection Agency (USEPA), National Primary Drinking Water Regulations, (2019), Available at: https://www.epa.gov/ground-water-and-drinking-water/national-primary-drinking-water-regulations (Access date December 2, 2019).

United States Environmental Protection Agency (USEPA), 2001. National primary drinking water regulations; arsenic and clarifications to compliance and new source contaminants monitoring. Fed Reg 66, 6975-7066.

Van der Leeden, F., 1990. The water encyclopedia. CRC Press.

Wallace, S.H., Shaw, S., Morris, K., Small, J.S., Fuller, A.J., Burke, I.T., 2012. Effect of groundwater pH and ionic strength on strontium sorption in aquifer sediments: Implications for Sr-90 mobility at contaminated nuclear sites. Applied Geochemistry 27, 1482-1491.

Wang, C., Luo, H.J., Zhang, Z.L., Wu, Y., Zhang, J., Chen, S.W., 2014. Removal of As(III) and As(V) from aqueous solutions using nanoscale zero valent iron-reduced graphite oxide modified composites. Journal of Hazardous Materials 268, 124-131.

Wang, H., Robinson, J.T., Diankov, G., Dai, H., 2010. Nanocrystal Growth on Graphene with Various Degrees of Oxidation. Journal of the American Chemical Society 132, 3270-3271.

Wang, P.L., Zhou, X., Zhang, Y.G., Yang, L.P., Zhi, K.K., Wang, L.L., Zhang, L.T., Guo, X.F., 2017. Unveiling the mechanism of electron transfer facilitated regeneration of active Fe2+ by nano-dispersed iron/graphene catalyst for phenol removal. RSC Advances 7, 26983-26991.

Wang, S.B., Sun, H.Q., Ang, H.M., Tade, M.O., 2013. Adsorptive remediation of environmental pollutants using novel graphene-based nanomaterials. Chemical Engineering Journal 226, 336-347.

Weber, T.W., Chakravorti, R.K., 1974. Pore and Solid Diffusion Models for Fixed-bed Adsorbers. Aiche Journal 20, 228-238.

Wen, T., Wu, X.L., Tan, X.L., Wang, X.K., Xu, A.W., 2013. One-Pot Synthesis of Water-Swellable Mg-Al Layered Double Hydroxides and Graphene Oxide Nanocomposites for Efficient Removal of As(V) from Aqueous Solutions. ACS Applied Materials & Interfaces 5, 3304-3311.

World Health Organization (WHO), Arsenic in Drinking-water: Background Document for Development of WHO Guidelines for Drinking-water Quality, WHO/SDE/WSH/03.04/75. 2003.

World Health Organization (WHO), Guidelines for Drinking-water Quality, World Health Organization, 2004.

World Health Organization (WHO), Arsenic Fact Sheet, 2018, Available at: https://www.who.int/news-room/fact-sheets/detail/arsenic. (Access November 23, 2019)

Wu, C., Tu, J.W., Liu, W.Z., Zhang, J., Chu, S.Q., Lu, G.N., Lin, Z., Dang, Z., 2017. The double influence mechanism of pH on arsenic removal by nano zero valent iron: electrostatic interactions and the corrosion of Fe0. Environmental Science-Nano 4, 1544-1552.

Wu, K., Jing, C.Y., Zhang, J., Liu, T., Yang, S.J., Wang, W.D., 2019. Magnetic Fe3O4@CuO nanocomposite assembled on graphene oxide sheets for the enhanced removal of arsenic(III/V) from water. Applied Surface Science 466, 746-756.

Wu, L.K., Wu, H., Zhang, H.B., Cao, H.Z., Hou, G.Y., Tang, Y.P., Zheng, G.Q., 2018. Graphene oxide/CuFe2O4 foam as an efficient absorbent for arsenic removal from water. Chemical Engineering Journal 334, 1808-1819.

Xu, L., Yan, K., Mao, Y., Wu, D., 2019. Enhancing the dioxygen activation for arsenic removal by Cu0 nano-shell-decorated nZVI: Synergistic effects and mechanisms. Chemical Engineering Journal, 123295.

Yan, W., Vasic, R., Frenkel, A.I., Koel, B.E., 2012a. Intraparticle Reduction of Arsenite (As(III)) by Nanoscale Zerovalent Iron (nZVI) Investigated with In Situ X-ray Absorption Spectroscopy. Environmental Science & Technology 46, 7018-7026.

Yan, W.L., Ramos, M.A.V., Koel, B.E., Zhang, W.X., 2012b. As(III) Sequestration by Iron Nanoparticles: Study of Solid-Phase Redox Transformations with X-ray Photoelectron Spectroscopy. Journal of Physical Chemistry C 116, 5303-5311.

Yoon, Y., Park, W.K., Hwang, T.M., Yoon, D.H., Yang, W.S., Kang, J.W., 2016. Comparative evaluation of magnetite-graphene oxide and magnetite-reduced graphene oxide composite for As(III) and As(V) removal. Journal of Hazardous Materials 304, 196-204.

Yoon, Y., Zheng, M., Ahn, Y.-T., Park, W.K., Yang, W.S., Kang, J.-W., 2017. Synthesis of magnetite/non-oxidative graphene composites and their application for arsenic removal. Separation and Purification Technology 178, 40-48.

Yu, X.W., Wei, Y.F., Liu, C.B., Ma, J.H., Liu, H., Wei, S.D., Deng, W., Xiang, J.N., Luo, S.L., 2019. Ultrafast and deep removal of arsenic in high-concentration wastewater: A superior bulk adsorbent of porous Fe2O3 nanocubes-impregnated graphene aerogel. Chemosphere 222, 258-266.

Zhu, J., Lou, Z.M., Liu, Y., Fu, R.Q., Baig, S.A., Xu, X.H., 2015. Adsorption behavior and removal mechanism of arsenic on graphene modified by iron-manganese binary oxide (FeMnOx/RGO) from aqueous solutions. RSC Advances 5, 67951-67961.

CHAPTER 4. DESORPTION PROFILE OF ARSENIC FROM GRAPHENE OXIDE-METAL OXIDE NANO-HYBRID

4.1. Introduction

Arsenic (As) is a class one carcinogenic metalloid which presents in groundwater as oxyanions with different oxidation states [As(III) and As(V)] (Jomova et al., 2011). The drinking water maximum contaminant level (MCL) level for arsenic is 10µg/L (WHO, 2017). Throughout the world, more than 200 million people are exposed to arsenic contaminated water and cause great concern for public health (Podgorski and Berg, 2020). Groundwater arsenic contamination is spread throughout the world from Southeast Asia (India, Bangladesh, Pakistan, Nepal, Vietnam, Cambodia), to Europe (Turkey, Greece, Romania, Slovakia, Croatia, Serbia, Hungary, Spain), South America (Argentina, Bolivia, Chile, Uruguay, Mexico) and the USA. (Murcott, 2012; WHO, 2017; Ahmad et al., 2020; Podgorski and Berg, 2020). In the United States, several region's groundwaters recorded arsenic contamination above the MCL level which affected ~2.1 million people (Ayotte et al., 2017).

Arsenic is non-biodegradable and long persistence in the environment, separation of inorganic arsenic from aqueous media is the most logical way to treat arsenic. Adsorption, coagulation-flocculation, precipitation, ion exchange, and membrane filtration are the proven technology for arsenic treatment. Among all these techniques adsorption is the most feasible option to adopt and promoted globally. An ideal adsorbent for a filter treatment unit should have the following characteristics like high arsenic adsorption capacity, quick reaction kinetics, and work for a longer period without losing its efficiency. Further, it should work globally from rural to an urban settings with minimum external energy and monitoring and maintenance.

It is evident from the literature that metal oxide nano adsorbents are more efficient in terms of adsorption capacity and quick reaction rate compared to other adsorbents (Lata and Samadder, 2016) (Baig et al., 2015; Nicomel et al., 2016). Adsorption of arsenic by metal oxide nanoparticles are extensively studied over the last two decades (Mohan and Pittman, 2007; Gallegos-Garcia et al., 2012; Lata and Samadder, 2016; Hao et al., 2018). These nanoparticles could not work with its full potential as it agglomerates immediately after the synthesis process and that reduces adsorption efficiency. Embedding nanoparticles on a suitable support media (Carbonaceous material, clay, zeolites) can reduce the agglomeration and improve the contact between nanoparticles surface and contaminant which can enhance the removal efficiency. Among these support media graphene oxide (GO) promises great potential. GO is a 2D layer of honeycomb carbon network with very high specific surface area (320-940 m^2/g) and attached with functional groups (−OH,−COOH, −O−). The metal oxide-nanoparticles synthesized on the surface GO sheets (nanohybrids) are well dispersed (Chandra et al., 2010; Hoan et al., 2016; Fu et al., 2017; Wu et al., 2019). This new class of material is designed as graphene oxide metal oxide nanohybrids or nanocomposites are showed to be very efficient adsorbents for arsenic removal and perform better than bare nanoparticles.

For the last ten years, wide categories of nanohybrids are evaluated for their superior arsenic removal performance (Figure 4.1). The nanohybrids recorded very high adsorption capacities and better reaction kinetics compared with bare nanoparticles. In our previous studies, we reported that GO supported iron and GO supported cerium oxide nanohybrids showed very high adsorption capacities for As(V) (431 mg/g for GFeN and 212 mg/g for GO-CeO_2) and quick reaction kinetics (less than 10 mins with As(V) concentration 100 µg/L) which made both the nanohybrids suitable for use in the arsenic treatment system. While the sorption of arsenic on this

nanohybrid system is well investigated, information regarding the desorption of arsenic from the nanohybrids is lacking. The mechanisms of desorption are not well understood. Secondary desorption of arsenic from the nanohybrids under changeable environmental conditions is a real concern for practical application. As these nanohybrids have very high adsorption capacities, so filter media fabricated with this material will be expected to have a longer operational lifespan (at least 4-5 years). So, it is necessary to understand the fate of exhausted nanomaterial over time while the treatment system is still working. A complete desorption profile of arsenic saturated nanohybrids is very important. To provide this scientific and practical information, in this study we investigated the desorption behavior of arsenic from As(V) saturated GFeN and GO-CeO_2 under the variable environmental condition both short duration and long-duration time frame (two years). We also investigated changes in adsorbed arsenic complexation of nanohybrids over time. This study will facilitate the assessment of arsenic release from the nanohybrids inside filter bed media and help to understand the changes undergoes in arsenic saturated nanohybrid over time.

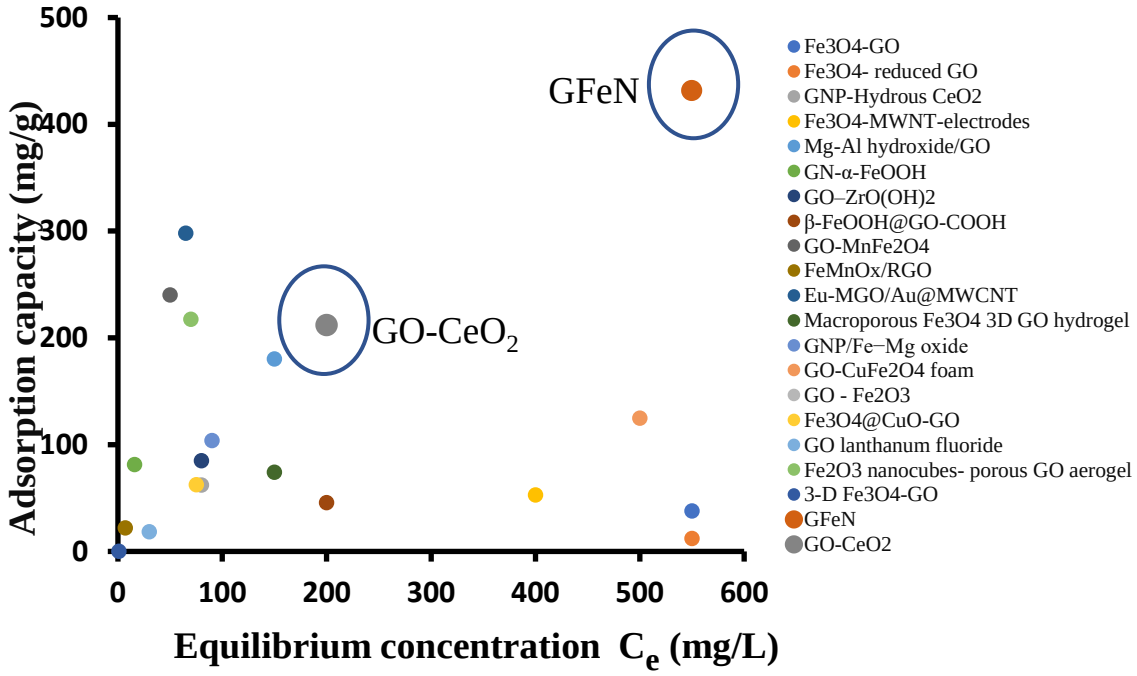

Figure 4.1. High arsenic adsorbing graphene oxide metal oxide nanohybrids.

4.2. Material and methods

4.2.1. Chemicals

Analytical grade $Ce(NO_3)_3 \cdot 6H_2O$ (99%) Sigma-Aldrich, ferrous sulfate ($FeSO_4 \cdot 7H_2O$, >99.5%, Merck, Germany), sodium borohydride ($NaBH_4$, >97%, Alfa Aesar, USA), and ammonium hydroxide (ACS reagent grade) were used. The 1000 ppm arsenic standard (III and V) in nitric acid solution was obtained from Environmental Express (USA). The graphene oxide (GO) was obtained from Garmor LLC (USA) for GO CeO_2 synthesis and from Graphenea (Spain) for GFeN.

4.2.2. Material synthesis

GO-CeO_2 was prepared as per Sakthivel et al (2017). Briefly, GO (240 mg) was dispersed in DI water (20 mL) mixed with cerium(III) nitrate hexahydrate (1.73 g), and pH was adjusted to 10. The resultant mixed solution was transferred into synthesis vessels and put in an oven for 4 h at 140 °C. The synthesized material was washed in copious amounts of DI water to

remove the unreacted chemicals followed by oven drying (80 ℃) to get GO-CeO_2. GFeN synthesis was done as reported earlier. In brief, $FeSO_4.7H_2O$ solution (2.25 g in 50 mL DDI water) was mixed with 250 mg GO in a round bottom flask and the solution pH was adjusted to ~6. $NaBH_4$ solution was added to the GO solution under continuous stirring and N_2 environment and kept at 60 ºC for 4 h to allow for the reaction to complete. The black colored end product was washed using a copious amount of DDI water and ethanol and dried in a vacuum oven under a nitrogen environment.

4.2.3. Characterization

Transmission electron microscopy (TEM) images were obtained using a JEOL JEM-2100 LaB6 transmission electron microscope (JEOL USA, Peabody, MA, USA) ran at 200 kV. Powdered nanohybrid was placed in 100% ethanol and sonicated. A drop of the suspension was placed on a lacey-carbon support film on a 300-mesh copper TEM grid (Ted Pella, Redding, California USA) for 30 sec, then wicked off with a filter paper and allowed to air dry. High-Resolution X-ray Photoelectron Spectroscopy (HR-XPS) analysis was performed on a Thermo Fisher ESCALAB 250Xi spectrometer (Thermo Fisher Scientific, Waltham, MA, USA) with a monochromated Al Kα X-beams (hν = 1486.7 eV). The specimens were set in the HR-XPS examination chamber ($5x10^{-9}$ Torr) where spectra for Fe2p, As3d, C1s, and O1s were recorded. Peak fitting was accomplished by utilizing the Avantage XPS program.

4.2.4. Desorption experiment

For the desorption experiment, a 1000 mL wide-mouth plastic bottle with caps was used. Each reactor was filled with 500 mL 200 mg/L As(V) solution and each measured amount (250 mg, i.e., 0.5 g/L) of a nanohybrid (GO-CeO_2 or GFeN) was added and then pH was adjusted to 7. The reactors were put in an end-over-end shaker (28 rpm) at room temperature (22±2 ºC) for 24

h to allow for arsenic adsorption. The nanohybrid after arsenic adsorption was separated using a vacuum filter (0.2 μm nylon membrane filter), and the nanohybrid was scrapped from the membrane and dried in the vacuum oven at 60 °C for 6 h under nitrogen environment. The initial and final arsenic concentration bulk solution was measured using an atomic absorption spectrometer (AAS) and the amount of arsenic adsorbed onto the nanohybrid was calculated using arsenic mass balance for the bulk solution. The dried nanohybrid was used for desorption experiments. The desorption behaviors of both the materials in DI and synthetic groundwater water (Table 4.1) were evaluated by conducting batch studies. For the batch experiments, 30 mg of each material was put into a 40 mL glass vial (reactor) and 30 mL water was added to it. The reactor was then rotated in the end-over-end shaker (28 rpm) at room temperature. The effects of solution pH (3-9) on desorption were also monitored (batch experiments) where the solution pH was adjusted using 0.1 M HCl/NaOH.

Table 4.1. Composition of synthetic groundwater (Van der Leeden, 1990).

Ions	**Na^+**	**Ca^{2+}**	**Cl^-**	**HCO_3^-**	**SO_4^{2-}**	**PO_4^{3-}**
Concentration (mg/L)	230	32	234	183	96	3

Sequential extraction of adsorbed arsenic from nanohybrids was done as per Dong et al., (2012), a method modified after Keon et al. (2001). Here, 30 mg of nanohybrid (with arsenic adsorbed) was put into a 30 mL of specific extraction solution in a 50 mL centrifuge tube and rotated in end over end shaker for a pre-decided time as per the method. Sequentially, we used four extraction solutions which included $MgCl_2$ (for ionically bound arsenic extraction), NaH_2PO_4 (for strongly adsorbed arsenic), oxalic acid (for arsenic coprecipitated with amorphous Fe oxyhydroxide), and HNO_3 (for arsenic coprecipitated with crystalline Fe oxyhydroxide). After each extraction reaction time, the reactors were taken out and centrifuged for 15 min at 3000 rpm

and decant the supernatant (do very carefully that no residual nanohybrids thrown away). The decant solution was filtered using a 0.2 μm syringe filter and stored for further analysis. The residual in the reactors was washed with 30 mL DI water. After that next extraction solution was added and followed the cycles as per Table 4.2.

Given that sequential extraction is a short-duration experiment and cannot be used to predict the long-term arsenic desorption behavior of an adsorbent, a 24-month study was conducted using synthetic groundwater. For this, 30 mg nanohybrids and 30 mL of synthetic groundwater were put in several sacrificial batch reactors (40 mL vials). The batch reactors were stored in a dark place at room temperature. A set of three reactors were taken out at specific time intervals, and the content was filtered using a 0.22 μm syringe filter (VWR, USA) and arsenic content in the filtrate (bulk solution) was analyzed.

Table 4.2. Sequential Extraction Procedure for As-loaded Nanohybrid.

Step	**Procedure**	**Target phase**	**Possible mechanism**
Mg	1 M $MgCl_2$, pH 8, 2h, 25 °C two repetitions + one water wash	Ionically bound As	anion exchange of Cl for As; possible Mg-As complex formed
PO_4	1 M NaH_2PO_4, pH 5, 24h, 25 °C one repetition + one water wash	Strongly adsorbed As	anion exchange of PO_4 for AsO_4
Oxalic acid	0.2 M oxalic acid, pH 3, 2 h, 25 °C one repetition + one water wash	As coprecipitated with amorphous Fe oxyhydroxides	ligand-promoted dissolution
HNO_3	16 N HNO_3, 2 h, 25 °C	As coprecipitated with crystalline Fe oxyhydroxides	proton dissolution

Modified method from Keon et al., (2001).

To mimic an actual filtration system, a sand block filter was developed with arsenic-sorbed nanohybrid (250 mg)with sand (30 g) and packing them into a column with an effective column length of 10 cm. Such a column would represent a partially saturated drinking water arsenic removal unit. Synthetic groundwater was passed through the column continuously for 60

days in an up-flow mode at a flow rate of 1 mL/min. The effluent arsenic concentration was measure at different time points.

Total inorganic arsenic in all samples was measured using Graphite Furnace-Atomic Absorption Spectrophotometer (GF-AAS, Perkin Elmer AAS 900H) following standard operating procedure.

4.3. Result and discussion

4.3.1. Material characterization

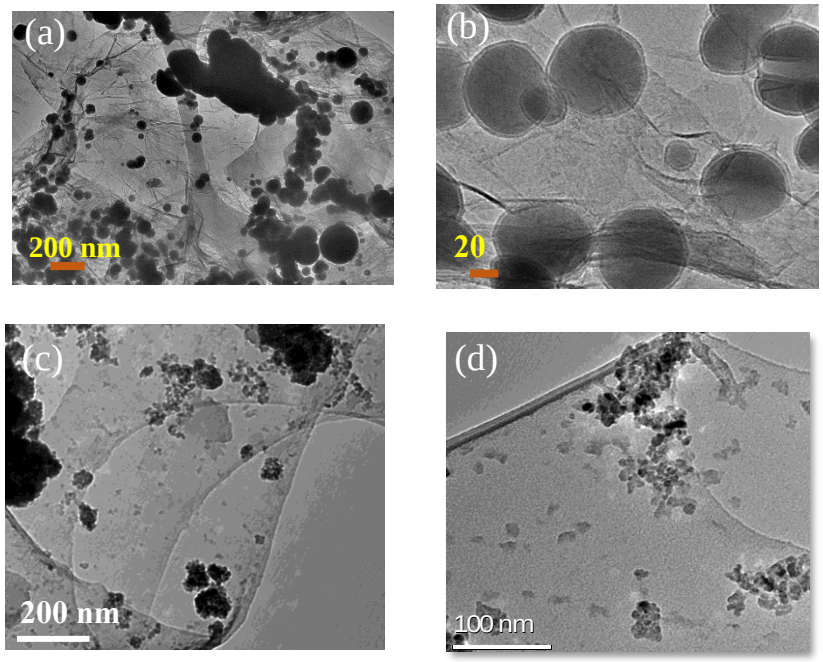

Figure 4.2. TEM micrograph of (a-b) GFeN and (c-d) GO-CeO_2 nanohybrids showed nanoparticles decorated on the graphene oxide surface.

In both the nanohybrids, nanoparticles were dispersedly deposited on the graphene oxide surface (Figure 4.2). A definite core-shell structure of FeNP was observed in the GFeN with a metallic core and an oxide shell (Figure 4.2a-b,). In the case of the GO CeO_2, the nanoparticles were circular (Figure 4.2c-d). The BET-specific surface area was found to be 159.62 m^2/g for GFeN and 129.24 m^2/g for GO CeO_2.

4.3.2. Arsenic saturation and desorption

4.3.2.1. Arsenic sorption

The arsenic loading in arsenic-sorbed nanohybrids was 111 mg of As/g for GFeN and 75 mg/g for GO-CeO_2 (Figure 4.3a). Arsenic sorption by GFeN happened through electrostatic attraction and surface complexation, and the adsorbed arsenic then got transformed to more stable forms in the nanohybrid (Das et al., 2020). XPS analysis of arsenic-sorbed GFeN recorded a strong peak for As(V) at 45.7 eV and a significant change in surface-bound hydroxyl groups (64% with arsenic sorbed to 50% when it sorbed arsenic). As(V) was sorbed onto the GFeN surface through surface complexation and inner-sphere monodentate ($FeOAsO_2OH$) or bidentate [$(FeO)_2AsO_2$)] complexes were formed (Das et al., 2020). GO-CeO_2 attracts arsenate through electrostatic interaction and made a stable surface complex by reacting with Ce^{3+} sites. (Sakthivel et al., 2017) The XPS analysis of arsenic adsorbed GO-CeO_2 showed a strong peak for As(V) (45.4 eV).

The adsorbed arsenic can be present in different forms depending on their surface reaction with the nanohybrids. The sequential extraction of arsenic from the two nanohybrids (with $MgCl_2$, NaH_2PO_4, oxalic acid, and HNO_3) was done to quantify the adsorbed arsenic fractions into (i) ionically bound, (ii) strongly adsorbed, (iii) coprecipitated with amorphous Fe oxyhydroxides, (iv) crystalline Fe oxyhydroxides and (v) residual (i.e., not extractable) (Figure 4.3b). In GFeN, a significant amount (64.31 %) of adsorbed arsenic was associated with the amorphous iron oxyhydroxide phase (oxalic acid fraction) of GFeN (Figure 4.3b) where 34.62 % present as residual. This means that if the environmental conditions (e.g., pH, redox, presence of microorganism) are changed the 64.31% arsenic may get resolubilize in drinking water. Small fractions of the sorbed arsenic were present as ionically bound ($MgCl_2$ fraction, 1.05%), strongly

adsorbed (phosphate, 1.57 %), and crystalline oxyhydroxide (HNO_3, 1.06%). In GO-CeO_2 nanohybrid, 97.15 % of adsorbed arsenic was in the residual form indicating that the arsenic-cerium complexes were strongly bound and would not potentially come out from the adsorption media. As can be seen from the discussion in the previous paragraph, 34.62% of adsorbed arsenic was strongly bound to GFeN and that value is 97.15% for GO-CeO_2. Based on these analyses, it was expected that desorption of arsenic from both the nanohybrid would be minimal with GO- CeO_2 showing the least desorption over time.

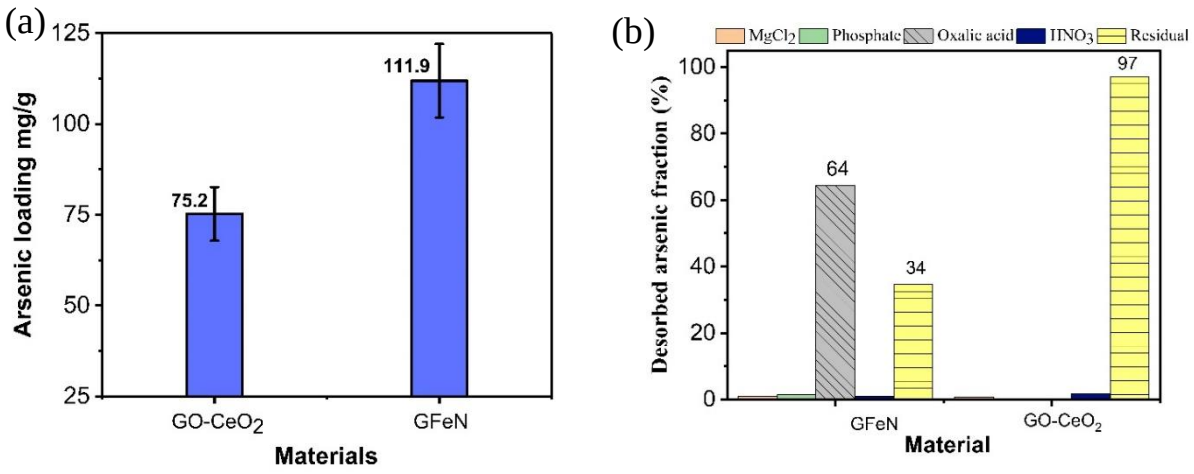

Figure 4.3. (a) Arsenic adsorbed on the nanohybrids from a 200 mg/L As(V) solution in 24 h. (b) The fraction of sorbed arsenic extracted from the nanohybrids. The $MgCl_2$ extracted arsenic was ionically bound arsenic, the phosphate extracted part was strongly adsorbed arsenic, the oxalic acid extracted part is arsenic coprecipitated with amorphous oxyhydroxide, and the arsenic extracted with HNO_3 was coprecipitated with crystalline oxyhydroxide.

4.3.2.2. Desorption studies

4.3.2.2.1. Short-term study

Both the nanohybrids were evaluated for their arsenic desorption (leaching) behavior in DI water and synthetic groundwater system. During the first 3 days, only 2.63% (in GFeN) and 0.56% (in GO-CeO_2) of total adsorbed arsenic desorbed in DI water system (pH ~ 7) under continuous shaking in an end-over-end shaker (28 rpm) at room temperature. In the simulated

groundwater system (pH ~8), there was 0.31% desorption of total adsorbed arsenic from GFeN and 0.32% from GO-CeO_2 over a period of 24 h under continuous shaking. Increase in total dissolve phosphate concentration 0 to 3 mg/L in simulated groundwater increased arsenic desorption slightly from 0.31 to 0.44% in GFeN, and 0.32 to 0.46% in GO-CeO_2. This might have happened because phosphate (PO_4^{3-})and As(V), i.e., arsenate (AsO_4^{3-}), have similar ionic structures, so some ionically bound and loosely-held arsenate was replaced by phosphate (Zeng et al., 2008; DeVore et al., 2019). In both DI and groundwater environments, the total arsenic desorption from the nanohybrids was low compared to the total amount adsorbed by them. This indicates that the complexation between arsenate and nanohybrids is quite stable. A comparison between two nanohybrids indicates that GO-CeO_2 showed slightly lower desorption than GFeN. The total arsenic loading in GFeN was 111.9 mg/g meaning a 1% release from GFeN equal to 1.119 mg/g, while 1% release from GO-CeO_2 equals to 0.752 mg/g (total arsenic loading 75.2 mg/g).

Solution pH is another important environmental parameter that can affect arsenic desorption behavior. Arsenic desorption from the two materials was evaluated using solutions (DI water) over a wide pH range (3-9). For GFeN, arsenic desorption increased marginally from 0.84% at pH 3 to 1.21% at pH 7, and then to 2.01% at pH 9. As the pH increased, hydroxyl ions replaced arsenic ions from the iron oxide sorption sites and caused the desorption of arsenic oxyanions. (Al-Abed et al., 2007; Yuan et al., 2018) On the other hand, arsenic desorption decreased with an increase in pH from 0.73% (pH 3) to 0.38% (pH 7) and then 0.33% (pH 9) for GO-CeO_2. At alkaline conditions (pH>7) the transformation of Ce^{4+} to Ce^{3+} or vice versa is very much limited, therefore, so the surface-bound Ce-As complex remains more stable.

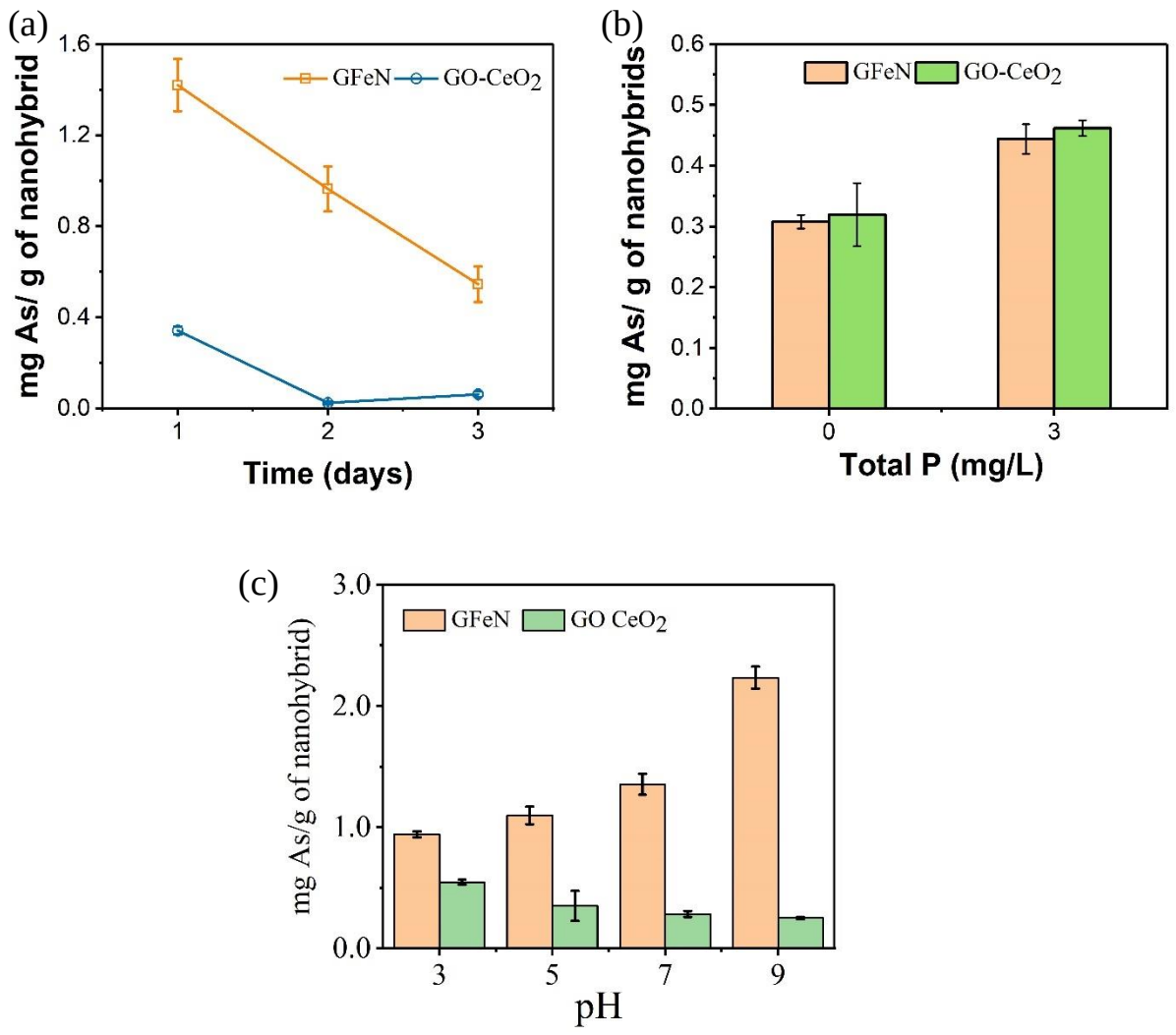

Figure 4.4. Release of adsorbed arsenic release from nanohybrids in (a) DI water over a period of 3 days, (b) synthetic groundwater with phosphate concentration, and (c) DI water system at different pH (3-9).

4.3.2.2.2. Long-term study

The short-term evaluation of arsenic desorption from nanohybrids showed minimal release of arsenic apparently because the arsenic metal oxide complex remained stable during this period. However, short-term studies cannot predict the long-term release behavior of arsenic from the media. Given that these arsenic adsorption media will be used in water filter units which are expected to last for 6 months to a year, it would be pertinent to conduct long-term arsenic release studies under environmentally relevant conditions to know the remobilization of

arsenic from the solid phase (the nanohybrids) to the aqueous phase. Chromatographic release of toxic arsenic to the drinking water system may affect unsuspecting water consumers. So, to understand the release behavior of arsenic from the adsorbed (solid) phase over time, an arsenic desorption study was conducted for 2 years using sacrificial batch reactors and in simulated groundwater.

Arsenic saturated GFeN material exhibited slow but prolonged arsenic desorption (Figure 4.5 a-b). For GFeN on Day 1, the desorption was 0.62% which slowly increased to 0.85% on Day 11 and 1.07 % on Day 21. At end of 31 days, the desorption was ~1.19% which increased to 3.93% on Day 180 and 4.61% on day 341. At the end of the study periods (day 696), GFeN recorded cumulative desorption of 5.73% of total adsorbed arsenic. For GO-$CeO_{2\backslash,}$ desorption was 0.68% on Day 1 and increased marginally to 0.71% on Day 11 and 0.75% on Day 21. In the case of GO $CeO_{2,}$ 0.80% was desorbed after 31 days, 0.57 % on Day 180), 0.83% on Day 341, and 0.94% 696 days (Figure 4.5 a-b). Comparing the two classes of nanohybrids indicated arsenic desorption is lower in GO-CeO_2 than GFeN. There was potentially strong complexation between Ce^{3+} and As(V) which remained stable till the end of the 2-year study.

Adsorbed arsenic release patterns from the nanohybrids were also evaluated under continuous flow conditions in column reactors for period of 60 days. The sand columns (packed sand column with arsenic-sorbed nanohybrids) were operated in continuous flow mode (1 mL/min) with synthetic groundwater (Figure 4.5c). the effluent arsenic concentration was monitored over two months. Initially, a bit higher amount (148.3- 51.3 µg/L) of adsorbed arsenic release in both the nanohybrids which might have come from the loosely held arsenic on the surface (ionically bound arsenic) (Figure 4.5c). As time proceeded, the desorption decreased and reached a steady-state after one week. At the end of the first week, the effluent arsenic

concentration for the GFeN column decreased from 148.3 to 45.9 µg/L. For GO-CeO_2, effluent arsenic decreased from 51.3 to 9.8 µg/L after a week, and it further decreased as time proceeds. The arsenic release from the GFeN based nanohybrids is higher than GO-CeO_2 which is in agreement with our long-term batch desorption studies which also record higher arsenic release from GFeN. The possible reason for this enhanced release from GFeN is the transformation of surface-bound Fe-As fraction (arsenic coprecipitated in iron oxyhydroxide and ionically bound fraction) under a continuous flow of simulated groundwater.

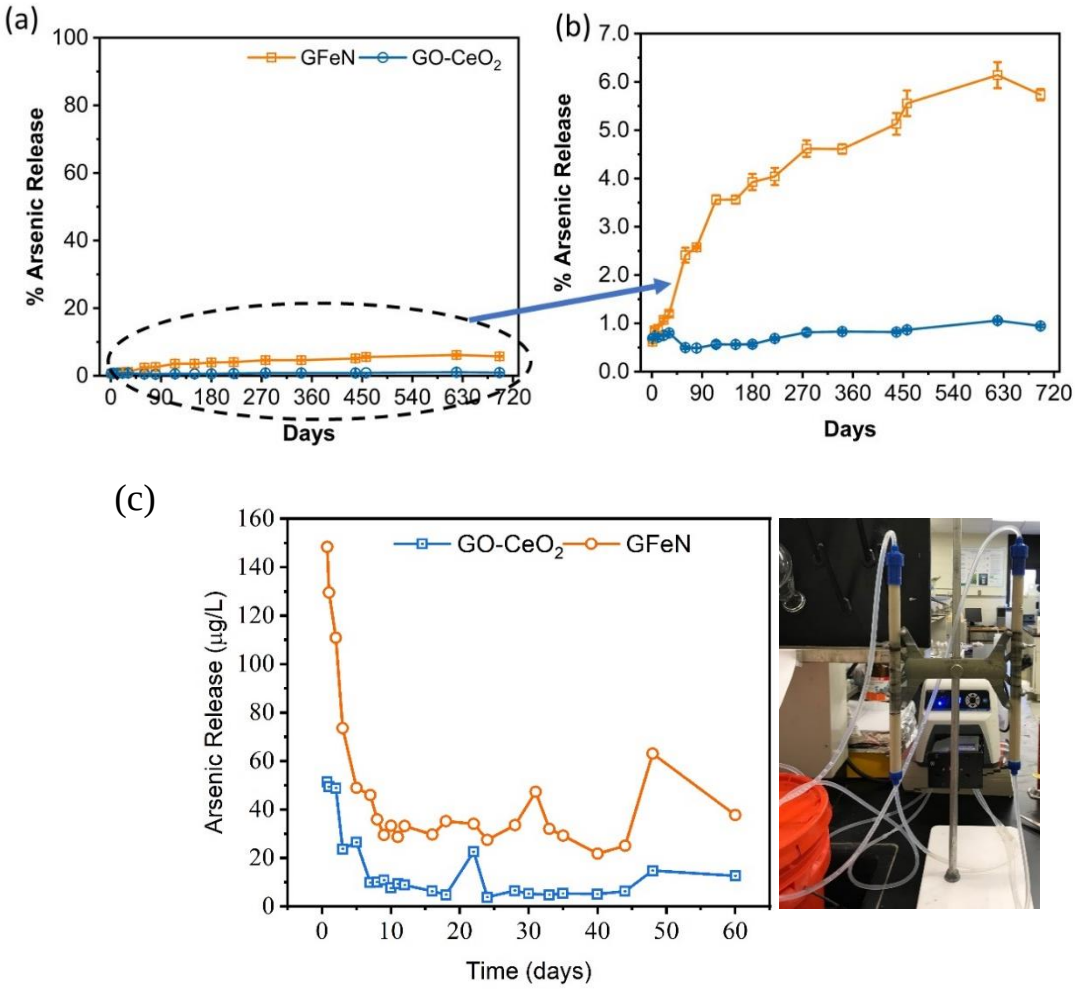

Figure 4.5. (a) Cumulative arsenic release from arsenic-sorbed nanohybrids in the batch reactors (synthetic groundwater) (b) Zoomed in the area from cumulative arsenic release plot (Figure 4.5a) (c) Arsenic release from the continuous flow columns. No arsenic was detected in the control run with fresh nanohybrids (no arsenic sorbed onto them).

4.3.3. Transformation of material surface composition

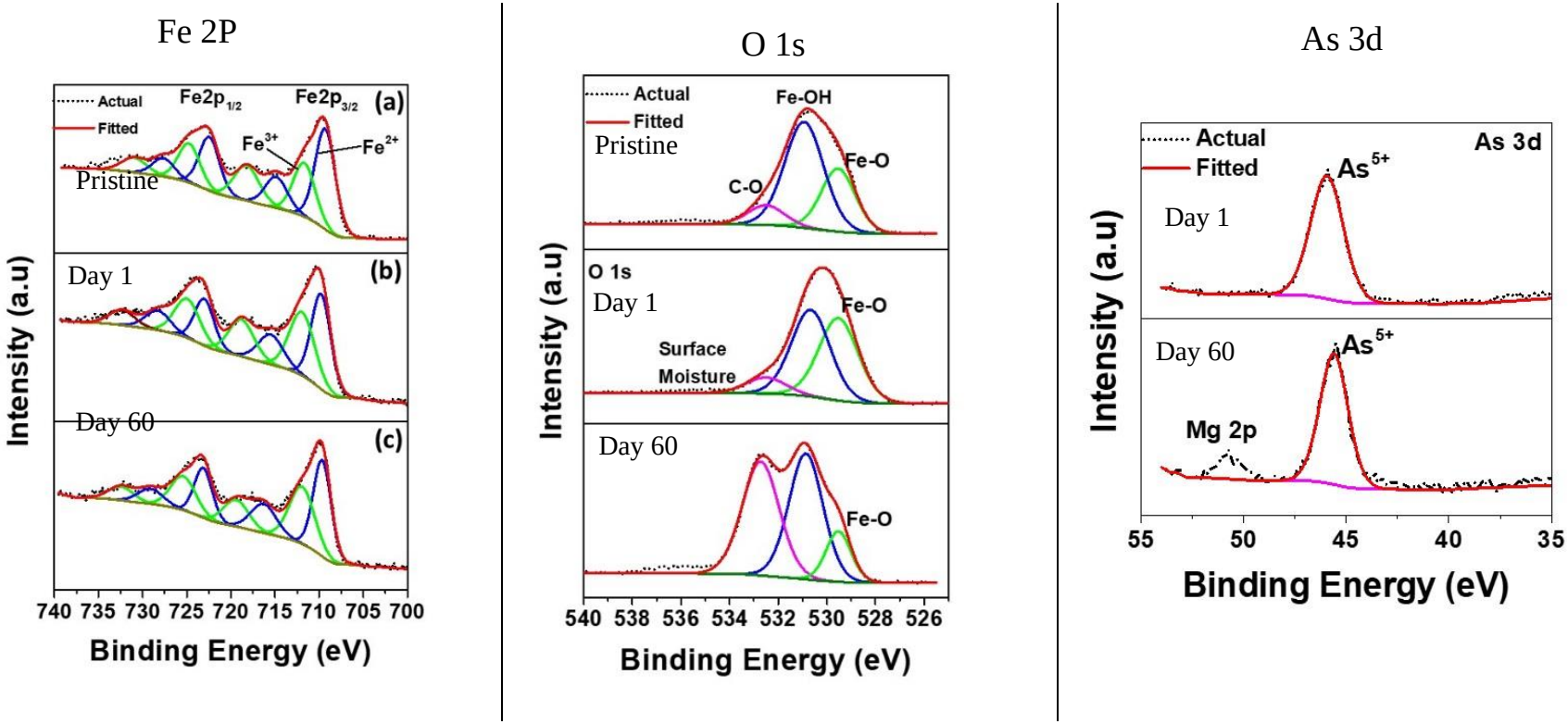

Figure 4.6. XPS spectra of pristine GFeN and arsenic adsorbed GFeN for Day 1, Day 60.

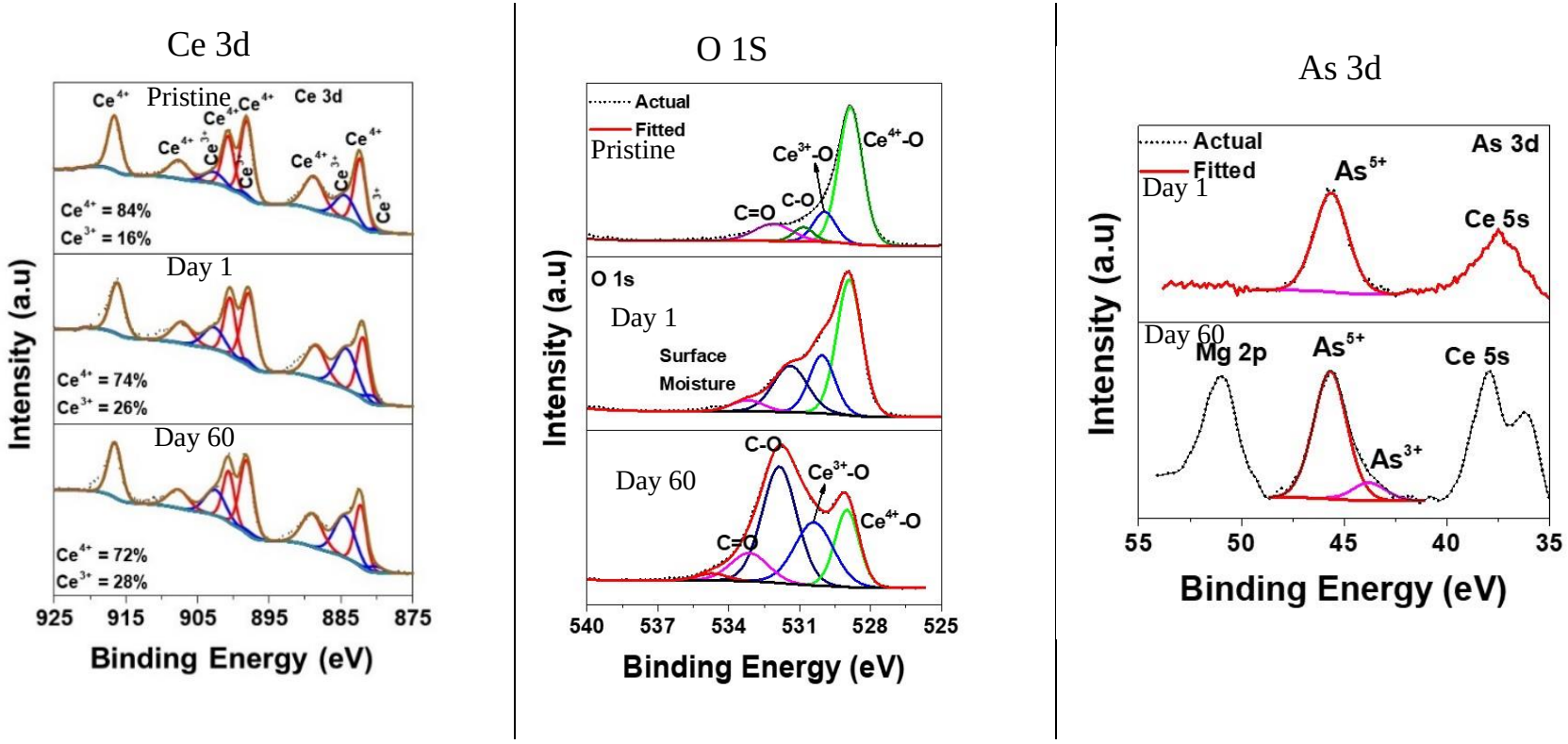

Figure 4.7. XPS spectra of pristine GO-CeO_2 and arsenic adsorbed GO-CeO_2 for Day 1, Day 60.

XPS analysis of both the nanohybrids before and after arsenic adsorption was performed to understand the transformation of surface composition. For pristine GFeN (Figure 4.6), the presence of Fe2p spectrum with the deconvoluted peaks of Fe($2p_{3/2}$), Fe($2p_{1/2}$) indicated the presence of Fe(II) and Fe(III) on the surface. Three prominent peaks were identified in the O1s spectrum of GFeN which were assigned to O^{2-} (~530 eV), OH (~531.8 eV), and OH_2 (~533.1 eV). The dominance of -OH peak (68%) with a broad peak of Fe–O (~23%) (Figure 4.6, see the O1s spectra of XPS) indicated that the surface iron was mostly FeOOH while there were small amounts of Fe_2O_3 and Fe_3O_4 (Das et al., 2020). Arsenic participates in surface complexation with GFeN forming bidentate and monodentate complexes with surface iron oxyhydroxide. After adsorption, at Day 1, the concentration of Fe-OH groups decreased, and Fe-O increased which confirms the complexation of As(V) with surface-bound Fe-OH groups and transformation of FeOOH to Fe_2O_3. After 60 days, material released a small amount (~1.87%, Figure 4.5b) of adsorbed As (V), and there are some changes in O1s spectra, Fe-O peak is decreased, and Fe-OH peak is increased. The means Fe_2O_3 is changing to FeOOH due to the interaction of the surface layer in the water with the presence of other ions. This transformation can facilitate the release of arsenic bound in the surface iron oxyhydroxide fraction which explains the small and slow arsenic release behavior from the sand-block filter study (between 7-60 days). GFeN, the oxidation state of surface adsorbed As (V) did not change over the 60-days study period.

The Ce 3d XPS spectra of GO–CeO_2 (Figure 4.7) contained Ce 3d5/2 and Ce 3d3/2 spin-orbit splitting which confirms the presence of both Ce^{3+} (16%) and Ce^{4+} (84%) (Sakthivel et al., 2017). Ce^{3+}/Ce^{4+} acts as a redox couple and can interchange the redox state due to their low redox potential (1.61 eV). In GO-CeO_2 after one day of adsorption concentration of Ce^{3+} increased from 16 to 26% where Ce^{4+} decreased (84 to 74%). This transformation of Ce^{3+}/Ce^{4+}

facilitated due to low redox couple which helped to form a stable complex of Ce-As(V). Further, there are some changes in O 1s spectra, Ce^{4+}-O peak is decreased and Ce^{3+}-O peak is increased after 60 days, which might help to keep Ce-As complex compound stable. After adsorption at day 1, all adsorbed arsenic remained in As(V) oxidation state which undergo reduction after 60 days, and 13% transformed to As (III) while 87% remain as of As (V). After 60 days, GO-CeO2 nanohybrid released only ~0.5 % of adsorbed As (V), so most of the adsorbed arsenic remain remained very stable in the adsorbed phase.

4.4. Conclusion

Graphene oxide-supported metal oxide nanohybrids were promoted as a superior arsenic adsorbing material based on its performance. The desorption behavior of As(V)-sorbed GFeN and GO-CeO_2 were evaluated under different environmental conditions (pH and the presence of co-existing ions). Both the nanohybrids have very high adsorption capacities and the adsorption mechanism is dominated by surface complexation. In batch reactors with simulated groundwater, arsenic-sorbed GFeN released ~5.73 %, and GO-CeO_2 released ~0.94% of total adsorbed arsenic over two years. The desorption behavior was also monitored for both the nanohybrids in a simulated filter bed system (nanohybrid mixed with sand) and continuous flow conditions for two months. While the overall arsenic release was minimal from the filter bed, the release from GFeN was slightly higher compared to that from GO-CeO_2. The surface oxide composition (Fe_3O_4/FeOOH) of GFeN changed over time which resulted in the desorption of the sorbed arsenic. While adsorbed As(V) remain stable (i.e., no change in oxidation state) on the surface of GFeN, part of As(V) reduces to As(III) in GO-CeO_2. This study provides detailed insight into the fate and transformation of adsorbed arsenic sorbed onto arsenic adsorbing nanohybrids. The

finding of this study will contribute towards the planning and design of sustainable arsenic removal adsorbent media.

4.5. References

Ahmad, A., van der Wens, P., Baken, K., de Waal, L., Bhattacharya, P., Stuyfzand, P., 2020. Arsenic reduction to < 1 mu g/L in Dutch drinking water. Environment International 134.

Al-Abed, S.R., Jegadeesan, G., Purandare, J., Allen, D., 2007. Arsenic release from iron rich mineral processing waste: Influence of pH and redox potential. Chemosphere 66, 775-782.

Ayotte, J.D., Medalie, L., Qi, S.L., Backer, L.C., Nolan, B.T., 2017. Estimating the High-Arsenic Domestic-Well Population in the Conterminous United States. Environmental Science & Technology 51, 12443-12454.

Baig, S.A., Sheng, T.T., Hu, Y.J., Xu, J., Xu, X.H., 2015. Arsenic Removal from Natural Water Using Low Cost Granulated Adsorbents: A Review. Clean-Soil Air Water 43, 13-26.

Chandra, V., Park, J., Chun, Y., Lee, J.W., Hwang, I.-C., Kim, K.S., 2010. Water-Dispersible Magnetite-Reduced Graphene Oxide Composites for Arsenic Removal. ACS Nano 4, 3979-3986.

Das, T.K., Sakthivel, T.S., Jeyaranjan, A., Seal, S., Bezbaruah, A.N., 2020. Ultra-high arsenic adsorption by graphene oxide iron nanohybrid: Removal mechanisms and potential applications. Chemosphere 253.

DeVore, C.L., Rodriguez-Freire, L., Mehdi-Ali, A., Ducheneaux, C., Artyushkova, K., Zhou, Z., Latta, D.E., Lueth, V.W., Gonzales, M., Lewis, J., Cerrato, J.M., 2019. Effect of bicarbonate and phosphate on arsenic release from mining-impacted sediments in the Cheyenne River watershed, South Dakota, USA. Environmental Science-Processes & Impacts 21, 456-468.

Dong, H., Guan, X., Lo, I.M.C., 2012. Fate of As(V)-treated nano zero-valent iron: Determination of arsenic desorption potential under varying environmental conditions by phosphate extraction. Water Research 46, 4071-4080.

Fu, D.D., He, Z.Q., Su, S.S., Xu, B., Liu, Y.L., Zhao, Y.P., 2017. Fabrication of alpha-FeOOH decorated graphene oxide-carbon nanotubes aerogel and its application in adsorption of arsenic species. Journal of Colloid and Interface Science 505, 105-114.

Gallegos-Garcia, M., Ramírez-Muñiz, K., Song, S., 2012. Arsenic removal from water by adsorption using iron oxide minerals as adsorbents: a review. Mineral Processing and Extractive Metallurgy Review 33, 301-315.

Hao, L.L., Liu, M.Z., Wang, N.N., Li, G.J., 2018. A critical review on arsenic removal from water using iron-based adsorbents. RSC Advances 8, 39545-39560.

Hoan, N.T.V., Thu, N.T.A., Van Duc, H., Cuong, N.D., Khieu, D.Q., Vo, V., 2016. Fe3O4/Reduced Graphene Oxide Nanocomposite: Synthesis and Its Application for Toxic Metal Ion Removal. Journal of Chemistry, 10.

Jomova, K., Jenisova, Z., Feszterova, M., Baros, S., Liska, J., Hudecova, D., Rhodes, C.J., Valko, M., 2011. Arsenic: toxicity, oxidative stress and human disease. Journal of Applied Toxicology 31, 95-107.

Keon, N.E., Swartz, C.H., Brabander, D.J., Harvey, C.F., Hemond, H.F., 2001. Validation of an arsenic sequential extraction method for evaluating mobility in sediments. Environmental Science & Technology 35, 2778-2784.

Lata, S., Samadder, S.R., 2016. Removal of arsenic from water using nano adsorbents and challenges: A review. Journal of Environmental Management 166, 387-406.

Mohan, D., Pittman, C.U., 2007. Arsenic removal from water/wastewater using adsorbents - A critical review. Journal of Hazardous Materials 142, 1-53.

Murcott, S., 2012. Arsenic contamination in the world. IWA publishing.

Nicomel, N.R., Leus, K., Folens, K., Van der Voort, P., Du Laing, G., 2016. Technologies for Arsenic Removal from Water: Current Status and Future Perspectives. International Journal of Environmental Research and Public Health 13.

Podgorski, J., Berg, M., 2020. Global threat of arsenic in groundwater. Science 368, 845-+.

Sakthivel, T.S., Das, S., Pratt, C.J., Seal, S., 2017. One-pot synthesis of a ceria-graphene oxide composite for the efficient removal of arsenic species. Nanoscale 9, 3367-3374.

Van der Leeden, F., 1990. The water encyclopedia. CRC Press.

WHO, 2017. Arsenic. WHO. World Health Organization.

Wu, K., Jing, C.Y., Zhang, J., Liu, T., Yang, S.J., Wang, W.D., 2019. Magnetic Fe3O4@CuO nanocomposite assembled on graphene oxide sheets for the enhanced removal of arsenic(III/V) from water. Applied Surface Science 466, 746-756.

Yuan, Z.D., Ma, X., Wu, X., Wang, X., Wang, S.F., Jia, Y.F., 2018. Effect of hydroquinone-induced iron reduction on the stability of Fe(III)-As(V) Co-precipitate and arsenic mobilization. Applied Geochemistry 97, 1-10.

Zeng, H., Fisher, B., Giammar, D.E., 2008. Individual and competitive adsorption of arsenate and phosphate to a high-surface-area iron oxide-based sorbent. Environmental Science & Technology 42, 147-152.

CHAPTER 5. CONCLUSIONS

5.1. Conclusion

The overarching goal of this research was to develop advanced nano-based safe materials for aqueous arsenic removal and elucidate the mechanisms involved in the arsenic removal process. In this research, graphene oxide-supported iron/iron oxide nanohybrid materials were synthesized and evaluated for their potential applications to treat arsenic contaminated water. First, the most efficient nanomaterial for arsenic removal was identified, and the material was further tested for arsenic removal under relevant environmental conditions. The underlying arsenic removal mechanisms were investigated, and the risks associated with its potential field application were assessed in terms of arsenic desorption from the used (arsenic-sorbed) materials.

In the first phase of this research, two iron-based nanomaterials~~,~~ viz., nanoscale zero-valent iron (FeNP) and magnetite (M), were deposited onto graphene oxide (GO) sheets to synthesize two nanohybrids. Graphene oxide nano zerovalent iron (GFeN) nanohybrid was obtained by depositing FeNPs on graphene oxide (GO) and graphene oxide magnetite (GM) nanohybrid was synthesized by depositing M on GO. Arsenic removal behaviors of the two nanohybrids (GFeN and GM) and their bare counterparts FeNP and M (no GO) were evaluated under the same experimental conditions of pH, adsorbent dose, temperature, initial arsenic concentration, and contact time to identify the best candidate for use in an arsenic treatment system. The deposition of nanoparticles on the GO surface (to form nanohybrids) improved arsenic removal significantly in both the nanohybrids (GFeN and GM) compared to their bare counterparts (FeNP and M), and this happened because of better dispersion of the iron nanoparticles (FeNPs and M) on the GO surface providing for better interaction between arsenic

species and reactive surfaces of the nanomaterials. The FeNP-based material showed better removal performance compared to the M-based material over a wide pH range (3 to 9) for both the inorganic arsenic species, As(III) and As(V), present in groundwater (drinking water). The magnetite (M)-based nanomaterials worked better (>90%) at low pH (pH- 3) but only for As(V) and most efficient As (III) removal (~80%) was found to be at high pH (pH = 9). The different iron (Fe) contents in FeNP- and M-based materials played a crucial role in the arsenic removal process, and it found that GFeN was the most efficient material in terms of arsenic removal per unit mass of iron present in the nanohybrid. The experimental and characterization data indicate that arsenic removal by FeNP-based nanomaterials was dominated by surface complexation. In M-based materials, As(V) removal was controlled by electrostatic interactions while As(III) removal was controlled by ligand exchange and surface complexation. At end of the first phase of this research, GFeN was identified as the most suitable candidate material for potential field application.

In the second phase of this research, the arsenic removal mechanism(s) and arsenic removal performance of the graphene oxide-iron nanohybrid (GFeN) were evaluate in more details. The isotherm data for arsenic removal by GFeN fitted well into the Langmuir model and the adsorption capacities were found to be 431 mg/g for As(V) and 306 mg/g for As(III) which are very high compared to other available nanohybrid reported by others (Table 3.6, Chapter 3). The kinetic data from arsenic removal studies with both high (5 mg/L) and low arsenic (100 μg/L) concentrations fitted well into pseudo-second-order kinetic models indicating that arsenic removal by GFeN is chemisorption. There were negligible interferences (90% removal) in the presence of potential coexisting ions (SO_4^{2-}, NO_3^-, HCO_3^-, PO_4^{3-}, SiO_3^{2-}) and organic matters (humic acid) at environmentally relevant concentrations. However, groundwater with high

dissolve SiO_4^{2-} ions was found to reduce the arsenic removal efficiency (70-88% removal). GFeN was able to remove both the arsenic species, As(III) and As(V), simultaneously without any pre-oxidation of As(III) otherwise required in the currently practiced treatment processes. GFeN worked very effectively to remove arsenic from actual arsenic contaminated groundwater (with 30-40 µg/L of total arsenic) and brought down the effluent arsenic concentrations to below the maximum contaminant level (MCL) of 10 µg/L within 2-3 min. Arsenic adsorption results and material characterization data from GFeN before and after arsenic adsorption suggested that arsenic was adsorbed onto the GFeN surface through surface complexation (dominant process) and electrostatic interaction. In the GFeN nanohybrid, the GO layer played a significant role in enhancing arsenic removal. First, the effective dispersion of iron nanomaterial (FeNPs) on the GO surface reduced the agglomeration of FeNPs and enhanced the interaction of arsenic with the nanomaterial. The enhanced interactions of arsenic with FeNPs potentially led to effective arsenic removal and fast kinetics. Second, the GO sheets acted as the reservoirs for the electrons released during the oxidation of Fe^0 (in FeNPs present ~~in~~ on GFeN) and then transferring the electrons back to the nanoparticles (FeNPs) surface to rejuvenate the adsorptive oxide layer (reduced back to Fe^0). The rejuvenation of the surface layer prolongs the effective life span of the GFeN by protecting the reactive Fe^0 core and stabilizing the adsorbed arsenic on the nanohybrid.

GFeN nanohybrid was found to be the most efficient in environmentally relevant conditions of pH, presence of other ions, and temperature. It recorded fast kinetics and high adsorption capacity (>300 mg/g for either arsenic species). These superior adsorption characteristics of GFeN made it a suitable candidate for use in filter media for arsenic treatment systems. Our calculations indicate that a point-of-use treatment unit with 100 g of GFeN can

potentially supply 20 liters of arsenic-free drinking (and cooking) water every day to a 4-member family for ~10 years without much operational and maintenance needs.

While the study established that GFeN is an effective candidate material for arsenic treatment, it is important to recognize that adsorbents with high arsenic adsorption capacity always pose a risk of secondary contamination through the release (desorption) of arsenic from the adsorbed phase. So, in the third phase of this research, experiments were conducted on the potential desorption (release) of arsenic from arsenic-sorbed GFeN nanohybrid. For comparison, the arsenic desorption behavior of another standard but a non-iron GO nanohybrid was studied alongside GFeN in batch experiments. The non-iron candidate selected was graphene oxide ceria (GO-CeO_2) nanohybrid. GFeN released ~5.73% and GO-CeO_2 released ~0.94% of total adsorbed arsenic over a period of 2 years. The sand block filters (a representative arsenic treatment unit) filled with arsenic-sorbed nanohybrids mixed with sand followed similar arsenic desorption trends like in the batch desorption studies with GFeN releasing more than GO-CeO_2. The arsenic release behavior was explained from the surface analysis of arsenic-sorbed nanohybrids. Additional sequential chemical extraction indicated that 66% of the sorbed arsenic in GFeN was ionically bound indicating potential future chromatographic release. In GO-CeO_2, the major fraction (97%) of arsenic was present as very stable Ce-As complexes where the arsenic was very strongly bound onto the ceria, and, thus, making it a potentially safer arsenic treatment medium.

5.2. Future directions

With this research, an ultra-high arsenic adsorbent graphene oxide-iron nanohybrid was synthesized using a facile sol-gel method and an in-depth mechanism study was also done. However, the applicability of the adsorbent in actual drinking water systems will still needed be

evaluated. To translate this research into application, two major tasks will be needed. First, a scale-up of the nanomaterial production process must be achieved. The current laboratory synthesis process yields only ~700-750 mg of material per batch. Second, the development and evaluation of pilot-scale water treatment systems using the nanohybrid. For pilot studies, the nanohybrids can be mixed with sand and a standard functional adsorbent (e.g., activated carbon) to develop point-of-use treatment units. Nanoscale powdery materials have some operational challenges like the movement of nanomaterial through the filter bed and potential clogging. To address this issue, polymeric beads and capsules can be potentially used. However, the polymers to be used should be toxicant-free and cost-effective. Further, economic feasibility, application viability, and stakeholder (societal included) acceptability of the developed technology should be evaluated through community-level studies. The major concern associated with any nano-enabled water treatment system is the potential leaching of nanomaterials from the system. To ensure consumer safety, possible nanomaterial leaching from the system should be extensively studied.

APPENDIX

A.1. XPS spectra of FeNP and GO

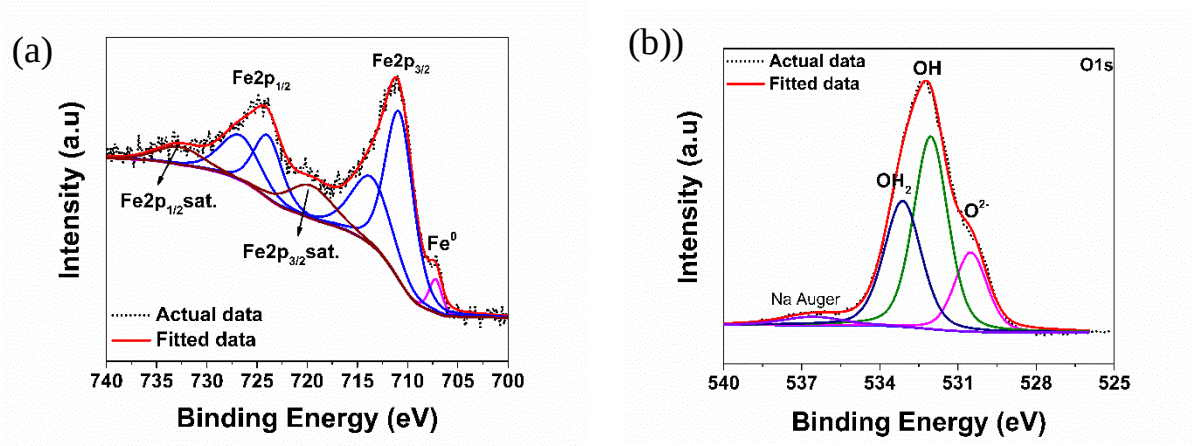

Figure A1. XPS spectra of bare FeNP (not on GO) for (a) Fe 2p indicating presence of iron oxide and elemental iron on the surface layer, and (b) O1s indicating that majority of surface oxides have –OH bond.

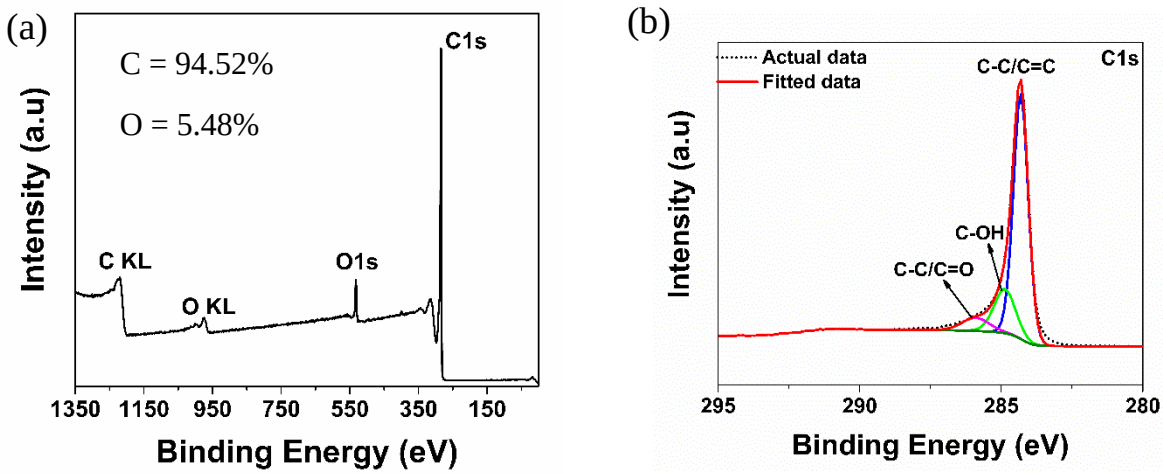

Figure A2. XPS spectra for bare GO (a) Survey, and (b) C1s indicating presence of surface functional groups. The survey spectrum of GO shows 94.52% of Carbon and 5.48% of Oxygen. No impurities are present in the GO material.

A.2. Iron content determination in nanomaterials

To measure the amount of iron in each nanomaterial (adsorbent) we followed Yoon et al. (2016) (Yoon et al., 2016). Here, 50 mg of an adsorbent was digested with 15 mL of 7 M HCl by first shaking (250 rpm) the mixture for 2 h in a 50 mL test tube and then keeping it in a water

bath (80 ºC) for 1 h. The digested sample was filtered using a membrane filter (0.22 µm, VWR, USA) and iron content in the filtrate was measured using Flame AAS (Perkin Elmer AAS 900H).

A.3. FeNP surface corrosion reactions

The following corrosion reactions (Eqs. A1-A9) have been proposed by others to represent the corrosion systems on FeNPs (Kanel et al., 2006; Wu et al., 2017) .

$$Fe^{o} + 2H_2O \rightarrow Fe^{2+} + H_2 + 2OH^- \quad (A1)$$

$$Fe^{o} + O_2 + 4H_2O \rightarrow Fe^{2+} + H_2 + 6OH^- \quad (A2)$$

$$4Fe^{2+} + O_2 + 2H_2O \rightarrow 4Fe^{3+} + 4OH^- \quad (A3)$$

$$6Fe^{2+} + O_2 + 6H_2O \rightarrow 2Fe_3O_4\,(S) + 12H^+ \quad (A4)$$

$$Fe^{2+} + 2OH^- \rightarrow Fe(OH)_2(S) \quad (A5)$$

$$4Fe_3O_4 + O_2 + 18H_2O \leftrightarrow 12Fe\,(OH)_3(S) \quad (A6)$$

$$4Fe_3O_4 + O_2 \rightarrow 6Fe_2O_3(S) \quad (A7)$$

$$Fe^{3+} + 3H_2O \rightarrow Fe(OH)_3 + 3\,H^+ \quad (A8)$$

$$Fe\,(OH)_3 \rightarrow FeOOH + H_2O \quad (A9)$$

A.4. Composition of synthetic groundwater

We prepared the synthetic groundwater keeping concertation of all ions close to the typical values found in natural groundwater (Van der Leeden, 1990) .

Table A1. Composition of synthetic groundwater.

Ions	Concentration (mg/L)
Na^+	230
Ca^{2+}	32
Cl^-	234
HCO_3^-	183
SO_4^{2-}	96
PO_4^{3-}.	3

A.5. Effect of humic acid and ionic strength

Fig. A3 is provided here.

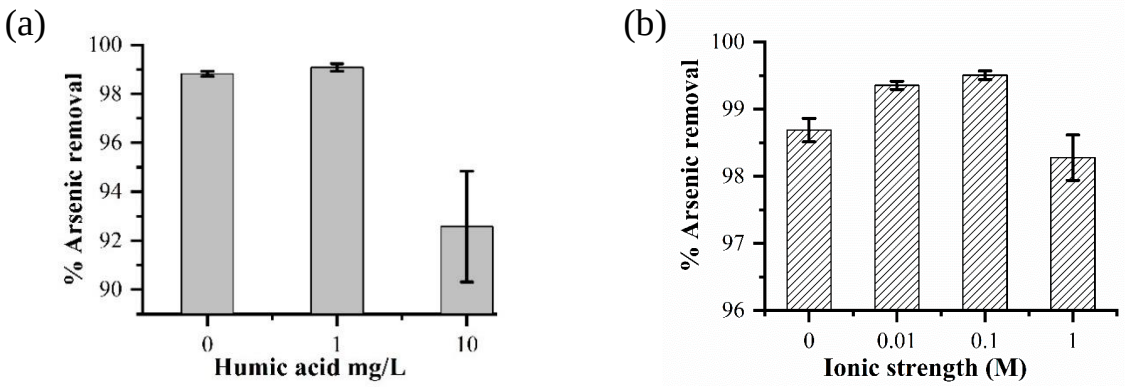

Figure A3. Effects of (a) humic acid (b) ionic strength (NaCl) on arsenic removal by GFeN.

A.6. References

Van der Leeden, F., 1990. The water encyclopedia. CRC Press.1990